K. S. ARSAVA METU 2011

FIRE TESTS OF CUT AND COVER TUNNEL ROOF SEGMENTS AT POSITIVE MOMENT REGION

KEMAL SARP ARSAVA

JANUARY 2011

FIRE TESTS OF CUT AND COVER TUNNEL ROOF SEGMENTS AT POSITIVE MOMENT REGION

A THESIS SUBMITTED TO
THE GRADUATE SCHOOL OF NATURAL AND APPLIED SCIENCES
OF
MIDDLE EAST TECHNICAL UNIVERSITY

BY

KEMAL SARP ARSAVA

IN PARTIAL FULFILLMENT OF THE REQUIREMENTS
FOR
THE DEGREE OF MASTER OF SCIENCE
IN
CIVIL ENGINEERING

JANUARY 2011

Approval of the Thesis:

FIRE TESTS OF CUT AND COVER TUNNEL ROOF SEGMENTS AT POSITIVE MOMENT REGION

Submitted by **KEMAL SARP ARSAVA** in partial fulfillment of the requirements for the degree of **Master of Science in Civil Engineering Department, Middle East Technical University** by,

Prof. Dr. Canan Özgen
Dean, Graduate School of **Natural and Applied Sciences** _____________

Prof. Dr. Güney Özcebe
Head of Department, **Civil Engineering** _____________

Asst. Prof. Dr. Alp Caner
Supervisor, **Civil Engineering Dept., METU** _____________

Examining Committee Members:

Prof. Dr. Çetin Yılmaz
Head of Jury, Civil Engineering Dept., METU _____________

Asst. Prof. Dr. Alp Caner
Supervisor,Civil Engineering Dept., METU _____________

Asst. Prof. Dr. Afşin Sarıtaş
Civil Engineering Dept., METU _____________

Asst.Prof.Dr. Burcu Burak
Civil Engineering Dept., METU _____________

Asst.Prof.Dr. Burcu Güneş
Civil Engineering Dept., Atilim University _____________

Date: 25/01/2011

I hereby declare that all information in this document has been obtained and presented in accordance with academic rules and ethical conduct. I also declare that, as required by these rules and conduct, I have fully cited and referenced all material and results that are not original to this work.

Name, Last name : KEMAL SARP ARSAVA

Signature :

ABSTRACT

FIRE TESTS OF CUT AND COVER TUNNEL ROOF SEGMENTS AT POSITIVE MOMENT REGION

Arsava, Kemal Sarp
M.Sc, Department of Civil Engineering
Supervisor: Asst. Prof. Dr. Alp Caner

January 2011, 129 pages

The most important issue during a tunnel fire is safety of human life. The tunnel fire structural research and investigations have gained more importance in the last decade but studies show variable results depending on the concrete quality and tunnel design fire. For instance, a certain type of concrete with high moisture content can tend to explode in the first 10-15 minutes of fire with rapid increase of heat release rate. A sudden collapse of the tunnel roof during the fire is unacceptable. Especially in Netherlands, the possible sagging of cut and cover tunnel roof is undesired and prevention systems are applied. The main purpose of this research is to investigate fire response of the positive moment region of cut and cover tunnel roof through an experimental and analytical program without use of any protection. In this context a standard one cell rail road cut and cover tunnel has been designed for loads of backfill, lateral earth pressure and self weight. The typical concrete cover used in

Turkish railroad tunnels is 6 centimeters. Four pairs of representative sample tunnel roof segments have been manufactured and only one segment out of each pair are tested under 2 hours extreme design tunnel fire in a furnace. Out of these four types, two types have been internally pre-stressed to simulate the internal loads at the positive moment region of the tunnel roof. Four pairs of sample segments are simply supported during the static load test and static load is applied at the mid-span to measure the difference in the post-fire structural performance. Compressive strength of concrete, tensile strength of reinforcing bars, electron microscope evaluation of concrete, moisture content of concrete are recorded during the test program. A finite element based solution is developed to simulate the results of static load tests. Post-fire structural performances of burnt segments are observed to be not much different than the unburnt segments.

Keywords: Fire test, ACI 216, Eurocode2, Spalling, Tunnel Linings.

ÖZ

AÇ-KAPA TÜNEL ÜST DÖŞEME AÇIKLIK MOMENTİ BÖLGESİNDE YANGIN TESTLERİ

Arsava, Kemal Sarp
Yüksek Lisans, İnşaat Mühendisliği Bölümü
Tez Yöneticisi: Yrd. Doç. Dr. Alp CANER

Ocak 2011, 129 sayfa

Bir tünel yangını sırasında en önemli unsur insanların can güvenliğinin sağlanmasıdır. Tünellerde yapısal yangın araştırmaları son on sene içinde hız kazanmasına rağmen elde edilen sonuçlar betonun özelliğine ve tünel içindeki yangının yapısına göre değişiklik göstermektedir. Örnek olarak, belirli bir beton malzeme anlık şiddetli bir yangının ilk 10 – 15 dakikasında patlama özelliği gösterebilir. Bir tünel yapısının uzun süreli bir yangın sırasında aniden çökmesi kesinlikle istenilen bir durum değildir. Aç-kapa tünellerin yapısal yangın güvenliğinin deneysel ve analitik olarak ele alınması bu projenin esas amacını oluşturmaktadır. Bu nedenle aç-kapa yapım metodu uygulanarak inşa edilecek tek açıklıklı standart bir demiryolu tüneli, maruz kalacağı dolgu, yanal toprak basıncı ve zati ağırlık gibi yükler esas alınarak tasarlanmıştır. Tünel üst döşemesinin pozitif moment bölgesinde oluşan yüklere göre dizayn edilmiş sekiz numune hazırlanmıştır.

Numunelerin boyutları deney fırınına girecek şekilde seçilmiştir. Bu sekiz numunenin dördü, iki saatlik yangın testine maruz bırakılmıştır. Bu dört numunenin ikisine de tünel üst döşemesine gelen yükleri yansıtmak için öngerme verilmiştir. Numunelerin yapısal performansını ölçmek için ise basit mesnet üzerine oturtulmuş numuneler ortadan tekil yüklemeye maruz bırakılmıştır. Sonuçlar numunelerimizin geniş derin kiriş gibi çalıştığını göstermektedir. Beton basınç dayanımı, çelik çekme dayanımı, betonun elektron mikroskobu taraması ve betonun içindeki nem oranı yangın testinden önce ve sonra olarak kaydedilmiştir. Yangın testine maruz kalmış numunelerin yapısal performansında, yanmamış numunelere kıyasla bir fark gözlenmemiştir.

Anahtar Kelimeler: Yangın Testi, ACI 216, Eurocode 2, Parçalanma, Tünel Yapıları.

To My Family

ACKNOWLEDGEMENTS

I wish to express my deepest gratitude to my supervisor Assist Prof. Dr. Alp CANER for his kind and friendly guidance and continuous help, support and encouragement.

I would also like to thank to Prof. Dr. Çetin YILMAZ, Assoc Prof. Dr. İsmail Özgür YAMAN, Asst. Prof. Dr. Burcu BURAK, Asst. Prof. Dr. Afşin SARITAŞ from Civil Engineering Department of Middle East Technical University and Asst. Prof. Dr. Eray BARAN, Asst. Prof. Dr. Tolga AKIŞ, Asst. Prof. Dr. Burcu GÜNEŞ, Asst. Prof. Dr. Ayhan GÜRBÜZ from Civil Engineering Department of Atilim University and also Dr. Serkan Kayılı for their advice and help in steps throughout the study.

I also thank to SINTA Precast Element Manufacturing Company in Bursa, TARU Engineering, METU-BAP for their support in the study.

I want to express my special thanks to Prof. Dr. O. Cahit ERALP who we unfortunately lost for few months ago.

Finally, I would like to offer my special thanks to my family and my wife for their unyielding patience and endless support throughout my life.

TABLE OF CONTENTS

LIST OF TABLES

TABLES

LIST OF FIGURES

FIGURES

LIST OF SYMBOLS AND ABBREVIATIONS

SYMBOLS

a :Depth of Equivalent Rectangular Stress Block

Ac: Cross Sectional Area of Concrete (mm^2)

Al: Aluminum

A_s : Total Area of Not pre-stressed Tension Reinforcement

$A_{S\rho}$:Total Area of the Pre-stressing Strands

b :Width of Compression Face of Member

b_w: Width of Beam (cm)

CR: Creep Loss

C: Carbon

Ca: Calcium

d: Distance from Extreme Compression Fiber to Centroid of Tension Reinforcement

d_b: Diameter of Reinforcement

DL: Dead Load

e: Eccentricity

Ec: Elastic Modulus of Concrete (MPa)

E_{c28}: Modulus of Elasticity of 28 Days Old Concrete

Ep_v: Vertical Soil Load on Conduit

Epha: Horizontal Soil Load on Conduit

Es: Elastic Modulus of Steel (MPa)

ES: Elastic Shortening Loss

fc: Concrete Strength (MPa)

f_c^T: Concrete Compressive Strength at Temperature T (MPa)

f_c' : Specified Compressive Strength of Concrete (MPa)

f_{pk}: Rupture Characteristics of Pre-stressing Strands

fy: Specified Yield Stress of Not pre-stressed Reinforcement (MPa)

f_y^T: Yield Strength of Steel Reinforcement at Temperature T (MPa)

Fe: Iron

h :Height of Unit

j: Lever arm

K: Calculation Coefficient

K_a: Active Earth Pressure

l_e: The Equivalent Thickness of the Member

L: Span Length

M: Moment

Mg: Magnesium

Mn: Nominal Moment Strength at Section

N: Axial Load

O: Oxygen

P: Force

RE: Strand Relaxation Loss

SH: Shrinkage Coefficient

Si: Silicon

SW: Self Weight

T: Temperature (^{o}C)

u: Concrete Cover Over Main Reinforcing Bar or Average Effective Cover

$u^{'}$: Perimeter in Contact with Environment

W: Dead Load

w: Applied Load (Dead + Live)

$\gamma_{concrete}$: Self Weight of Concrete(t/m^3)

γ_{soil}: Self Weight of Soil (t/m^3)

ρ: Calculation Coefficient

σ_{DL}: Stress Due to Dead Load

σ_{p}: Stress Due to Axial Loading

σ_{co}: Stress in Concrete under Sustained Loading

σ_{pe}: Stress Due to Eccentricity

$\phi_{f1}, \phi_{f1}, \beta_d, \beta_f, Ø_{ce}$: Creep Coefficient

$\varepsilon_{s1}, \varepsilon_{s2}, \beta s$: Shrinkage Coefficient

ABBREVIATIONS

ACI: American Concrete Institute

ASTM: American Society for Testing and Materials

CEN: Comite Europeen de Normalization

C-H: Calcium Hydroxide

C-S-H: Calcium Silicate Hydrate

METU: Middle East Technical University

MW: Mega Watt

NFPA: National Fire Protection Association

PC: Portland Cement

RWS: Rijkswaterstaat Hydrocarbon Curve

CHAPTER 1

INTRODUCTION

1.1 General View

The “TUNNEL” between Karaköy and Beyoğlu designed and constructed by a French engineer, Henry Gavand in 1875, is one of the first underground rail transportation systems in the world, and after 100 years the implementation of transit rail systems in our country gained popularity. The municipalities in cities like Istanbul, Ankara, İzmir, Bursa, Konya, Eskişehir and Antalya are now operating various types of mass transportation facilities (heavy and light rail transportation, modern trams and street-cars). Other cities like Adana, Kayseri, Gaziantep, Denizli and Samsun are planning to solve their traffic problems by providing rail transportation systems. The capacities of the operating systems in İstanbul, Ankara, İzmir, Bursa, Konya and Antalya have already reached their limits and extension projects and planning of new lines are underway.

Highways and railroads are aiming to carry person and freight in the shortest time and by the safest way. The recent developments in vehicle and road systems are not sufficient alone for the required and approached safety. The motorways and railways together with their sub and super structures and related infrastructural elements such as crossings, bridges, tunnels and other similar structures gain importance in the operational systems of mass transportation.

In the underground structures like highway and rail tunnels the restrictions due to physical and environmental conditions are relatively high and therefore the issue of safety becomes one of the most important topics. As per the reports of the Turkish highway authority, following the completion of ongoing tunnel constructions and planned projects, Turkey will become the third nation in Europe with regard to the length of the tunnel network [1]. In addition to the projects tendered out by the highway authority, the municipalities are investing in big urban transportation projects where the portions of tunnels are not negligible.

The demand for provision of mass transportation systems in cities increased the problem of finding free land and corridors for the operation of such systems. It is almost no more possible to operate systems at grade in city centers and close environment due to already congested traffic passenger accumulation. Operating the system underground is closely related with tunnel depth, access to and from stations, high construction and operating costs and therefore has to be optimized. The result of such an optimization is to construct tunnels using cut and cover construction method by leaving sufficient space above the deck slab for utilizes such as gas, water, sewerage, pipe work, power and telecommunication cables. The backfill on top of tunnel slab has no bearing capacity; it is only a load on the tunnel. This requires the tunnel slab to be designed and constructed in such a quality and safety that it does not collapse and causes severe damage.

Practical ways of assessment of backfill, traffic and load from other structures is developed over the years. Together with the self weight of the structure and taking into consideration all the other loads the system could be modeled and designed.

1.2 Objective

Over the years many tunnel fires developed resulting in economic loss, structural degradations and human loss (See Appendix A). The first priority in a tunnel fire is to provide life safety through rescue operations. Therefore, with in the early hours of fire the structural system shall not loose its stability.

The engineers and tunnel operators are more concerned in the behavior of reinforced concrete elements being exposed to fire which is regarded as a critical safety problem. The tunnel has to provide its stability even after having faced to high temperatures for a long period of time. In previous experimental researches, TBM tunnel structural fire performance is investigated. Experimental fire research on cut and cover tunnel is limited. However sagging of cut and cover tunnel roof is possible during the fires. The objective of this study is to evaluate the structural post-fire performance of sample cut and cover tunnel roof segments at positive moment region without using a protection. Degradation of the material is also studied in this research.

1.3 Scope

In this master thesis, eight concrete segments grouped in four different pairs are casted using the mix-design adapted for bored and cut-and-cover tunnels of the Marmaray project in Istanbul. One segment from each pair are tested in a furnace to evaluate the conditions of a concrete member being exposed to high temperatures; to determine the amount of decrease in strength of steel and concrete, and to observe the phenomena of surface damage like cracking, spalling, and rupture. All segments are simply-supported during the static load test following the furnace tests. Compressive strength of concrete, tensile strength of reinforcing bars, electron microscope evaluation of concrete, moisture content of concrete are recorded during the test program. A finite element based solution is developed to simulate the results of static load tests.

CHAPTER 2

LITERATURE REVIEW

Tunnels planned and built today are getting longer and more complex, and there is a growing need for refurbishing existing tunnels. Serious accidents happened in tunnels caused damage to persons and property (Appendix A). These accidents enforced the tunnel authorities and operators to focus more on provision of safety in tunnels. [6]

A decisive criterion against which, tunnel safety is measured, is the scenario of an accident involving a fire. Due to limitations of a tunnel, tunnel fires make escape, rescue and repair measures rather difficult, and are regarded to be the greatest risk to people, vehicles and the tunnel structure itself. Safe escape routes, fire load containment along escape and rescue routes, and the integrity of electrical systems are basic elements of safety concepts of underground transport systems [6]. Other aspects have been gaining significance, namely the prevention of spalling in structural concrete, which results from quickly rising temperatures and extreme heat radiation, and the installation of efficient smoke extraction systems.

If a fire occurs in a tunnel, the unprotected structural concrete is exposed to rapidly rising temperatures and considerable heat radiation [6]. This weakens the load bearing capacity and stability of the structure, and exposes tunnel users and rescue teams to additional risks. Once the concrete has started to spall, the heat can penetrate deep into the material and change the structural reinforcement, further reducing its strength and favoring the development of hairline cracks [6].

Fire developments in the underground train carriages, on the passenger platforms, escalators and railway have the following critical security features:

- Limited space and a great number of people which result difficulties for passenger evacuation.
- A lot of up to 10kV live power cables in the underground tunnels.
- A lot of live electric wiring in the carriages.
- A high rate of air exchange causing a high rate of temperature growth up to the values of a thousand and more degrees; actually in 3-5 minutes after the fire start the situation for the people in the tunnel becomes hazardous, herewith it is necessary to evacuate a few hundred people, when the fire develops.
- Fast smoke spreading over the escape ways.
- Possible panic rise among the passengers. [9]

2.1 Concrete Spalling

Concrete is generally considered to be a fire-resistant construction material, since it offers adequate heat insulation properties and is non-combustible.

Spalling of concrete is the separation of pieces of concrete from the main body during fire. A generally accepted division of spalling into three types is the following.

First one is general or destructive spalling. This violent type of spalling is progressive in time and may lead to extensive damage.

The second type is local spalling, and consists of three subtypes: surface spalling (local removal of surface material due to moisture), aggregate splitting (due to physical changes in crystalline structure) and corner separation (due to tensile stress). [17]

The third type, explosive spalling of concrete (Sloughing off type) is a thermo-hydraulic process which is based on the following mechanisms [Figure 2.1]. In a fire, water that physically and chemically inside the concrete is released due to the quickly rising temperatures. As the water changes to the gaseous state, its volume increases by a factor of 1,100. As a result of pressure compensation in near-surface concrete layers, the concrete dries in this region, whereas condensation produces zones that are almost completely water-saturated in deeper regions of the concrete. As the ambient temperatures continue to rise, the concrete has to sustain very high steam pressure on the inside [6]. Once the tensile strength of the concrete is exceeded, the material reacts with explosive spalling, a behavior which becomes more marked with increasing strength of the structural concrete: the pore volume in high-strength concrete is reduced, lowering its permeability. Explosive spalling relationship of moisture content and pressure is shown in Figure 2.2.

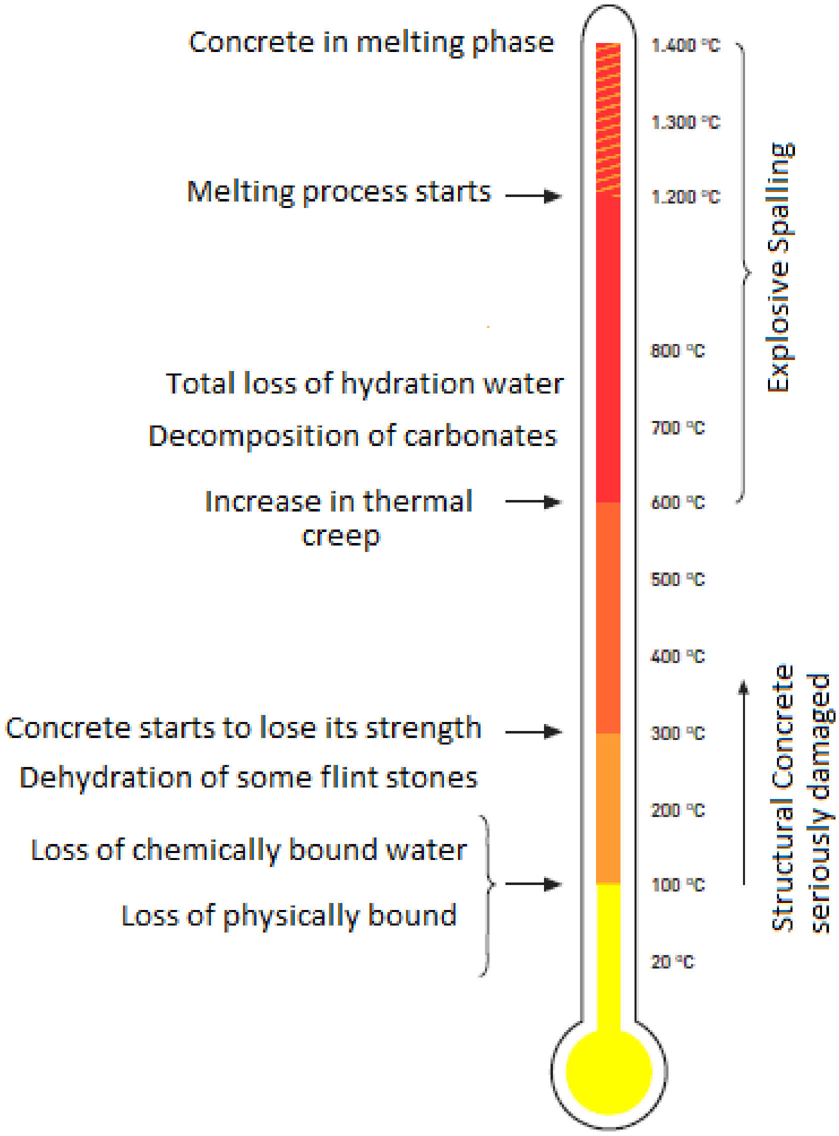

Figure 2.1 Behavior of Concrete under Temperature Effect [6]

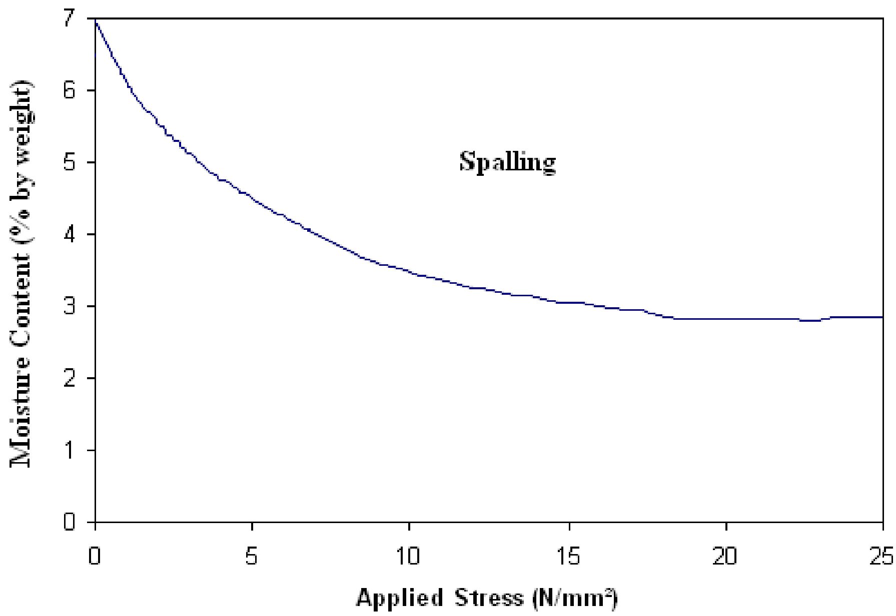

Figure 2.2 Explosive Spalling Relationship of Moisture Content and Pressure [18]

2.2 Fire Curves

Measured temperatures during major fires are given in Table 2.1. It has been observed that the maximum recorded temperature is around 1100 °C.

Table 2.1 Some Major Tunnel Fires [20]

Incident	Concrete Strength (MPa)	Maximum Temperature (°C)	Fire Duration (h)	Length Affected	Segment Depth Affected
Great Belt (1994)	28 days strength: 76	800-1000	7	16 segment rings (1.65 m long)	Peak of spalling: 270 mm
Channel (1996)	110	1100	9	500 m with 50 m severely effected by spalling	Up to 100% (400 mm) of thickness spalled
Mont Blanc (1999)	Not reported	1000	50	900 m tunnel crown most effected	Serious structural damage

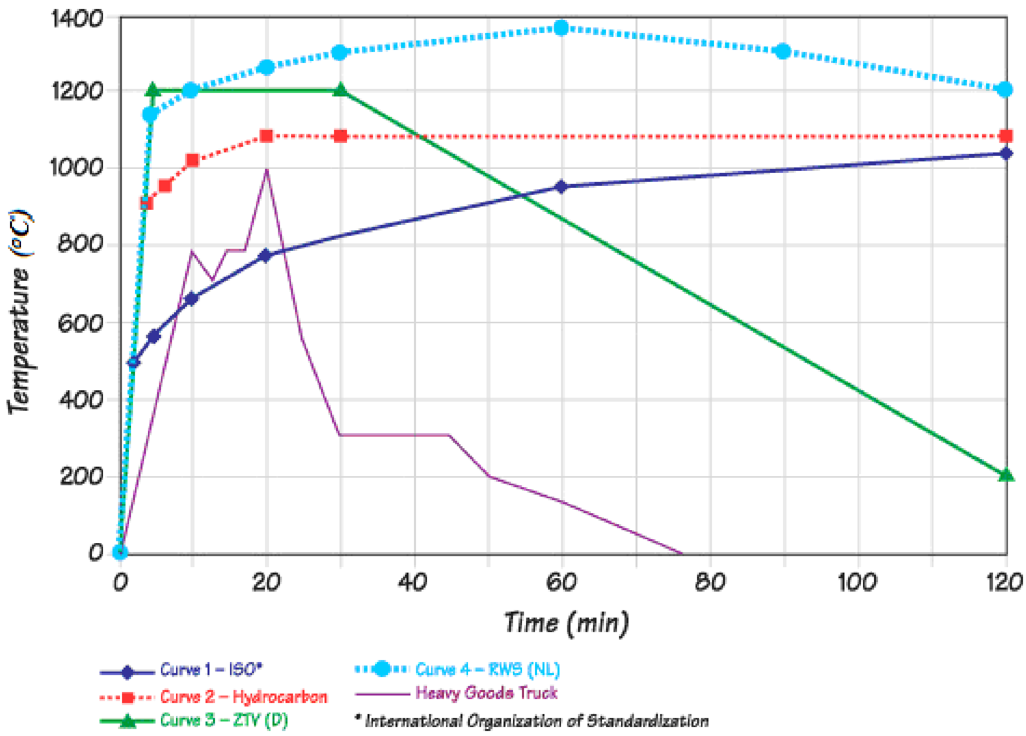

Figure 2.3 Fire-Air Temperature Curves for Tunnels [8]

To model various types of fires that would result in different combustion rates, duration and peak temperature, fire curves are developed [Figure 2.3]. The most common types of these curves are as follows:

- Curve 1: Cellulosic curve that is based on the burning rate of materials found in general building materials and contents.
- Curve 2: Hydrocarbon curve that applies to cases where small petroleum fires might occur.
- Curve 3: RABT curve represents a case in which temperatures rapidly raise to 1200°C in 5 min.
- Curve 4: It simulates burning of a petroleum tanker with a fire load 300 MW.

2.3 Fire Tests and Analytical Evaluations

Tests are carried out on samples to verify the theoretical assessments and evaluation of structures exposed to fire. These tests could be categorized as:

Stressed test

The result of the stressed test are most suitable for representing fire performance of concrete in a column or in the compression zone of a beam, because in this test, a preload, often in the range of 20-40% of the ultimate compressive strength at room temperature, is applied to the concrete specimen prior to heating and sustained during the heating period. Heat is applied at a constant rate until a target temperature is reached and maintained until thermal steady state is achieved. Load or strain is then increased at a prescribed rate until the specimen fails [7].

Unstressed test

The results of the unstressed test are most suitable for representing fire performance of concrete in tension zone of a beam or concrete in an element that has small compressive load, because in this test, the specimen is heated, without preload, at a constant rate to the target temperature and maintained until a thermal steady state is achieved. Load or strain is then applied at a prescribed rate until failure occurs [7].

Unstressed residual-strength

The results of the unstressed residual-strength test are suitable for use in assessing post-fire properties of concrete, because in this test the specimen is heated without preload at a prescribed rate to the target temperature and maintained until a thermal steady state is achieved. The specimen is then allowed to cool, also following a prescribed rate, to room temperature. Load or strain is applied at room temperature until the specimen fails [7].

<u>METU Research</u>

Civil Engineering Department of METU has contributed a lot with theoretical and in-field research projects to the safety in highway and rail tunnels. The Department is specifically investigating theoretically and analytically the behavior of tunnel linings opposed to high temperatures in case of a fire and also carrying out small scale tests to verify the theoretical approach and the analytical analysis. ”Structural Fire Safety of Circular Concrete Tunnel Linings” [15], “Structural Fire Performance of Concrete and Shotcrete Tunnel Liners” [8] and “Structural Fire Safety of Standard Circular Railroad Tunnels Under Different Soil Conditions” [4] are specific references for such contribution.

In the study of Caner A., Zlatanic S. and Munfah N. [8], an analytical method is provided for assessing the structural fire performance of concrete or the shotcrete tunnel liners, by comparing the structural demand and the capacity of the liners in the time domain. The analysis is a combination of a heat transfer analysis and a non linear structural analysis that involves such factors as type of fire [Figure 2.3], concrete mix design, temperature induced material degradation and ground tunnel linear interaction. A case study involving a tunnel section with an internal diameter of 5,900 mm is provided. As a conclusion, some key findings based on the evaluation method and case study presented as follows:

- The structural concrete can be designed to withstand fire up to a certain period of time while accepting some minor, repairable damage to the liner.
- After the fire, the concrete exposed to temperatures in excess of 300 ^{o}C should be removed. For local repairs, a similar concrete mix design should be used to ensure that the structural integrity of the affected section is similar to that of original design as well as the remainder of the tunnel. [8]

The second research of Caner A. and Böncü A. [15] which is taken as one of the references in this master thesis, focuses on structural fire safety of circular tunnel linings in terms of reduction in service load safety due to time and temperature dependent material degradation and increase in load demand in tunnel fire, and to develop recommendations for preliminary assessment of structural fire endurance of circular tunnel linings. For this purpose Hydrocarbon fire tests on TBM tunnel segments (Tunnel Boring Machine) are applied at METU Mechanical Engineering Department laboratory. Three TBM segments are tested under fire and other three are kept as control. Conclusions are as follows:

- Initial level of design loads increase spalling slightly since the temperature induced strains are much higher than initial strains induced by design loads.
- Minor repairs shall be targeted after tunnel fires instead of using fire proofing materials. [15]

2.4 Structural Fire Codes

No specific structural fire code or specification is available to be used in design of tunnel linings. The available codes are related to building type of structures. However magnitude of tunnel fires can be extremely high compared to buildings due to confined space.

- Eurocode2 – Comite Europeen de Normalisation (CEN)
- ACI-216 (Guide for Determining the Fire Endurance of Concrete Elements)
- NFPA-130 (Standard for Fixed Guideway Transit and Passenger Rail Systems)
- PIARC (World Road Association)

Rail operators and organizations are also published regulations and recommendations following their research program and investigations such as:

- European Technical Specification for Interoperability "Safety In Railway Tunnels"
- Rail Infrastructure Management Board

New codes and standards are now defining the thickness of the concrete cover to reinforcing bars in reinforced concrete design and construction as a basic protective action to prevent damage of the reinforcing bars. The codes are covering this issue as shown below:

<u>Eurocode 2</u>

According to Eurocode, there are three standard fire exposure conditions that may need to be satisfied.

R = Mechanical resistance for load bearing.

E = Integrity of separation.

I = Insulation.

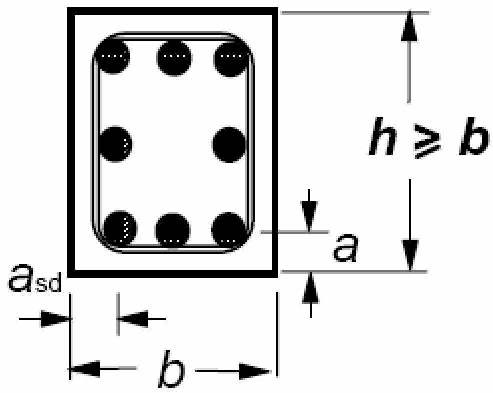

Figure 2.4 Cross-Section Properties According to Eurocode 2 [3]

Table 2.2 Concrete Cover Thicknesses According to Eurocode 2 [3]

Standard Fire Resistance		Minimum Dimension (mm)		
		One Way Slab	Two Way Slab	
			$L_y/L_x \leq 1.5$	$1.5 \leq L_y/L_x \leq 2.0$
REI 60*	h	80	80	80
	a	20	10	15
REI 90*	h	100	100	100
	a	30	15	20
REI 120*	h	120	120	120
	a	40	20	25
REI 240*	h	175	175	175
	a	65	40	50

* The number written next to the REI represents the duration of fire in minutes.

<u>ACI-216</u> (Guide for Determining the Fire Endurance of Concrete Elements)

ACI 216 suggests controlling the concrete cover for fire protection. For building type structures suggested minimum concrete cover thickness for slabs is 2 cm per ACI 216.

Fire endurance computations developed in ACI 216 is presented in below steps.

1) Determine the nominal moment strength of the beam element, M_n.

$$M_n = A_s \times f_y \times (d - \frac{a}{2}) \qquad \text{Eqn. (2.1)}$$

Where "A_s" is the tension reinforcement area, "f_y" is the yield strength of rebar without material degradation, "d" is the depth of tension reinforcement from extreme compression fiber and "a" is the effective depth of concrete compression block.

2) Determine the unfactored moment M under operating conditions.

3) Determine M/M_n ratio determined in obvious steps.

4) Determine the "w" for the section.

$$w = \frac{A_s \times f_y}{b \times d \times f_c'} \qquad \text{Eqn. (2.2)}$$

Where "b" is the width of beam and "f_c'" is the characteristic strength of concrete with no material degradation.

5) Determine the minimum required concrete cover corresponding to "w" and M/M_n ratio from Figure I.1

Turkish Standard (Regulation on protection of buildings from fire incidents)

The local fire code "regulation for protection of buildings from fire" upgraded in 2007 is an indication of understanding the risk of fire and the necessity of developing fire fighting criteria, norms and standards. Especial congested areas such as shopping malls, theatres and cinemas and commercial centers increased the demand of using fire retarding and insulating materials and products.

As a minimum protective measure it is required to provide a concrete clear cover of at least 4 cm to the steel members in a concrete cross-section (reinforcing bars or embedded steel profiles).

Others

There are also papers focused on the relationship between concrete cover and fire resistance of reinforced concrete members. One of them which also referenced in the thesis is named "Influence of Concrete Cover on Fire Resistance of Reinforced Concrete Flexural Members" [5]. The result of the test carried out by Xudong Shi; Teng-Hooi Tan; Kang-Hai Tan and Zhenhai Guo are given in the Table 2.3

Table 2.3 Concrete Cover Thicknesses by Xudong Shi; Teng-Hooi Tan; Kang-Hai Tan and Zhenhai Guo [5]

Duration of Fire Resistance (min)	Minimum Cover (mm)
30	20
60	30
90	40
120	60
180	70
360	80

2.5 Cut and Cover Tunnels

The railway tunnels constructed by applying cut-and-cover techniques have a relative shallow overburden. As the overburden is a backfill character and has no self carrying capacity in case of failure in the tunnel top slab, the top slab should be designed providing stability under the worst loading conditions.

Due to growing population and dense accumulation of people in cities, the public transportation is gaining popularity and the demand for reliable, safe and fast operation systems increase. As land in cities is also getting valuable and rare, it is not always possible to run the rail transportation system at grade [10]. Further to the congested urban conditions, the risk giving of damage to neighboring facilities increases where the tunnels are drilled at deeper levels which also bring additional construction, operation and maintenance costs. It is the task of the engineer to find the optimum solutions for relative easy and fast construction, minimize risk of giving damage to neighboring facilities but also to enable certain utilities to be placed above the tunnel deck [10].

Cut-and-cover is a simple method of construction for shallow tunnels. Two basic forms of cut-and-cover tunneling are available:

- *Bottom-up method*: A trench is excavated, with ground support as necessary, and the tunnel is constructed in it. The trench is then carefully back-filled and the surface is reinstated [12].
- *Top-down method*: Here side support walls and capping beams are constructed from ground level by such methods as slurry walling, or contiguous bored piling. Then a shallow excavation allows making the tunnel roof of precast beams or in situ concrete. The surface is then reinstated except for access openings. This allows early reinstatement of roadways, services and other surface features [12].

Another important issue is the sagging of cut and cover tunnel roof at mid-span, where is the most critical region, under extreme temperature effect [Figure 2.5]. Cut and cover tunnels are generally constructed more porous concrete mixes and the steel reinforcement in the mix is required to prevent sagging of the ceiling. The greater levels of porosity and the lower strength of the concrete, mean that explosive spalling of the concrete is not necessarily the main failure mechanism of these tunnels under fire conditions. If the sagging in the reinforcement of the roof is not prevented, this would lead to a leakage and possibly collapse of the tunnel ceiling. [19]

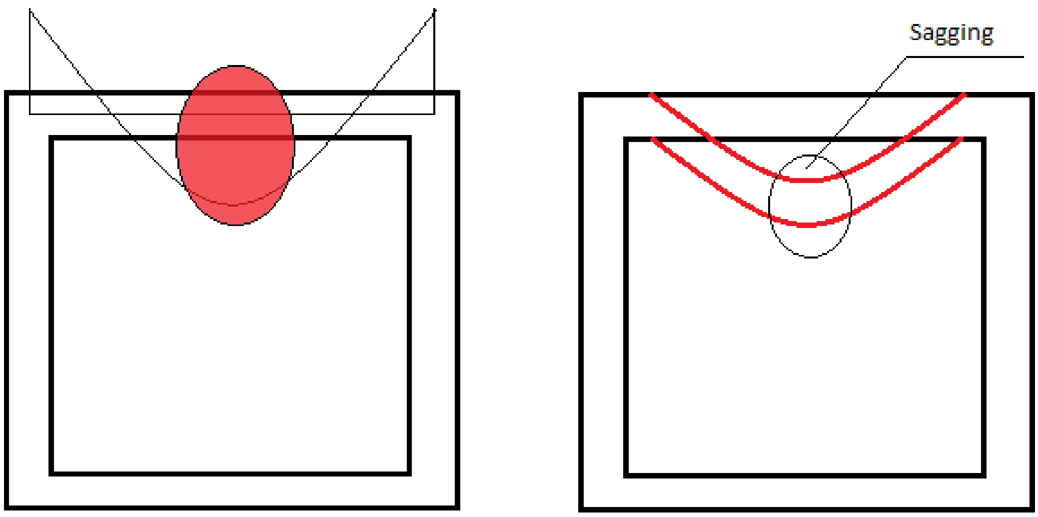

Figure 2.5 Sagging of Cut and Cover Tunnel Roof

CHAPTER 3

TEST DESCRIPTION

3.1 Introduction

In the scope of the test program a variety of tests have been conducted to evaluate the fire endurance of burnt specimens and to compare the structural performance of burnt and unburnt specimens. These tests are:

- Fire Tests (Furnace)
- Static Load Tests of Specimens
- Core Sampling
- Cube, Cylinder Crashing Tests
- Tensile Test for Reinforcement Bars
- Electron Microscope
- Moisture Content Evaluation

Test segments and conditions used in this research are a close simulation of the real life conditions. Test segment design represents the design of positive moment region of a cut and cover tunnel roof.

3.2 Cut and Cover Tunnel Design

In a typical cut and cover tunnel design, a 2-D structural model is constructed for analysis. Generally a 1 meter strip of tunnel in longitudinal direction is analyzed under acting loads for this particular strip (Appendix B). Cross-section properties and design loads are taken from existing tunnel designs of Yedikule-Kazlıçeşme metro line, Adana and Bursa light rail train tunnels (Figure 3.1).

Boundary conditions (soil springs) representing ground interaction is typically computed from subgrade reaction modulus. In this study, the soil type above the tunnel cross-section is sandy gravel (Taken form tunnel line design of Yedikule-Kazlıçeşme) and for this type of soil a typical subgrade reaction modulus of 2000 t/m^3 is used.

Tunnel Cross-section

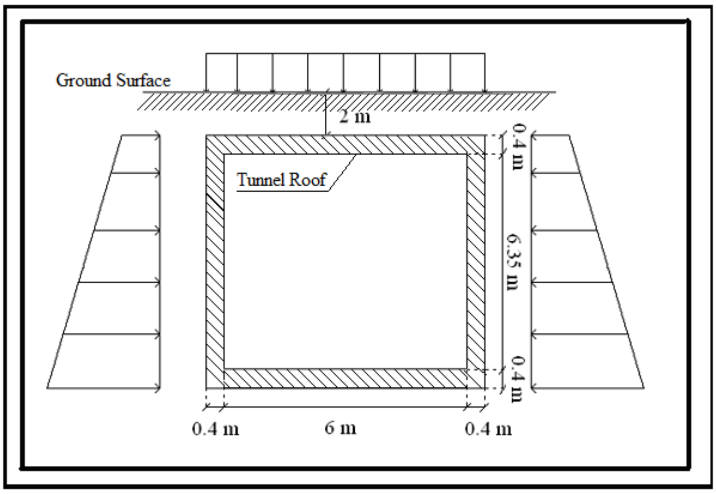

Figure 3.1 Tunnel Cross-Section and Loads

Structural Analysis and Design Loads

The structural analysis of the tunnel cross-sections are carried out by using a commercial program SAP 2000. The load acting on the concrete element is modeled as a self weight [Figure 3.2] of the concrete member, 2 meter high backfill [Figure 3.3] and the horizontal earth pressure on the tunnel walls [Figure 3.4]. As fire is considered as an unusual and rare load condition, all load factors in a fire load combination are taken as 1.0 (ACI 216). The same material properties used in existing tunnels are selected in design as:

Concrete Class: C40 (40 MPa)

Steel Class: S420 (420 MPa)

1) <u>Self Weight of Tunnel (SW)</u>

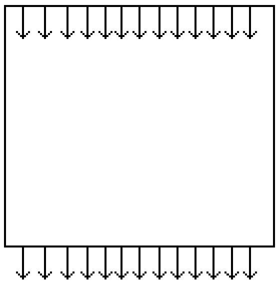

Figure 3.2 Self Weight Load on Tunnel

Self weight of the structure is calculated by activating the gravitational option in the program. The unit weight $\gamma_{concrete}$ is taken as 24 kN/m^3.

2) <u>Overburden (E_{pv})</u>

Overburden pressure can be computed from:

$$q_1 = h_1 \times \gamma_{soil} \qquad \text{Eqn. (3.1)}$$

Where "h_1" is the overburden thickness (2 m in this case) and "γ_{soil}" is the unit weight of soil (γ_{soil}=19 kN/m^3).

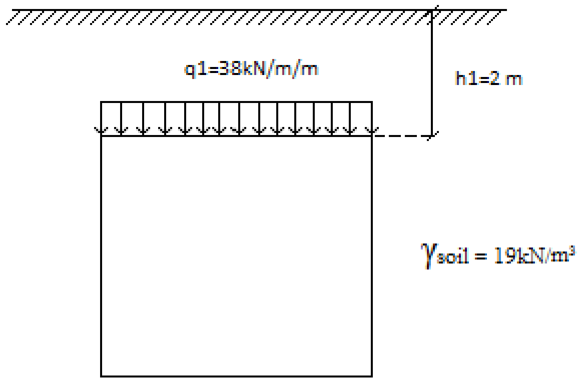

Figure 3.3 Overburden Soil Load on Tunnel

3) Lateral Pressure (E_{pha})

Active earth pressure can be determined from the following equations:

$$q_i = \gamma \times K_a \times h_i \qquad \text{Eqn. (3.2)}$$

Where "q_i" is the computed earth pressure at soil. Depth of "h_i" and "K_a" is the active earth pressure coefficient. K_a can be determined from:

$$K_a = \frac{1 - Sin\phi}{1 + Sin\phi} \qquad \text{Eqn. (3.3)}$$

Where "ϕ" is the shear strength parameter. "ϕ" is taken as 30°, since the soil type above the tunnel is sandy-gravel in our case. (Tunnel line of Yedikule-Kazlıçeşme)

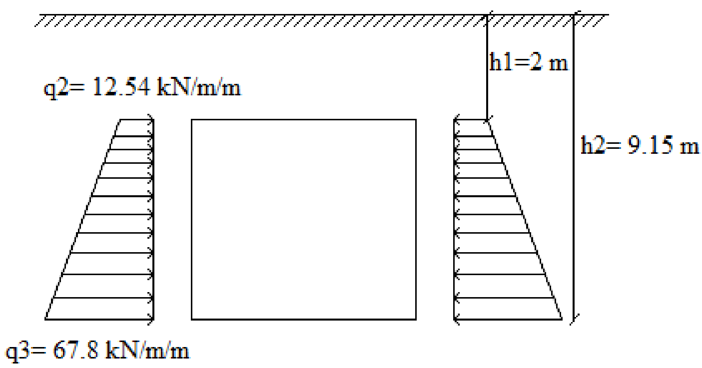

Figure 3.4 Horizontal Soil Load on Tunnel

3.3 Test Specimens

Design of specimens (segments) can be found in Appendix C.
The dimensions of the segments are chosen based on restriction induced by size of the test furnace [Figure 3.5].

The reinforcement design for test specimens is carried out for the positive moment region (mid-span) of the tunnel roof slab. The reinforcing configuration is as shown below, 4 specimens are reinforced with 5Ø12, the other four with 5Ø14 and the concrete cover is decided as 6 cm (from center of the tensile reinforcement) [Figure 3.5]. The 6 cm concrete cover is a standard concrete cover for cut and cover tunnels.

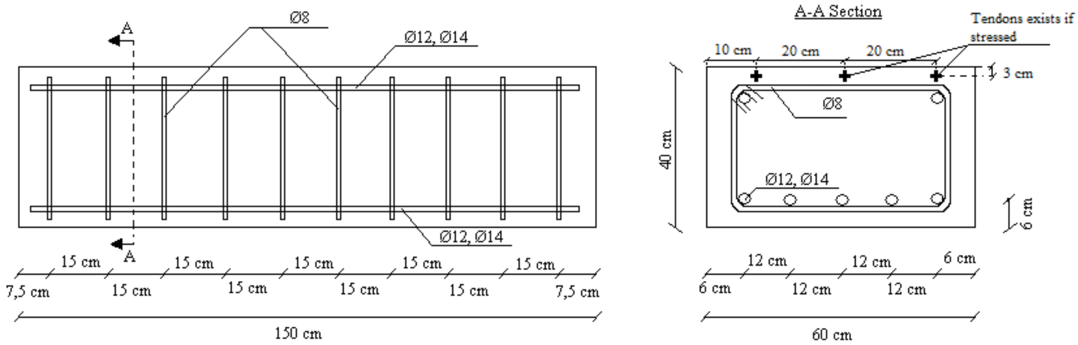

Figure 3.5 Configuration of Reinforcement

Two pairs of segments are stressed with pre-stressing tendons to simulate the internal design loads of tunnel roof. The two other pairs are unstressed as in the case of overburden is removed from tunnel roof region.
Four pairs are listed below:
Pair 1: Ø12 Unstressed
Pair 2: Ø14 Unstressed
Pair 3: Ø12 Stressed
Pair 4: Ø14 Stressed
The specimens are specified using the following formula: #L-#

First # indicates rebar size.

Ø12 rebar size $\rightarrow$ 1

Ø14 rebar size $\rightarrow$ 2

First letter indicates stressed condition.

Unstressed $\rightarrow$ A

Stressed $\rightarrow$ B

Last # indicates exposure to fire.

Exposed to Fire $\rightarrow$ -1

Not Exposed to Fire $\rightarrow$ -2

As an example: Type1A -1 indicates $\rightarrow$ rebar size Ø12, unstressed specimen, exposed to fire. The casting days and segment types are listed below.

Specimen Types:		Casting Dates:
Type 1A-1: Ø12 Unstressed		13/04/2010
Type 1A-2: Ø12 Unstressed		14/04/2010
Type 2A-1: Ø14 Unstressed		16/04/2010
Type 2A-2: Ø14 Unstressed		17/04/2010
Type 1B-1: Ø12 Stressed		20/04/2010
Type 1B-2: Ø12 Stressed		29/04/2010
Type 2B-1: Ø14 Stressed	[Figure 3.7]	30/04/2010
Type 2B-2: Ø14 Stressed		04/05/2010

Figure 3.6 Specimens that Prepared For Fire Test

The three pre-stressing tendons each has a cross-sectional area of 1.27 cm^2 are located 3 cm depth of the top of beam as shown in Figure 3.7. The jacking force of the each tendon is 135kN/cm^2. These tendons are cut at end of each beam after concrete reached the target compressive strength to initially stress the beams. These beams are manufactured in a close factory. Moist cure is used for concrete at production stage.

Prior to pouring the concrete into form work the tendons are stressed and thermocouples are placed at the selected locations.

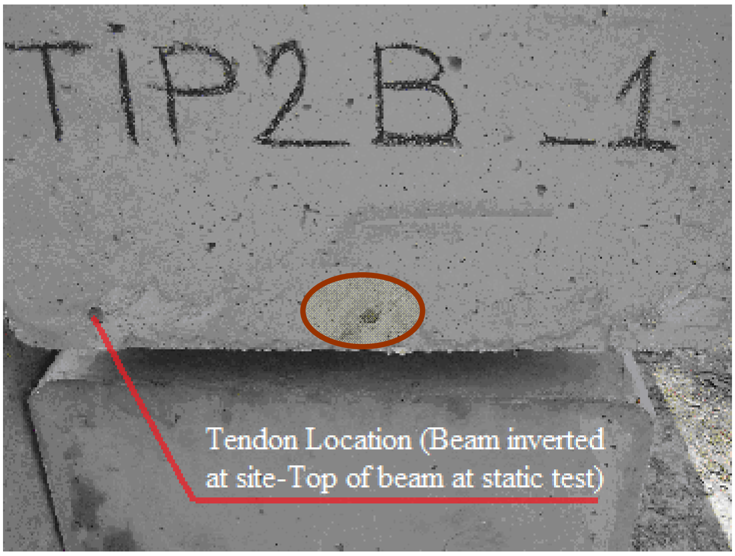

Figure 3.7 Stressed Specimens

The Marmaray Project put comprehensive emphasis in design and manufacturing of concrete. It was aimed to follow the same mix-design as implemented in Marmaray Project structures. Due to the complexity of the mix-design, specific aggregate and cement requirements, the standard mix-design is used for production of C40 concrete of the SINTA Pre-cast Concrete production company [Table 3.1].

Table 3.1 Mix Designs of Specimens

Mix-Design (kg/m^3)	
Cement	400
Water	160
Aggregate Type 1 (Sand)	783
Aggregate Type 2 (4.11,2 mm)	465
Aggregate Type 3 (11,2.22,4mm)	598
Additive	%2.0
Total	2.414

The concrete compressive strength is measured using 150x150x150 mm cubes. The factory tested compressive strength of concrete using 3 cubes at day 1 and day 7. The factory spared 3 more cubes for each segment (specimen) for future testing of concrete compression strength at fire and static test days.

3.4 Test Details

Test details for elements and materials are summarized in Table 3.2 and Table 3.3 respectively. The coding presented in the previous section is used in identification of elements.

Table 3.2 Element Test Details

Test Type	Segments			
Fire Test	Type 1A-1	Type 2A-1	Type 1B-1	Type 2B-1
Static Load Test	Type 1A-1 Type 1A-2	Type 2A-1 Type 2A-2	Type 1B-1 Type 1B-2	Type 2B-1 Type 2B-2

Table 3.3 Material Test Detail

Test Type	Segments that Specimens Gained from	Number of Specimens Gained From Segments
Core Sampling	Type 2B-2, Type 1A-1 Type 1B-1	3 from Type 1A-1, 3 from Type 1B-1
Cube Crashing	Type 1A-1, Type 1A-2, Type 2A-1, Type 2A-2, Type 1B-1, Type 1B-2, Type 2B-1, Type 2B-2	3 Cube Specimens for Each Segment
Tensile test for rebar	Type 1A-2, Type 2B-1	2 from Type 1A-2, 2 from Type 2B-1
Electron Microscope	Type 1B-1	3 specimens from depths 5, 10, 20 cm
Moisture Content	Type 2B-2, Type 1A-2 ,Type 2A-1	1 specimen from each segment

3.4.1 The Furnace, Its Components and Fire Testing

The furnace in the Fluid Mechanics Laboratory of Mechanical Engineering Department of METU is used for the fire test. The body of the furnace is of steel and is insulated with ceramic fiber and rock wool. It includes five inspection windows, two of them on the front and the others are on the side walls. The inner dimensions of the furnace are 130 cm in width, 250 cm in length and 100 cm in height [Figure 3.8]. To achieve the target fire curve adjustments are made by shifting the location of inner compartment wall. This steel wall is a rectangle shaped one with 20 mm thickness.

Figure 3.8 Furnace

1) <u>Burner</u>

As for the fire source, an Alarko Lamborghine natural gas burner is used [Figure 3.9]. A special burner operator is controlling the burner system during the fire under supervision of mechanical engineers. In case the temperature drops or rises the burner operator was adjusting the knob based on his experience. The control of inside temperature is measured through thermocouples connected to data logger.

Figure 3.9 Alarko Lamborghine Natural Gas Burner

2) Ceramic Fiber and Rock Wool

Since the furnace was damaged, it is needed to be repaired and refurbished. The inner walls of the furnace are insulated with ceramic fiber and rock wool [Figure 3.10]. By this way, the furnace was protected against the destructive effect of the fire, which reaches up to 1250 ^{o}C.

Figure 3.10 Ceramic Fiber Isolation on the Furnace Flap

3) Thermocouples

A K type thermocouple is used to collect the heat data. A K type thermocouple uses nickel-chromium and nickel-aluminum alloys to generate voltage. They are available in the -270 °C to +1370 °C range [11].

In order to measure the temperature distribution in the concrete, thermocouples were placed at 5, 10, 15 cm from top surface in the construction phase of segments. In the second test three thermocouples were placed to measure the temperature in the furnace.

4) Data Acquisition System

Data transfer and record from thermocouples to computer were done by Elimko E680 Data Logger device and software [Figure 3.11]. The change in temperature can be recorded every second and can be observed from the computer screen simultaneously with the fire test. Data logger can measure up to 30 channels and also recording the ambient temperature outside the furnace.

Figure 3.11 Data Acquisition System

5) Fire Testing

In fire tests of stressed and unstressed specimens, tension faces are allowed to touch by the flames of the burner. The flame temperature is targeted to be close to a fire temperature that can be generated by a 2 hour "Hydrocarbon" fire as shown in Figure 2.3. The industry standard for such design fire duration is typically around 2 hours. The main reason for such a short duration is the life safety. The structure has to maintain its integrity during initial hours of fire to allow rescue operations.

Two specimens are placed side by side as shown in Figure 3.12. The ceramic fiber and rock wool is used to insulate the specimens from each other and from walls of furnace. The results are presented in the next chapter.

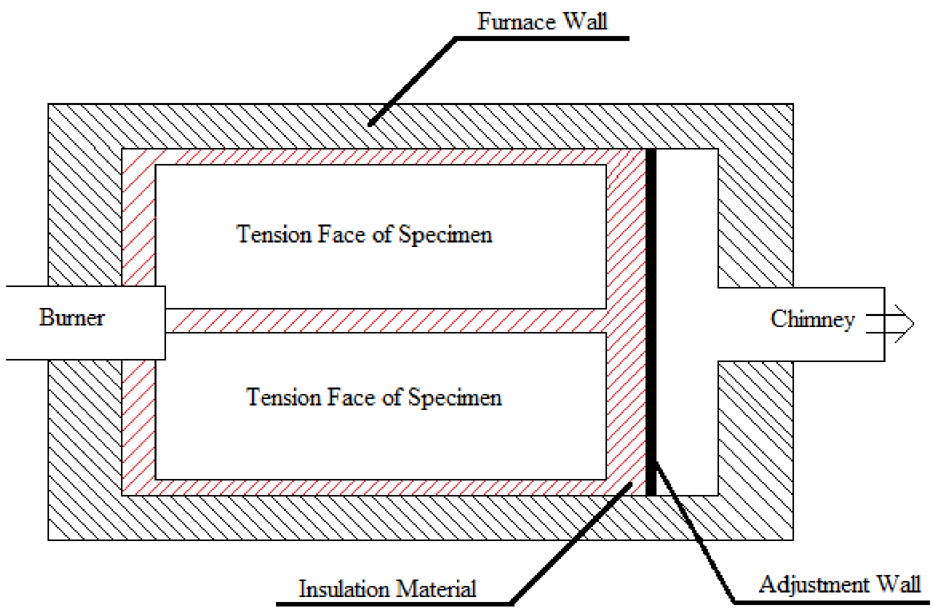

Figure 3.12 Plan View of Inside of Furnace

3.4.2 Static Load Set-up

To evaluate the structural performance of the specimens they are loaded by a point static load at mid-span. The specimens are simply supported on the test apparatus and loads are measured with a load cell. Displacement transducers are placed to measure the displacements, three at the center; two at the supports [Figure 3.13, Figure 3.14, and Figure 3.15].

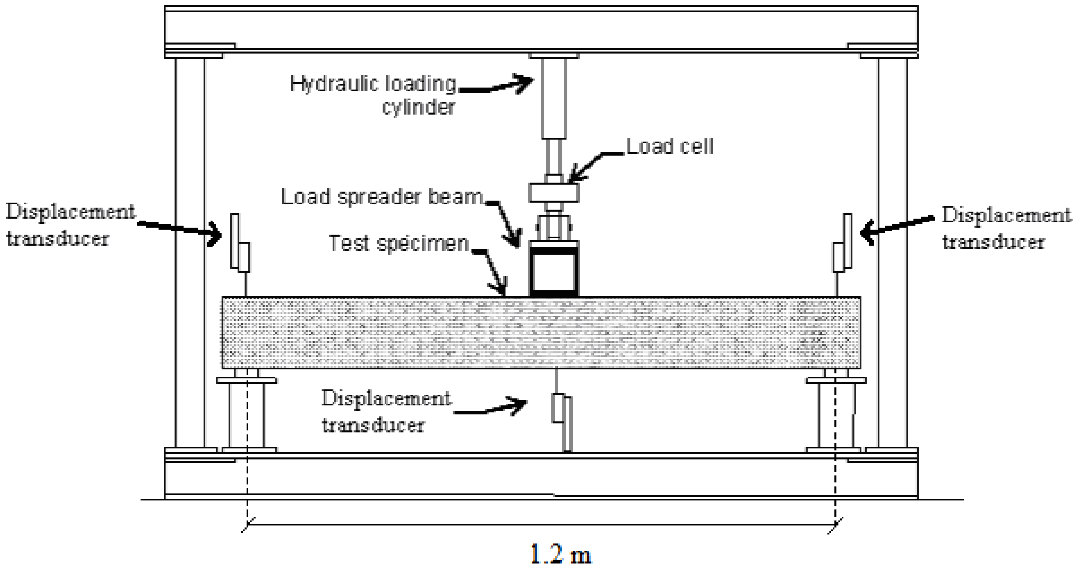

Figure 3.13 Static Load Set-up -1

Prior to tests, the load cells and displacement transducers are calibrated. The loading frame has a 500 kN loading capacity. Special short support columns are provided to support the beams. On top of each column a steel support of a hinge or a roller is used. The beams are not physically connected to the supports but they are in contact with steel supports by gravitational forces. The tests have been continuously monitored. The pressure to the hydraulic cylinder is applied through a hand type pump. The speed of loading is manually increased. At every increments of 100 kN the test has been stopped to observe the structural changes in the system.

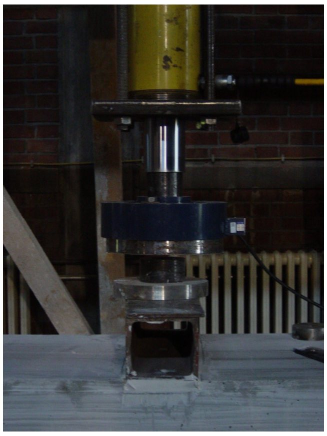

Figure 3.14 Load Cell

Figure 3.15 Static Load Set-up -2

3.4.3 Material Tests

Five different material tests have been utilized in this research. The cylindrical cores taken from the burnt and unburnt specimens and factory manufactured cubes are tested for compression under uniaxial test machine [Figure 3.16]. These tests are used to compare the compression strength of burnt and unburnt concrete. The cube test results are converted to cylindrical specimen results by a multiplier of 0.9 suggested by Ersoy U. [13]

Figure 3.16 Compression Test Samples

Following the fire tests, tensile reinforcement are taken out from the burnt and unburnt specimens by crushing the concrete using a hand held electrical concrete breaker. After the reinforcement bars are exposed, the bars are saw cut to a minimum length of 30 cm (To fit the tension testing machine). The sample bars are tested under tensile force to measure the tensile strength of reinforcement bars.

Electron microscopes can reveal the micro structure of many different types of materials and are widely used by scientists and industrialists working in materials, biology, geology, physics, and chemistry. The Scanning Electron Microscope (SEM) is mainly used to reveal surface topography at magnifications ranging from 10x to 50000x [Figure 3.17].

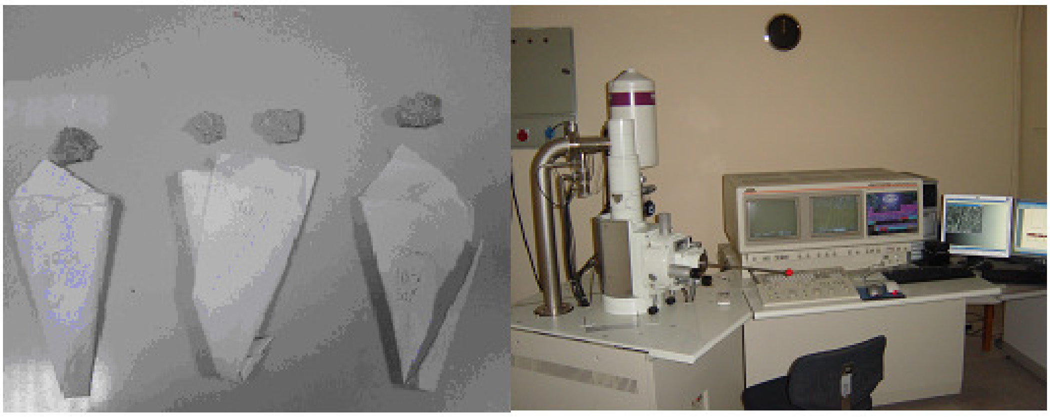

Figure 3.17 Electron Microscope

The chemical composition and crack patterns within the different depth of concrete can be evaluated using electron microscope results. Electron microscope samples are obtained from cores by experienced academicians [Figure 3.18]. If the electron microscope samples are taken from saw cut faces, samples become useless. Prior to the microscope observation the samples are gold plated for visual clearance. The samples are selected to contain cement and aggregate to observe the bonding detail between cement and aggregate.

Figure 3.18 Core Specimen

Samples are taken at 5, 10, 20 cm depths from the cored sample taken from the left side of the specimen type 1B-1 [Figure 3.17]. No internal cracking is visible on the face of cores.

METU Metallurgical Department's electron microscope is used for this purpose under supervision of an expert eye.

Moisture content, a measure of explosive spalling of concrete, need to be determined prior to fire testing. METU Civil Engineering Material Department provided testing equipments for these tests.

CHAPTER 4

RESULTS

4.1 Furnace Test Results

4.1.1 First Set

In the first set of the furnace fire tests, two segments called Type 2A-1 and Type 1B-1 are tested side by side simultaneously. Thermocouples are embedded in the Type 1B-1 segment at a depth of 5 cm, 10 cm, and 15 cm from hot surface. Two other thermocouples are placed on top of insulation (one close to center of furnace about 70 cm away from burner and one close to edge) to monitor the in-furnace temperature during the fire test [Figure 4.1]. The test took 2 hours as planned. A video of test is recorded at the start of the test. The top surface of concrete was about 20 cm lower than bottom face of burner allowing flame touch to top surface.

Figure 4.1 Inside of the Furnace and Thermocouple Placements

A concrete test cube is also placed next to segments in the furnace without any insulation i.e. all five faces are exposed to extreme temperature effect [Figure 4.2]. The cube is placed close to edge line away from the burner and observation glasses for protection purposes.

Figure 4.2 Placement of the Cube Specimen into Furnace

4.1.1.1 Recorded Furnace Internal Temperatures

At the first 10 to 20 minutes of the test, very minor explosive spalling is observed. The flying pieces settled on the surface of segments, insulation and thermocouples. The thermocouple located along the center line of furnace has more accumulation of ash and dust and had a lower reading of temperature in this period of time between 9:50 and 10:20 am.

The maximum recorded temperature from internal center thermocouples was around 1104 ^{o}C [Figure 4.3]. The direct flame temperature expected to be around 1250 ^{o}C is not able to be measured due to accumulation of dust. The maximum measured temperature of 1104 ^{o}C is a little bit above the hydrocarbon fire maximum temperature. The maximum temperature reading on edge line thermocouple was 1136 ^{o}C due to less accumulation of dust. On average the recorded thermocouple readings was 1120 ^{o}C and was about 1.8% more then the maximum temperature that recorded for a hydrocarbon fire.

ASTM E 119 fire test standards state that the furnace temperature-time curve can be used to determine the accuracy of furnace control by integrating the area under the fire temperature-time graph. The area underneath a hydrocarbon fire curve is around 128410 ^{o}C-min. The average recorded area under fire curves is around 120928 ^{o}C-min [Figure 4.3] and is about 6% less the hydrocarbon fire which is a representative curve. ASTM E 119 stated that if the difference in areas for 2 hours tests is less then 7.5%, the test control is achieved successfully [21]. The accumulation of dust preventing direct touch of flame to top undamaged surface is observed to have no disadvantage in terms of maintaining desired furnace temperature on surface of concrete.

Recorded temperature-time diagram is shown in Figure 4.3.

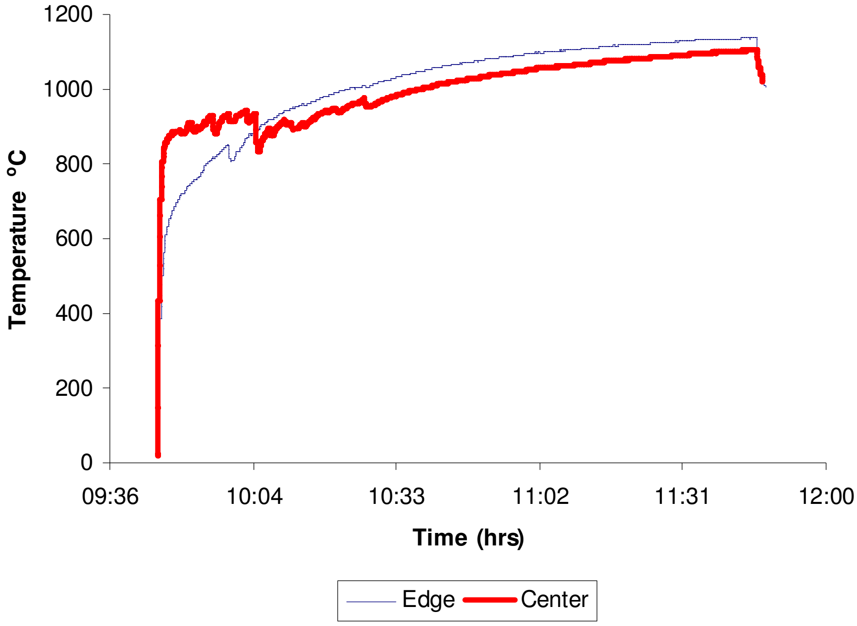

Figure 4.3 Temperature Data Gained from First Fire Test

4.1.1.2 Temperature Distribution in the Depth of Specimen

The results of thermocouple readings at depth of specimen presented below:

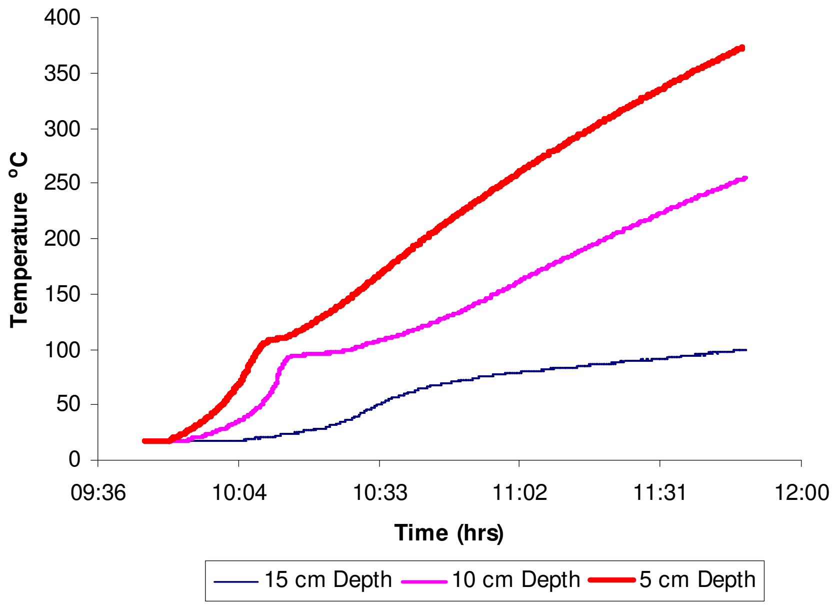

Figure 4.4 Temperature Distributions in the Specimen Measured from Hot Surface

After 2 hours, the maximum temperature measured at 5 cm depth is observed to be 377^{o}C. For the 10 cm depth, the maximum temperature measured is 255^{o}C, and for 15 cm depth the maximum measurement show 100^{o}C [Figure 4.4]. These results verify that the concrete has a low thermal conductivity. Concrete cover can be used as a passive fire protection. It is known from previous applications that concrete surface has to be replaced after exposed to a temperature in excess of 300^{o}C [4]. The concrete exposed 300 ^{o}C can loss 60% of its compression strength and exposed to 380 ^{o}C can loss about 50% of its compressive strength.

4.1.1.3 Post-fire Observations

The specimens are kept one more day in the furnace to cool down. A day after the furnace test, specimens are taken out and visual observations are done. It is observed that there is a 3-4 cm thickness of dust on segments and the concrete spalling is around 4-5 cm. The maximum depth of spalling found to be at mid-length of the segments where flames indirectly touched. It shall be also noted that most of the reflection of heat develops at the mid region of segments due to confined space of furnace insulated with white color material that increases radiation effects in the furnace. Reinforcement of specimens having a concrete cover of 6 cm's was not visible after fire tests [Figure 4.5 and Figure 4.6].

Figure 4.5 Concrete Face After Fire Test (Type 1B-1)

Figure 4.6 Concrete Face After Fire Test (Type 2A-1)

4.1.2 Second Set

After cleaning inside of the furnace and repairing insulation, second set of furnace fire test is carried out. In second test Type 1A-1 and Type 2B-1 segments are tested in the furnace. Two thermocouples are placed at similar spots as in the first set of test in furnace and test duration is again 2 hours. One other thermocouple is located on the fire flame path.

After having seen the problem of ash and dust covering the thermocouples placed too close to surface, thermocouples are placed at a higher position in the second test not to be affected from accumulation of dust and ash.

4.1.2.1 Recorded Furnace Internal Temperatures

In-furnace and flame temperature readings are shown below:

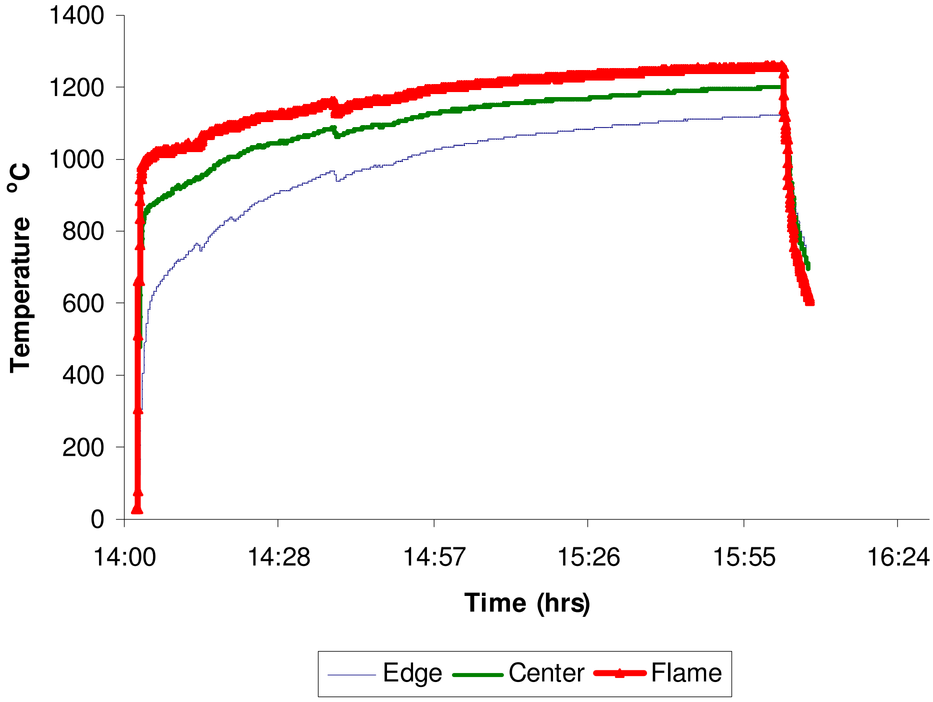

Figure 4.7 Temperature Data Gained from Second Fire Test

At the edge of the furnace maximum temperature of 1122°C is measured on surface of concrete. This value is lower than the temperatures measured in the other ones due to its location being too close to the insulated walls and away from flame.

The maximum temperature at mid-point is measured as 1201°C on surface of concrete, the maximum temperature measured at the thermocouple directly facing the flame is read as 1259°C [Figure 4.7]. These maximum temperatures are higher then hydrocarbon fire temperatures.

4.1.2.2 Post-fire Observations

The average area under fire curves is around 125026 °C-min and is about 2.6% less then hydrocarbon fire curve area. The flame temperature-time curve has about 9.8%

higher area then hydrocarbon fire curve area. The second set of test is found to be satisfactory when compared to threshold limit of 7.5% deviation [21]. Both tests are almost identical to each other in terms of temperature control. It is believed that the damage during a real tunnel fire will be less since the volume of heat sink will be larger compared to the very confined test condition in this research.

Figure 4.8 Concrete Face After Fire Test (Type 1A-1)

In the second fire test depth of spalling measured from the concrete surface is around 5-6 cm. Concrete cover reduces to 1-2 cm after exposing to fire. It is observed on segment Type 2B-1 the concrete cover of the reinforcing bars are heavily damaged locally and one of the bars became visible for 10 cm length [Figure 4.8 and Figure 4.9]. It is believed that if the fire continues and if flame directly touches these steel bars, reinforcement can melt and loose its strength.

Figure 4.9 Concrete Faces after Fire Test (Type 2B-1)

4.1.3 Observations after Fire Test

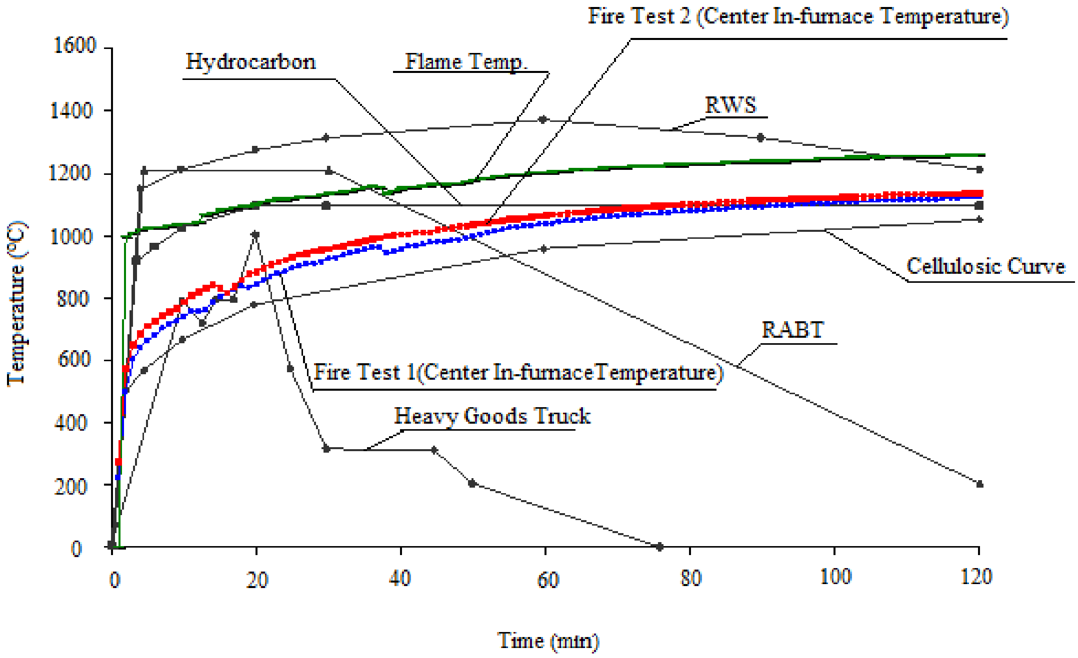

Figure 4.10 Temperature Curves after Tests

The temperatures in furnace on surface of concrete reached in our fire tests are very close to "Hydrocarbon" curve limits and temperature-time area computation indicate that the curves can be called "Hydrocarbon" curve. Measured flame temperature is above of the targeted "Hydrocarbon" curve in terms of temperature-time area. It is observed that in the first 15 minutes the explosive spalling take place [Figure 4.11]. The spalling duration was between 30-45 minutes. It is further observed that the specimens have lost 4-6 cm thick layer from their surface which is exposed to flames and concentration of reflection.

The cube is not exposed to direct flame but exposed to reflections of heat from the side walls. After the first test, it is seen that the 15x15 cm test cube was highly damaged and could not be used in the compressive strength crush test [Figure 4.11 b]. As noticed from the "Figure 4.11 b" bottom of the cube specimen was not damaged since the bottom part was in contact with the insulation material. It shall be noted that the part of the segment close to cube is not heavily damaged since segment volume serves as an effective heat sink.

(a)

(b)

Figure 4.11 (a) Concrete Face in Fire Test, (b) Cube Specimen after Fire Test

4.2 Compressive Strengths of Concrete Mixes

In METU Civil Engineering Department Material Laboratory, cubes are tested under compression with a uniaxial test machine. The curing, temperature, slump etc. details of cube specimens can be found in Appendix D. Prior to tests, dimensions of the tested cube specimens are entered as a data to the test machine. Uniaxial test machine loads the cubes with a rate of 6.8kN/s and gives the maximum stress and maximum load capacity of the sample.

Table 4.1 Concrete Compressive Strengths of Specimens

Segment	Compressive Strength (MPa)					
	1 Day	7 Days	28 Days	Fire Test Day (50-60 Days)	Static Loading Test Day (75-90 Days)	Corrected Values (75-90 Days)
Type 1A-1	41.4	49.5	58.4	58.6	58.6	52.7
Type 1A-2	43.4	57.9	63.9		68.7	61.8
Type 2A-1	44.4	55.9	60.4	61.0	64.0	57.6
Type 2A-2	44.1	58.4	64.5		68.7	61.8
Type 1B-1	44.8	58.6	63.4	68.0	68.3	61.4
Type 1B-2	45.4	56.6	61.0		67.3	60.5
Type 2B-1	51.5	58.1	65.0	66.7	68.5	61.6
Type 2B-2	43.9	54.2	52.0		56.2	50.5

Since the cylindrical compressive strength of concrete is used in calculations a factor of 0.9 is used to convert strength cube to cylinder. [13]

4.3 Tensile Test of Reinforcements

To measure the changes between pre-fire and post-fire tensile strength of reinforcement bars tensile test is carried out. For this purpose, concrete cover on segment Type 1A-2 and Type 2B-1 is cleaned and two samples for each segment are taken out. In the test; diameter, yield strength and ultimate tensile strength of the reinforcement bars are tested.

Table 4.2 Tensile Strength of Reinforcements

Properties	Unit	Type 1A-2 Taken From (Unburnt) Specimen1	Type 1A-2 Taken From (Unburnt) Specimen2	Type 2B-1 Taken From (Burnt) Specimen1	Type 2B-1 Taken From (Burnt) Specimen2
Length	mm	310	305	309	308
Weight	gr	0.375	0.362	0.382	0.373
Diameter	mm	14.0	13.8	14.1	14.0
Yielding Force	kN	76	78	85	84
Yield Strength	MPa	492	508	539	543
Ultimate Force	kN	94	94	102	100
Ultimate Tensile Strength	MPa	607	620	647	646

It is observed that the yield strength of steel is 520 Mpa and ultimate strength is 600 Mpa. In the further analysis these characteristics of steel is taken into consideration [Table 4.2]. The yield strength is about 24% higher then minimum required tensile strength of ST 420 steel.

4.4 Core Sampling

To determine the post-fire compressive strength of segments and to cut samples for the electron microscope scanning core samples are taken from the segments. A total number of 8 cores are taken from the segments Type 2B-2, Type 1B-1 and Type 1A-1. To investigate the post-fire characteristic of concrete compressive strength, three core samples from different locations (left, middle and right) of two burnt segments are extracted. The details of the samples and their approximate locations are described in Table 4.3 and Figure 4.12.

Table 4.3 Location of Core Sampling

Specimen No :	Number of Core Sampling	Location
Type 2B-2 (Unburnt)	2	Left, Right
Type 1B-1 (Burnt)	3	Left, Right, Middle
Type 1A-1 (Burnt)	3	Left, Right, Middle

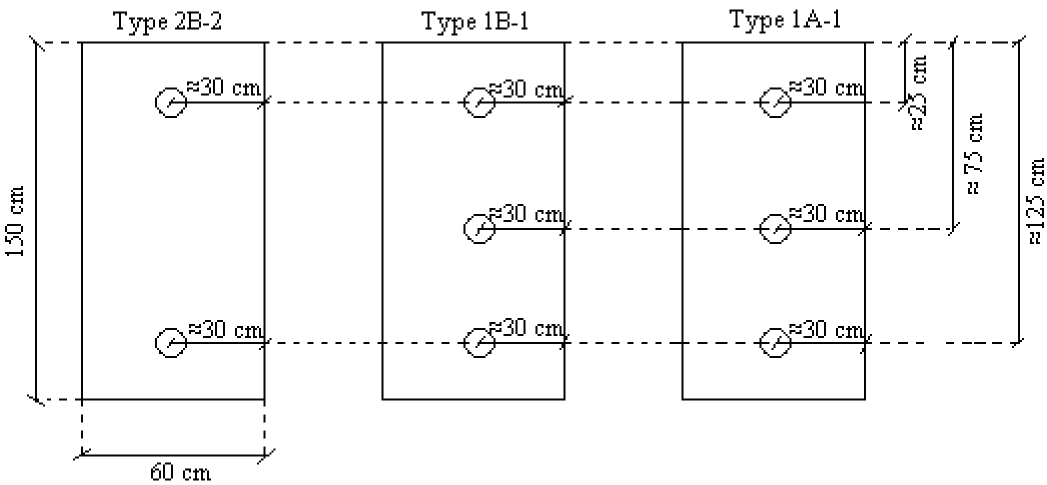

Figure 4.12 Location of Core Sampling-1

Core sampling machine can take samples of size up to 150 mm diameter with the help of thin wall diamond bits. The machine has an electric motor and makes its cooling arrangement with water. Machine can take 200-250 mm length cores. In our study samples are taken by laboratory experts, because the vibration during the extraction can break the core samples into 2-3 pieces. Another issue to pay attention is to measure the distance between the reinforcement bars and try not to drill through them. Cutting diamond bits are composed of very hard material but they can easily break from their connection points. These cores are taken from the degraded zones or zones exposed to high temperature. The cores are sulphur capped prior to the compression testing.

Figure 4.13 Location of Core Sampling-2

After coring and testing samples under compression, results are corrected according to ASTM. ASTM provides length-to-diameter correction factors that are used to reduce the compression strength measure by the testing machine. A core with a length-to-diameter ratio from 1.94 to 2.10 requires no correction factor [Table 4.4].

Table 4.4 Correction Factors According to ASTM [22]

Length-to-diameter Strength Correction Factor	
Length/Diameter Ratio	**Strength Correction Factor**
1.75	0.98
1.50	0.96
1.25	0.93
1.00	0.87

Post-fire compressive strengths of core samples are as follows:

Table 4.5 Core Sampling Results

<table>
<tr><th>Specimen</th><th>Diameter (mm)</th><th>Length (mm)</th><th>L/D Ratio</th><th>Correction Factor</th><th>Strength (MPa)</th><th>Average</th></tr>
<tr><td>Type 1B-1</td><td>92</td><td>170</td><td>1.84</td><td>≈1</td><td>49.4</td><td rowspan="2">48.1 MPa</td></tr>
<tr><td>Type 1B-1</td><td>92</td><td>175</td><td>1.90</td><td>≈1</td><td>46.8</td></tr>
<tr><td>Type 1A-1</td><td>92</td><td>190</td><td>2.06</td><td>≈1</td><td>41.4</td><td rowspan="2">43.0 MPa</td></tr>
<tr><td>Type 1A-1</td><td>92</td><td>170</td><td>1.84</td><td>≈1</td><td>44.6</td></tr>
</table>

4.5 Static Loading Test Results

Simply supported segments are tested under static loading. Tested segment characteristics are given in Table 4.6. In the test, yield capacity, ultimate capacity, support deflections and mid-span deflection are measured through data acquisition system. The load is applied from the unburnt face and burnt face positioned in the tension zone during the tests.

Table 4.6 Segment Characteristics

Segment	Tested		Bottom Reinforcement	Condition	Tests	
	f_{ck} (MPa)	f_{yk} (MPa)			Fire	Static
Type 1A-1	52.7	530	5Ø12	Unstressed	✓	✓
Type 1A-2	61.8	520	3 Ø12,2 Ø14	Unstressed		✓
Type 2A-1	61.8	530	5Ø14	Unstressed	✓	✓
Type 2A-2	57.6	520	5Ø14	Unstressed		✓
Type 1B-1	61.4	530	5Ø12	Stressed	✓	✓
Type 1B-2	60.5	520	5Ø12	Stressed		✓
Type 2B-1	61.6	530	5Ø14	Stressed	✓	✓
Type 2B-2	50.5	520	5Ø14	Stressed		✓

Firs test is performed on the segment Type 1A-1 at 09/07/2010 [Figure 4.14]. Since the segment surface is damaged in the fire test, bottom end surface of the segments that contacts with the supports are filled with gypsum to balance the system. Before static loading, the distance between segment top surface and load cell attached to test frame is measured. It is observed that the distance is not sufficient to apply loads. Because of this a 150 x 150 mm steel rectangular prism is placed at the middle of the segment top surface. After displacement transducers and load cell calibrated test is carried out. First cracking is observed at 200 kN and yield capacity of the segment is recorded as 450 kN. Ultimate strength of the segment is not reached, since the capacity of the loading frame is believed to be 500 kN of safe loading. To stay in safe zone, test is finished at 527 kN and the maximum mid-span deflection is measured as 12 mm [Figure 4.15]. Cracks spaced about 20 cm propagated from tension zone to upper regions.

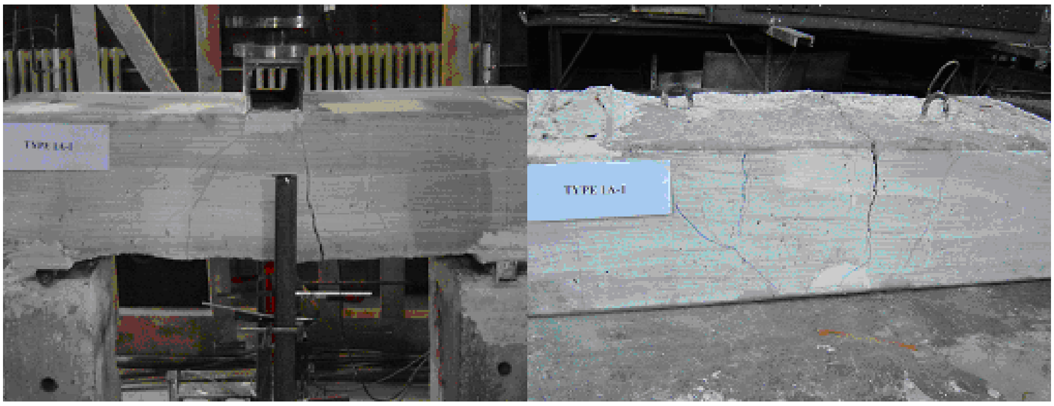

Figure 4.14 Type 1A-1 Specimen after Static Loading Test

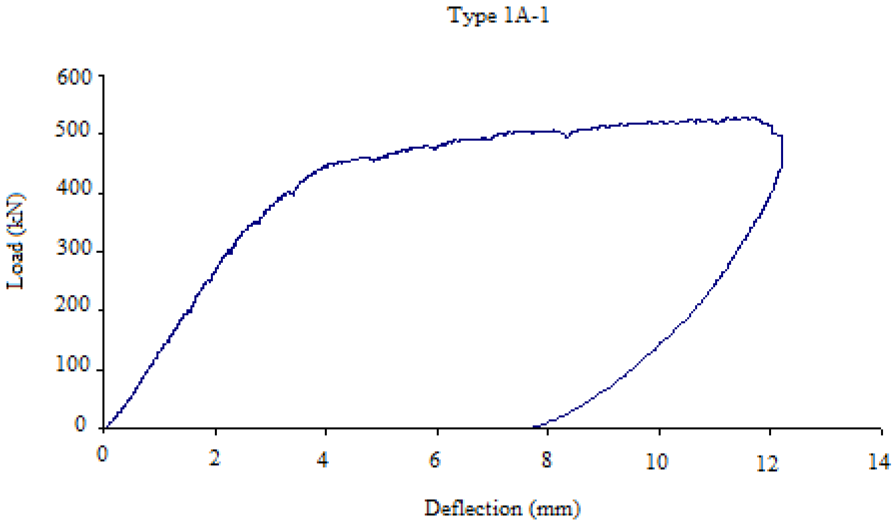

Figure 4.15 Load-Deflection Diagram (Type 1A-1)

(Type 1A-1: Ø12 Unstressed – Burnt)

In the static load test of Type 1A-2 at 14/07/2010 [Figure 4.16], first cracking is observed at 200 kN. This test is the fourth static loading test and capacity of the loading frame is observed to be more then 500 kN of safe loading. End of the test, yield capacity and ultimate capacity of the segment is measured as 460 and 529 kN respectively. It is also observed that the maximum mid-span deflection is about 22 mm [Figure 4.17]. This test is terminated after reaching degradation in load carrying mechanism of the segment.

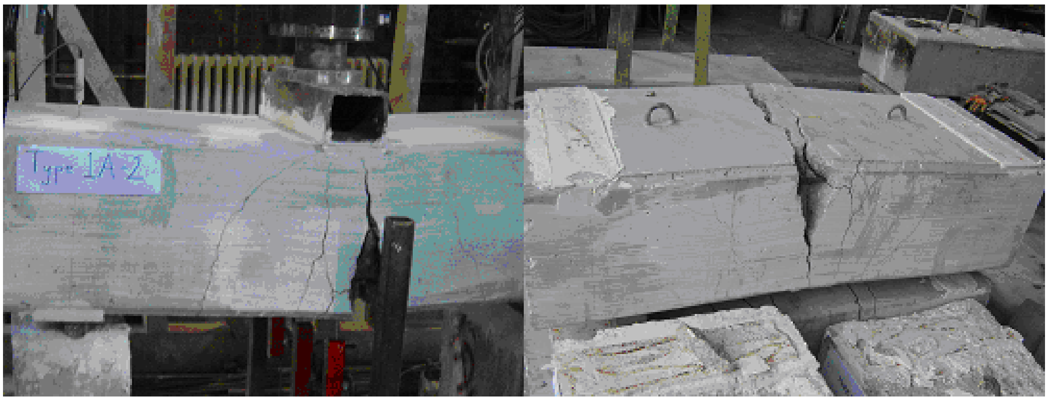

Figure 4.16 Type 1A-2 Specimen after Static Loading Test

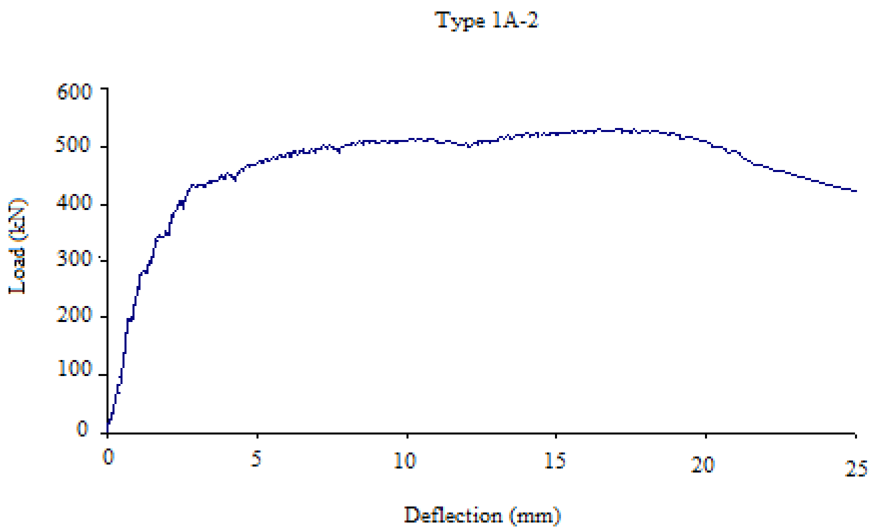

Figure 4.17 Load-Deflection Diagram (Type 1A-2)

(Type 1A-2: Ø12 Unstressed – Unburnt)

Static loading test of Type 2A-1 is done at 20/07/2010 [Figure 4.18]. At 180 kN initial cracking is observed. Yield capacity and ultimate capacity of the segment is measured as 495 kN and 557 kN respectively. Maximum mid-span deflection is measured as 28 mm [Figure 4.19].

Figure 4.18 Type 2A-1 Specimen after Static Loading Test

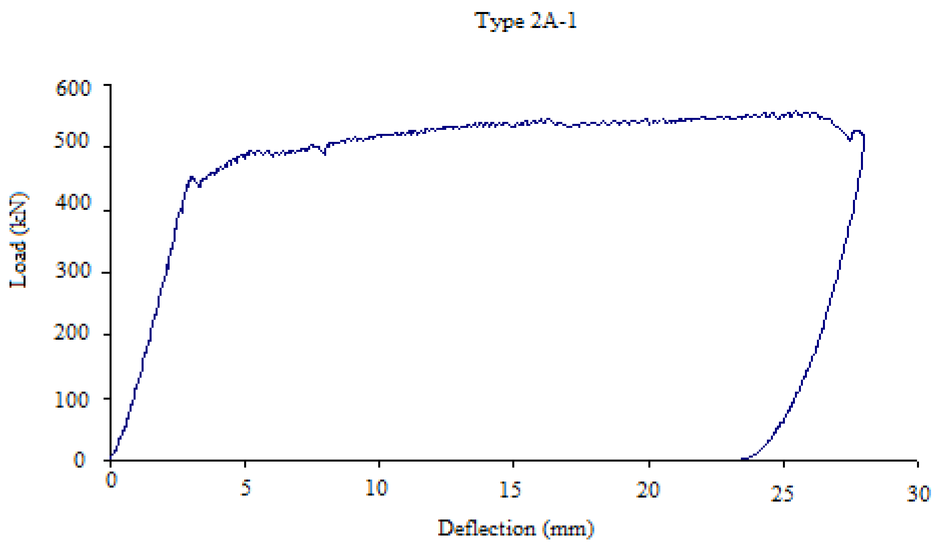

Figure 4.19 Load-Deflection Diagram (Type 2A-1)

(Type 2A-1: Ø14 Unstressed – Burnt)

Segment Type 2A-2 is tested at 13/07/2010 [Figure 4.20]. Segment started to crack at 200 kN. The ultimate capacity of the segment is not measured due to safety reasons believed to pertain to loading frame. Yield capacity of the segment is measured 490 kN and the maximum applied load is around 583 kN. Maximum mid-span deflection is measured as 27.4 mm [Figure 4.21].

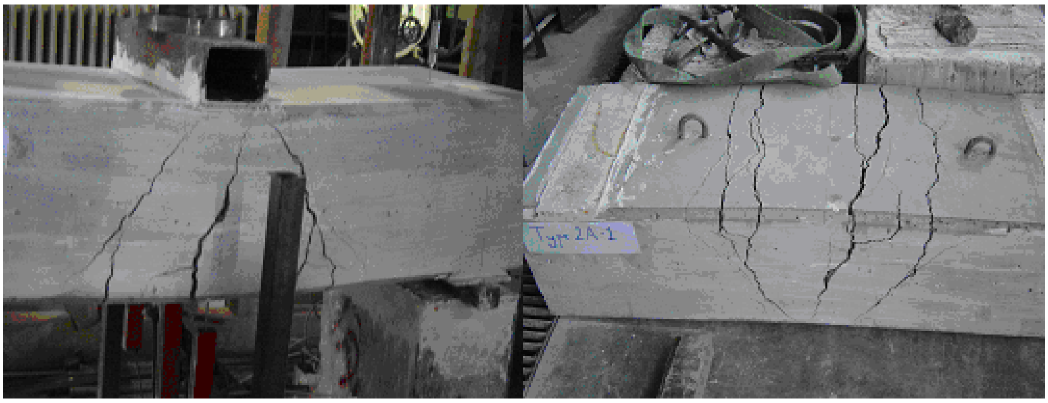

Figure 4.20 Type 2A-2 Specimen after Static Loading Test

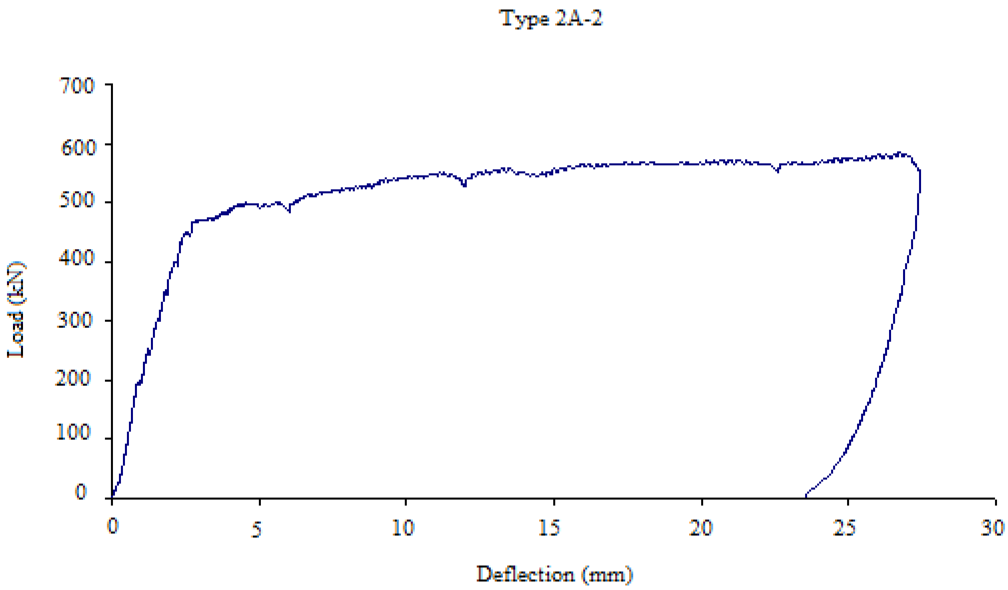

Figure 4.21 Load-Deflection Diagram (Type 2A-2)

(Type 2A-2: Ø14 Unstressed – Unburnt)

Static loading test of Type 1B-1 is done at 21/07/2010 [Figure 4.22]. At 150 kN initial cracking is observed. Yield capacity and ultimate capacity of the segment is measured as 353 kN and 446 kN respectively. Maximum mid-span deflection is measured as 41.2 mm [Figure 4.23].

Figure 4.22 Type 1B-1 Specimen after Static Loading Test

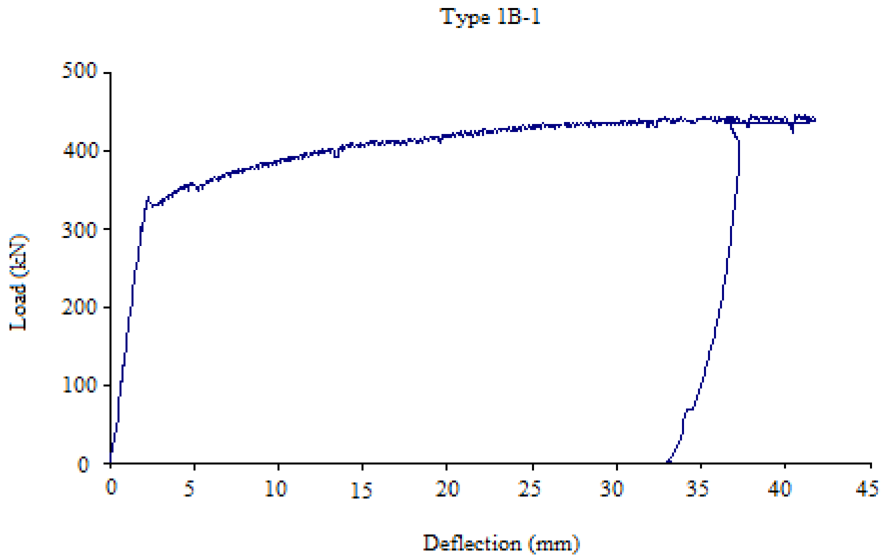

Figure 4.23 Load-Deflection Diagram (Type 1B-1)
(Type 1B-1: Ø12 Stressed- Burnt)

Static loading test of Type 1B-2 is performed at 21/07/2010 [Figure 4.24]. At 150 kN initial cracking is observed. Yield capacity and ultimate capacity of the segment is measured as 467 kN and 536 kN respectively. Maximum mid-span deflection is measured as 23.8 mm [Figure 4.25].

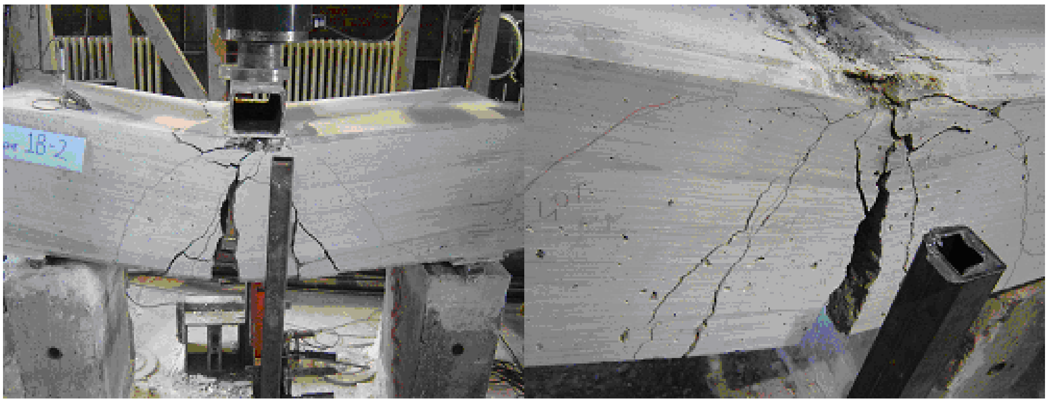

Figure 4.24 Type 1B-2 Specimen after Static Loading Test

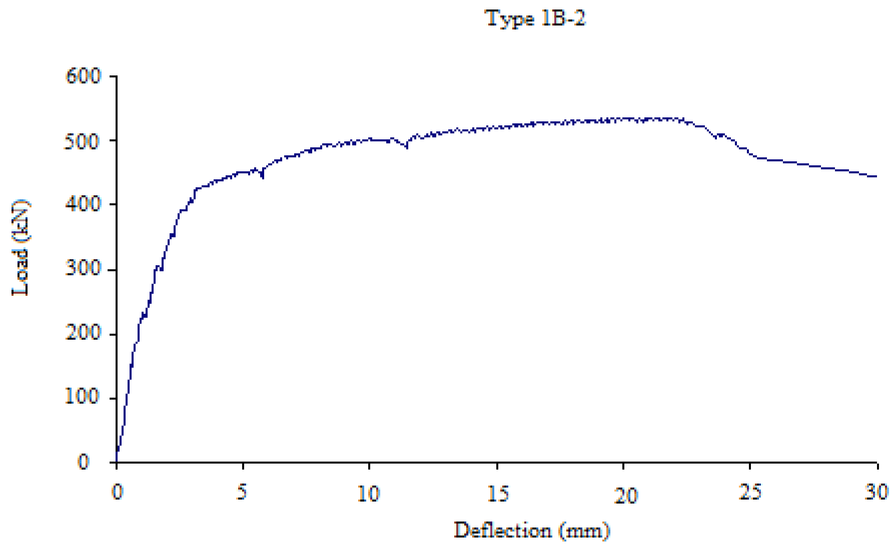

Figure 4.25 Load-Deflection Diagram (Type 1B-2)

(Type 1B-2: Ø12 Stressed – Unburnt)

In the static load test of Type 2B-1 at 12/07/2010 [Figure 4.26], first cracking is observed at 250 kN. In the test, the ultimate capacity of the segment is not measured due to safety reasons. End of the test, yield capacity of the segment is measured as 490 kN and the maximum applied load is measured about 590 kN. It is also observed that the maximum mid-span deflection is about 18.6 mm [Figure 4.27].

Figure 4.26 Type 2B-1 Specimen after Static Loading Test

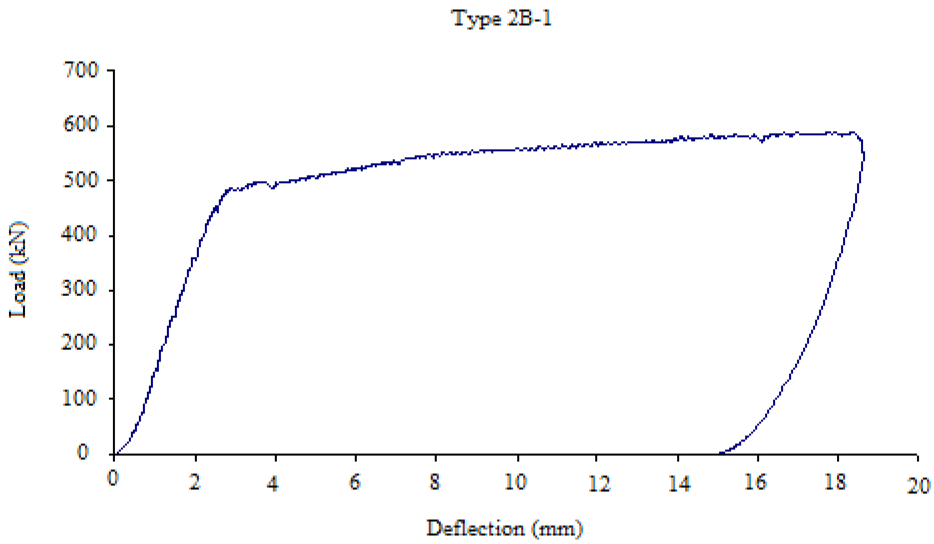

Figure 4.27 Load-Deflection Diagram (Type 2B-1)

(Type 2B-1: Ø14 Stressed – Burnt)

Static loading test of Type 2B-2 is done at 19/07/2010 [Figure 4.28]. At 180 kN initial cracking is observed. Yield capacity and ultimate capacity of the segment is measured as 520 kN and 606 kN respectively. Maximum mid-span deflection is measured as 13.1 mm [Figure 4.29].

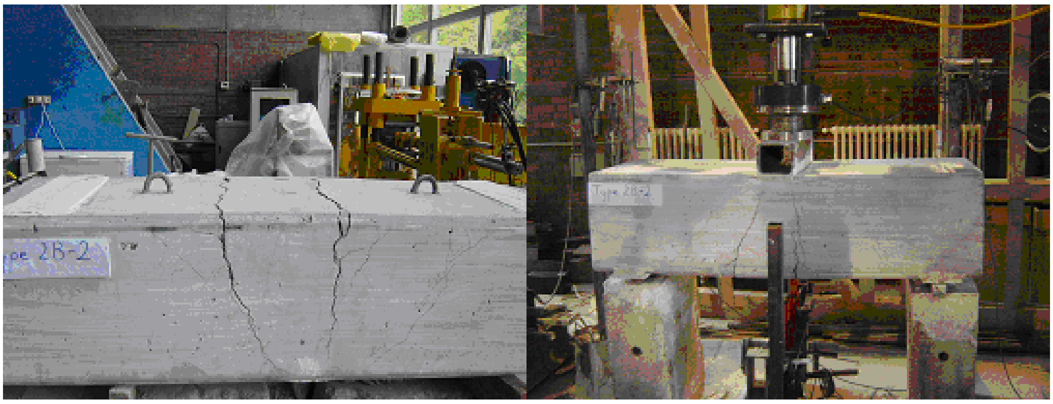

Figure 4.28 Type 2B-2 Specimen after Static Loading Test

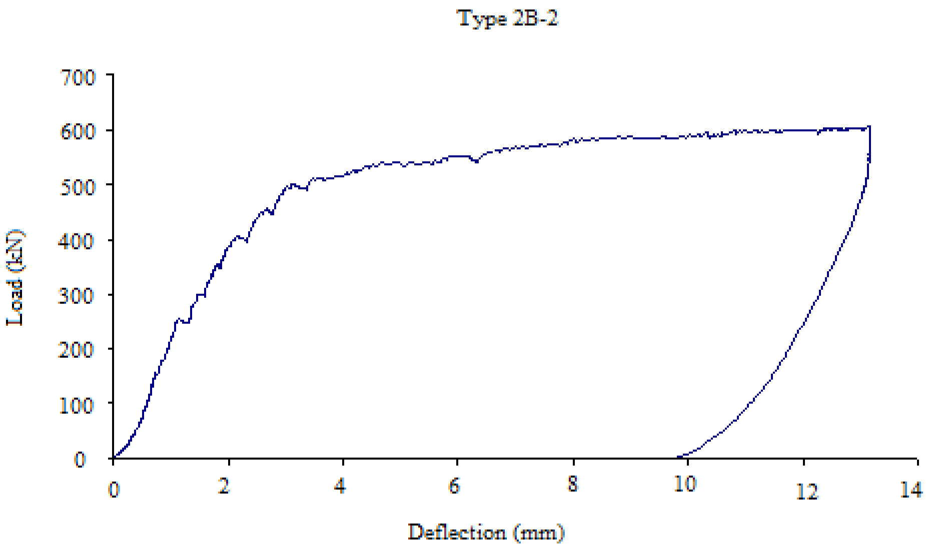

Figure 4.29 Load-Deflection Diagram (Type 2B-2)

(Type 2B-2: Ø14 Stressed – Unburnt)

Other test results and summary of static loading tests are as follows:

Table 4.7 Static Loading Test Results

Segment	Age (days)	Max. Applied Load (kN)	Situation	Yield Capacity (kN)	Ultimate Capacity (kN)	Max. Mid-span Deflection (mm)
Type 1A-1	89	527	Stopped	450	-	122
Type 1A-2	93	529	Tension Failure	460	529	220
Type 2A-1	95	557	Tension Failure	495	557	280
Type 2A-2	88	583	Stopped	490	-	274
Type 1B-1	94	446	Tension Failure	353	446	412
Type 1B-2	83	536	Tension Failure	467	536	238
Type 2B-1	74	588	Stopped	490	-	186
Type 2B-2	76	606	Tension Failure	520	606	131

4.5.1 Observations after Static Loading Tests

The static loading test set-up constructed for a different research has an allowable (safe) load capacity of around 500 kN. Therefore, the first sets of tests are interrupted around 500 kN to remain under allowable load capacity.

After the static loading tests [Figure 4.14 to 4.28], it is observed that the cracks are generally occurred in the mid-length of the stressed specimens; no distributions towards the supports are seen [Figure 4.28]. The unstressed specimens have provided the expected distributed crack pattern between the supports [Figure 4.20]. And the specimens started to crack under 150-250 kN.

It is also observed that a difference of 3-15 % loss in yield load capacity between the burnt and unburnt specimens.

Type 1A-2 should have 5 Ø12 bar as reinforcement. The reinforcement is checked following the static test and it is seen that instead of 5 Ø12, the specimen was reinforced with 3 Ø12 and 2 Ø14. In the further analysis, this actual rebar configuration is taken into consideration.

Except Type 1A-1, Type 2A-2 and Type 2B-1, all the beam tests are resulted in tension failure of steel. In type 1B-2 and 1A-2 the rebar is ruptured at failure.

The load-deflection comparisons are presented in Appendix E (Comparison between burnt and unburnt segments), Appendix F (Comparison between stressed and unstressed segments) and Appendix G (General comparisons of load deflection diagrams).

4.6 Electron Microscope Evaluations

<u>Sample Taken from 5 cm Depth</u>

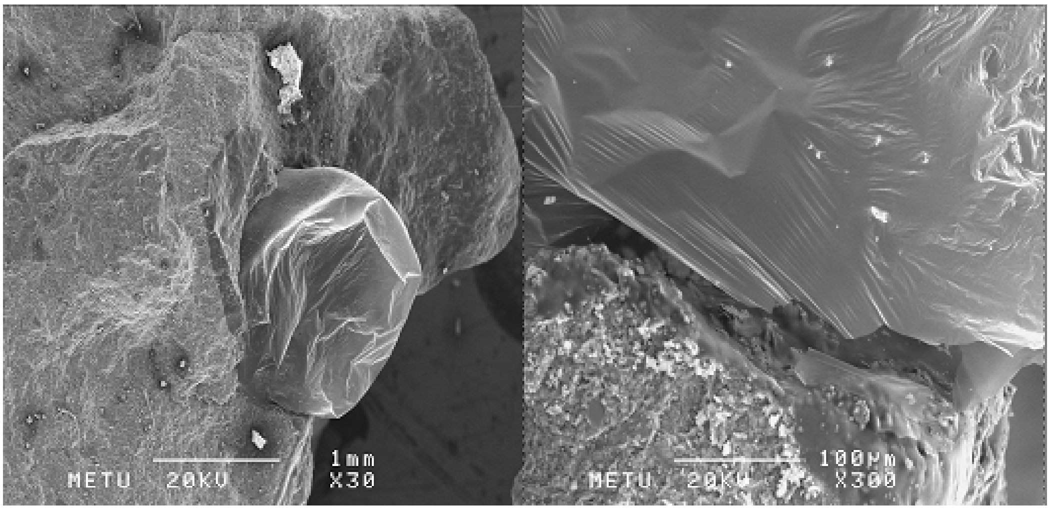

Figure 4.30 Scannings of Electron Microscope at 5 cm depth

In the Figure 4.30 the cement-aggregate bond is shown. On enlarged Figure 4.30 (the right) the cracks between the aggregate and cement appear more clear.

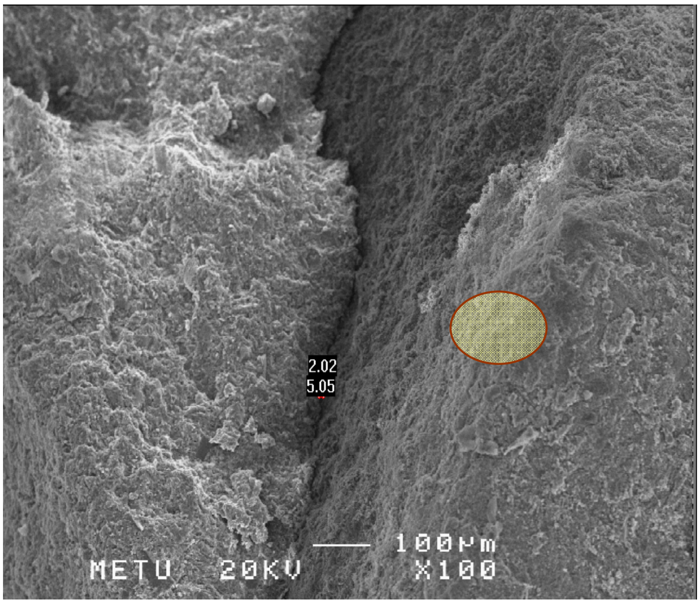

Figure 4.31 Internal Cracking in the Core

The Figure 4.31 is the general view of the sample from the top. The internal cracking is seen clearly. On this picture the location of EDX (EDX is a technique used for identifying the elemental composition of the specimen, or an area of interest.) is indicated and also the crack widths are dimensioned. The dimensions of the cracks are given in microns.

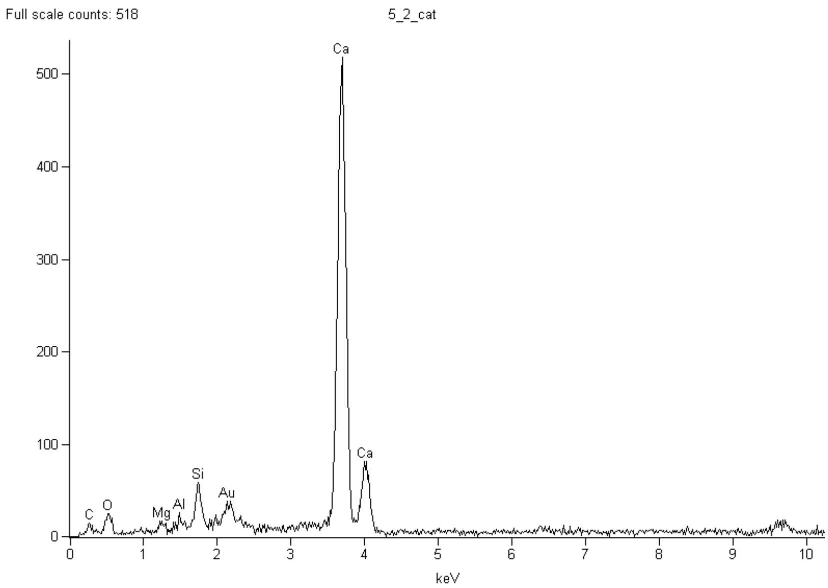

Figure 4.32 EDX Table at 5cm depth

The Figure 4.32 indicates the surface C-S-H gels. The C-S-H gel is not only the most abundant reaction product, occupying about 50% of the paste volume, but it is also responsible for most of the engineering properties of cement paste. This is not because it is an intrinsically strong or stable phase but because it forms a continuous layer that binds together the original cement particles into a cohesive whole. [14]

Sample Taken from 10 cm Depth

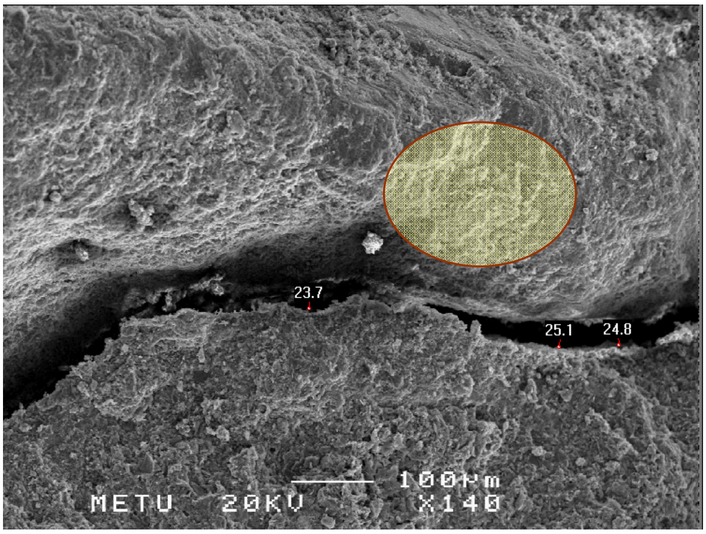

Figure 4.33 Scannings of Electron Microscope at 10 cm depth

The cracks are more visible at the depth of 10 cm [Figure 4.33]. There is no difference in the structural properties to the sample taken at 5 cm depth. The Figure 4.33 also shows the area from which EDX graph is derived.

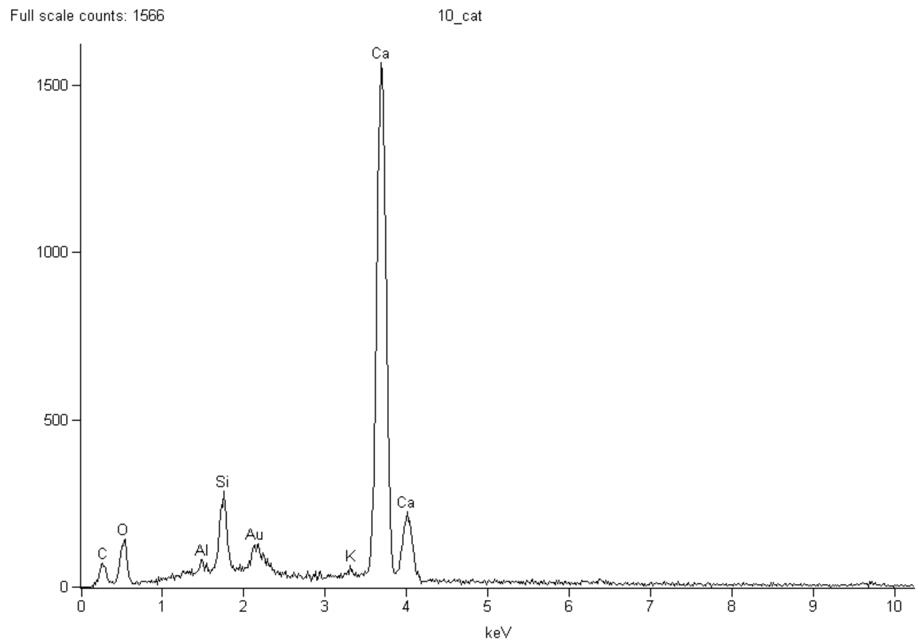

Figure 4.34 EDX Table at 10 cm depth

As stated above, no difference in structural properties are observed between the samples. The Figure 4.34 shows the C-S-H gel's chemical index.

Sample Taken from 20 cm Depth

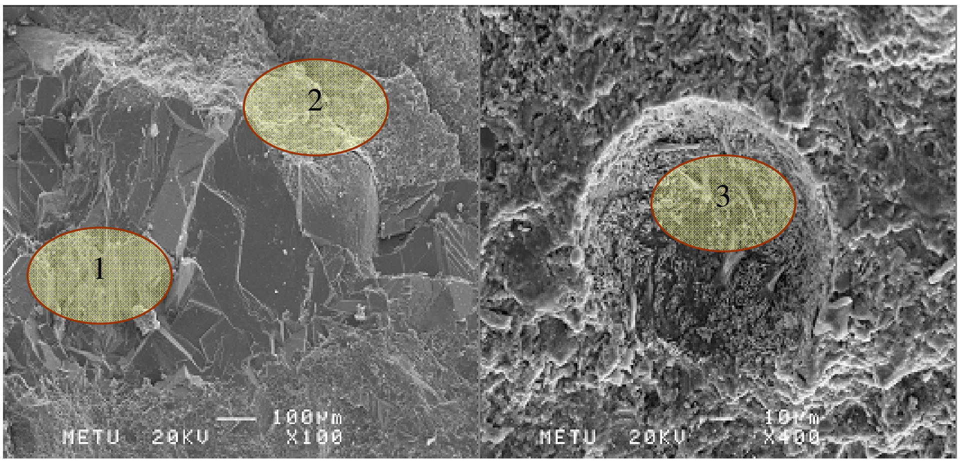

Figure 4.35 Scannings of Electron Microscope at 20 cm depth

The structure of specimen indicates a more heterogeneous structure at a depth of 20 cm [Figure 4.35]. The following EDX diagrams show the hydration products that seen in the concrete specimen from 20 cm [Figure 4.36, Figure 4.37, Figure 4.38].

1) <u>Calcium Hydroxide, $Ca(OH)_2$</u>

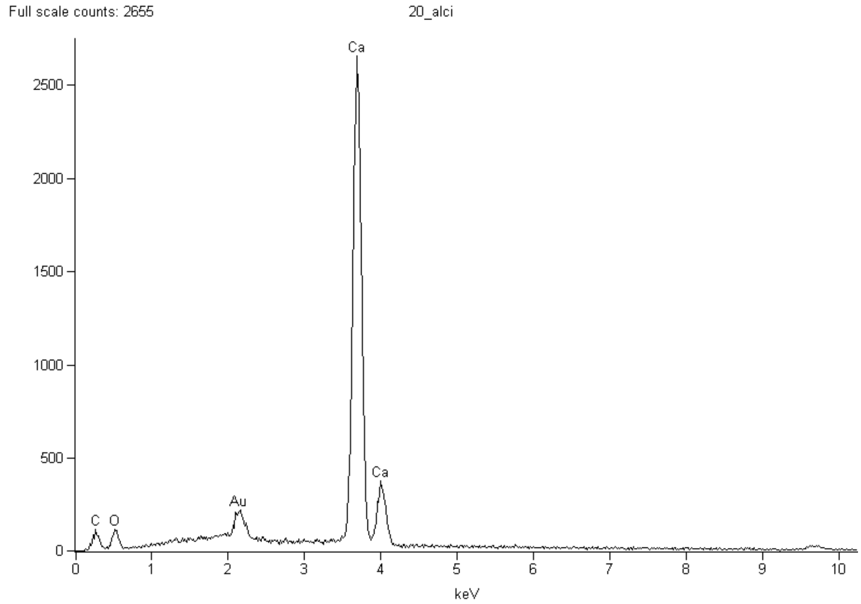

Figure 4.36 EDX Table at 20cm depth-1

2) <u>C-S-H Gel</u>

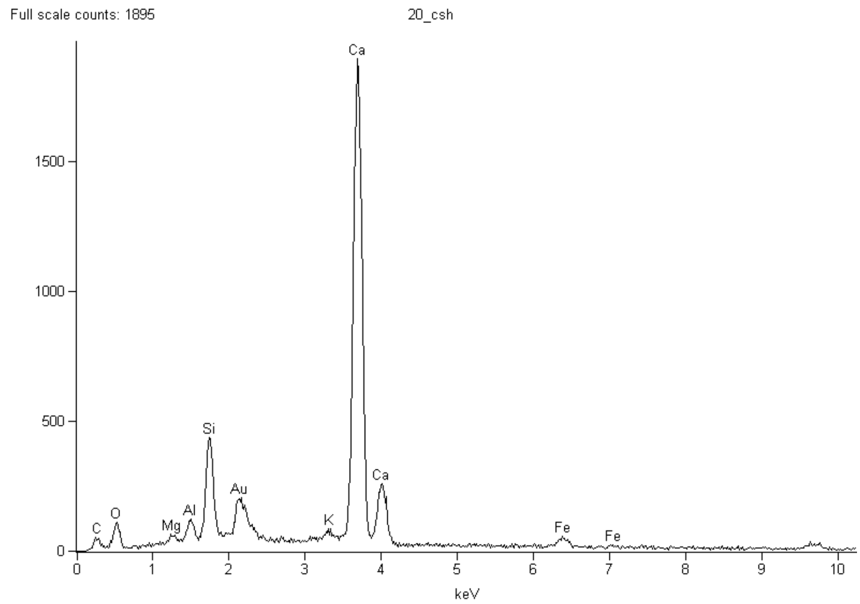

Figure 4.37 EDX Table at 20cm depth-2

3) Ettringite

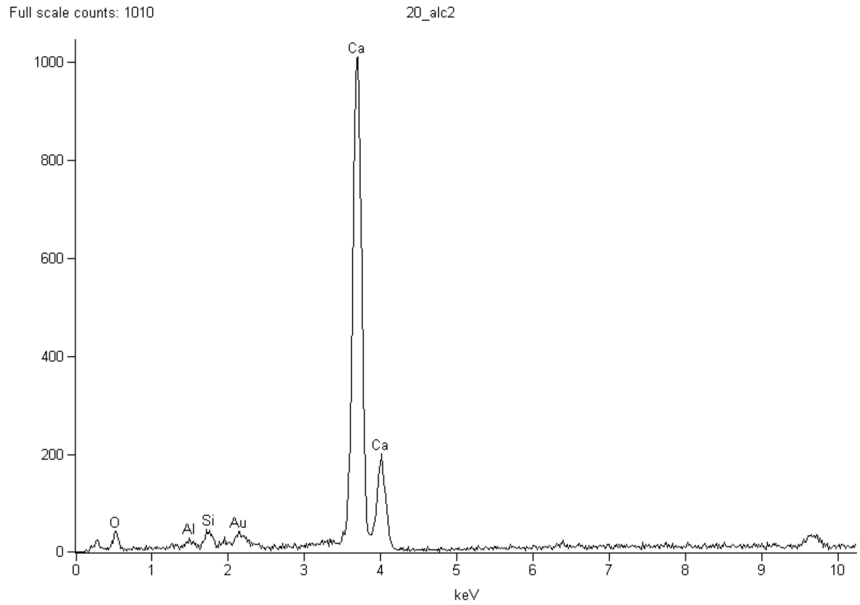

Figure 4.38 EDX Table at 20cm depth-3

The electron microscope scanning is carried out to observe the impact of fire in the concrete chemical properties. The results show:

1) Fire can develop internal cracking in the concrete at certain regions.
2) The approximate temperature of 80 ^{o}C measured at 20 cm depth from the surface of specimen exposed to 2 hours fire shows that, heat distribution does not lead to any chemical deformation at such depths.
3) When we investigated the specimens, which are taken 5 cm and 10 cm depth, it is observed that, they are more homogeneous due to extreme heat effect. Hydration products are eliminated in these regions and the concrete is dehydrated.

4.7 Determination of Moisture Content

Previous researches show that, the higher moisture content can ignite explosive spalling during a fire [15]. Because moisture in the concrete can rapidly turn into steam; in concrete with low permeability and high moisture content, the steam pressure can produce explosive spalling [4].

To investigate this theory samples are taken from specimens, type 2B-2, type 1A-2 and type 2A-1 to carry out laboratory analysis to determine the moisture content and evaluate the difference between the burned and unburnt specimens. (2B-2 unburnt, 1A-2 unburnt, 2A-1 burnt)

Specimens are tested in almost worst conditions in terms of moisture content in the Materials Laboratory of Civil Engineering Department of METU. They kept under 110 ^{o}C at 3 days in furnace [21]. High moisture content of 3% is observed in the specimen Type 2B-2. It was observed the moisture content of samples decreased during the fire tests as expected. The moisture that turned into the steam may cause to explosive spalling as mentioned in previous research. The table below indicates the difference of samples before and after the moisture tests, the loss in weight and percentage.

Table 4.8 Moisture Content

Samples From	Type 2B-2 (Unburnt)	Type 1A-2 (Unburnt)	Type 2A-1 (Burnt)
Weight Before Moisture Test (gr)	200.91	992.70	1907.56
Weight After Moisture Test (gr)	195.75	973.10	1893.60
Loss (gr)	5.16	19.60	13.96
% Loss	2.56 (High)	1.97 (High)	0.73 (Low)

The burnt segment has less moisture content as expected as indicate Table 4.8.

CHAPTER 5

EVALUATION OF TEST RESULTS

5.1 Temperature Distribution at Depth of Concrete

Temperature at top surface of concrete rapidly decreases at the inner depths of section due to poor conductivity of concrete. A non-linear heat transfer analysis is typically required to account for variation in thermal conductivity and specific heat of concrete. Temperature dependent variations of these thermal parameters are function of temperature, aggregate type and composition of concrete mix design. Therefore each concrete design has its own particular temperature profile at depth even if these different concretes can be subjected to the same fire. A comparison table of temperature readings from experimental and analytical works is presented in Table 5.1. Locations of thermocouples in the concrete cross-section are presented in the Figure 5.1.

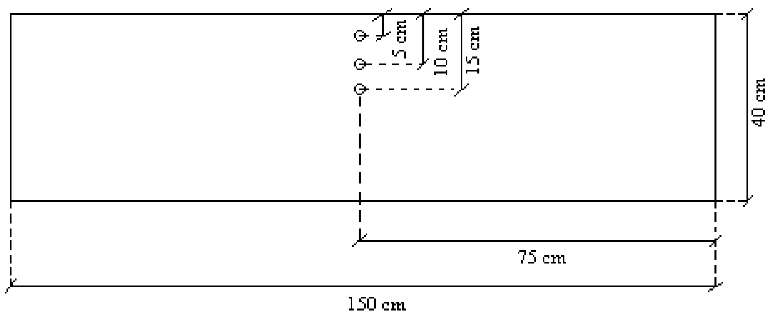

Figure 5.1 Locations of Thermocouples

Table 5.1 Comparison of Temperature Distribution into Concrete

			Temperature at Depth (^oC)		
Fire Type	Research	f_{ck} (MPa)	5 cm	10 cm	15 cm
Hydrocarbon	Arsava*	58	377	255	100
Hydrocarbon	Boncu [4]	75	Not Recorded	275***	Not Recorded
ASTM-E119 [21]	ACI 216 [2]	Normal	405	262	159
Hydrocarbon**	Caner et al [8]	28	434	284	174

* Current research.

** From unpresented work of Caner et al research [8].

*** Measured at 11 cm.

The result above comparison showing that the results obtained from the tests carried out in this project are in close proximity to other studies even if the fire and concrete mix designs are different.

5.2 Material Degradation

It has been known that at high temperatures concrete and steel material can have degradation in material properties due to changes in chemical composition. Material degradation models are developed by Shi et al [5], ACI 216 [2] and Eurocode 2 [3].

5.2.1 Shi et al [5] Degradation Model

In their study, the effect of high temperature on reinforced concrete flexural members that were designed and tested with proper steel content to observe ductile type of failure. And also different concrete cover thicknesses were tested [5]. Authors developed material degradation models some to calculate the compressive strength of concrete and yield strength of reinforcement exposed to elevated temperature [Eqn 5.1 and Eqn 5.2].

$$f_c^T = \frac{f_c}{1 + 24\left(\frac{T-20}{1000}\right)^6} \qquad \text{Eqn. (5.1)} \qquad f_y^T = \frac{f_y}{1 + 24{,}4\left(\frac{T-20}{1000}\right)^{4,5}} \qquad \text{Eqn. (5.2)}$$

Where "f_c^T" is the concrete compressive strength at temperature T and "f_y^T" is tensile strength of steel at temperature T.

Shi et al [5] material degradation models are used to compute material degradation of concrete and steel in this research. [Appendix H]

Table 5.2 Post-fire Compressive Strength of Specimens According [5]

Specimen		Type 1A-1	Type 2A-1	Type 1B-1	Type 2B-1
Initial Compressive Strength (MPa)		52.74	57.60	61.40	61.65
Compressive Strength After Fire Test (MPa)	5 cm	50.39	55.04	58.67	58.91
	10 cm	52.52	57.36	61.15	61.40
	15 cm	52.74	57.60	61.40	61.65
	Average	51.88	56.66	60.40	60.65

Table 5.3 Post-fire Tensile Strength of Reinforcement According [5]

Tensile Strength of Reinforcement (MPa)	According to Article	Yield Strength	420.43
		Ultimate Strength	485.12

5.2.2 ACI 216 [2] Degradation Model

ACI 216 provides graphical presentation of material degradation related to exposed temperature as shown in Figure 5.2. The steel rebar at 6 cm depth is subjected to 377 ^{o}C and about 10% degradation in material properties. The degraded yield strength of steel is estimated as 468 MPa. Steel gains back its strength after fire.

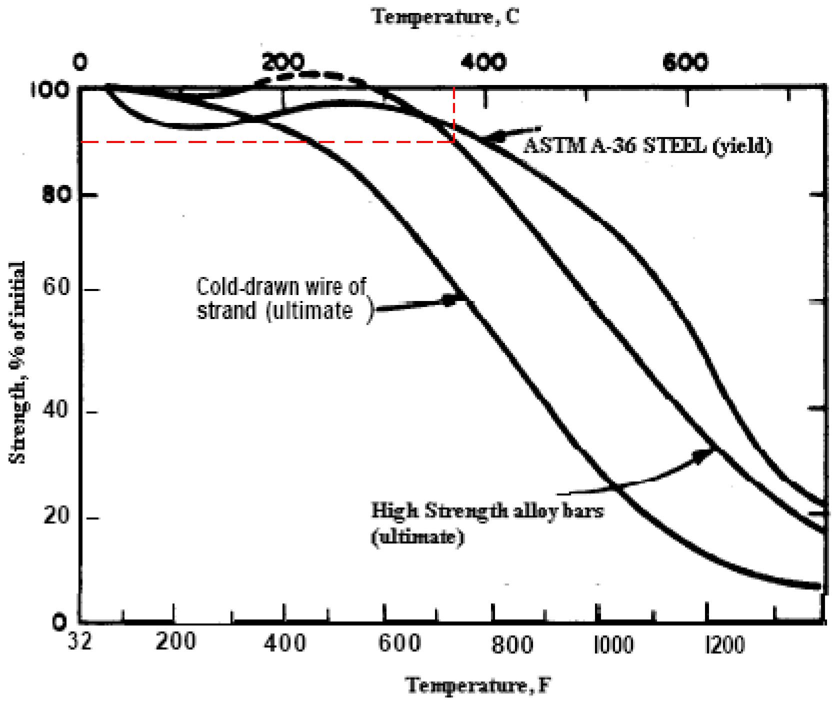

Figure 5.2 Strength of Certain Steels at High Temperatures [2]

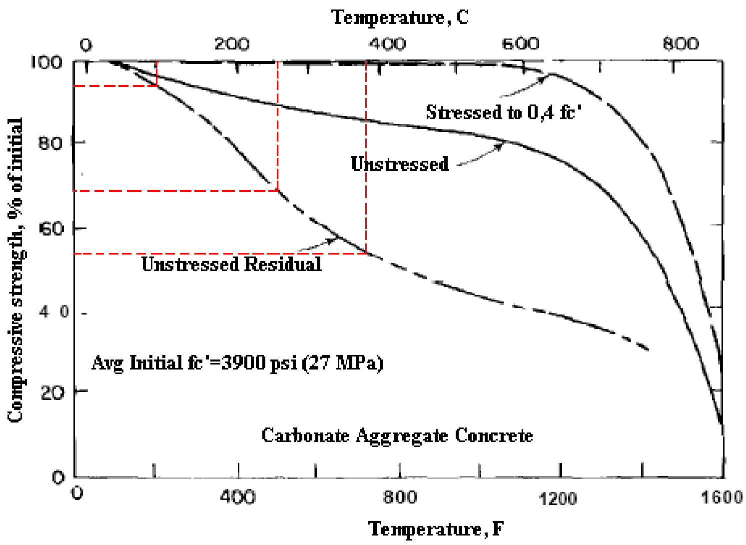

Figure 5.3 Compressive Strength of Carbonate Aggregate Concrete at High Temperature and After Cooling [2]

The concrete degradation continues after the fire stops. Therefore it is essential to evaluate the structural integrity with post-fire degradation models. Using Figure 5.3

of ACI 216 the concrete compression strength close to hot surface is presented in Table 5.5.

According to graph to "Unstressed Residual" curve,

Table 5.4 Decrease of Compressive Strength According to ACI 216

Temperature ^{o}C	Decrease in Compressive Strength %
377 (at 5 cm)	45
255 (at 10 cm)	30
100 (at 15 cm)	5

Table 5.5 Post-fire Compressive Strength of Specimens According to ACI 216

Specimen		Type 1A-1	Type 2A-1	Type 1B-1	Type 2B-1
Initial Compressive Strength (MPa)		52.74	57.60	61.40	61.65
Compressive Strength After Fire Test (MPa)	5 cm	29.00	31.68	33.77	33.90
	10 cm	36.90	40.32	42.90	43.15
	15 cm	50.10	54.72	58.33	58.65
	Average	38.66	42.42	44.97	45.23

5.2.3 Eurocode2 Degradation Model

Eurocode [3] suggest material degradation coefficients to compute the degraded material property for concrete and steel.

a. Steel Strength

The reduction of steel yield strength due to high temperature could be calculated by using reduction coefficient of k_s.

$$f_y^{\,T} = k_s \times f_y \qquad \text{Eqn. (5.3)}$$

$k_s = 1 \qquad 0 \le T \le 350^{O} C$

$k_s = 1.899 - 0.0025T \qquad 350 \le T \le 700^{O} C$

$k_s = 0.24 - 0.0002T \qquad 700 \le T \le 1200^{O} C$

$k_s = 0 \qquad 1200^{O} C \le T$

Yield Strength

$f_y^{377^o C} = 520 \times (1.899 - (0.0025 \times 377)) = 497.38 MPa$

Ultimate Strength

$f_u^{377^o C} = 600 \times (1.899 - (0.0025 \times 377)) = 573.90 MPa$

b. Concrete Strength

The reduction of concrete compressive strength due to high temperature could be calculated by using reduction factor k_c defined in Eurocode 2.

$$f_{ck}^{T} = k_c \times f_y \qquad \text{Eqn. (5.4)}$$

$k_c = 1 \qquad T \leq 100^O C$

$k_c = 1.067 - 0.00067T \qquad 100 \leq T \leq 400^O C$

$k_c = 1.44 - 0.0016T \qquad 400 \leq T \leq 900^O C$

$k_c = 0 \qquad 900^O C \leq T$

Table 5.6 Reduction Factor According to Eurocode2 [3]

Temperature ^oC	Depth (cm)	k_c
377	5	0.814
255	10	0.896
100	15	1

Table 5.7 Post-fire Compressive Strength of Specimens According to Eurocode2 [3]

Specimen		Type 1A-1	Type 2A-1	Type 1B-1	Type 2B-1
Initial Compressive Strength (MPa)		52.74	57.60	61.40	61.65
Compressive Strength After Fire Test (MPa)	5 cm	42.95	46.88	49.98	50.18
	10 cm	47.25	51.61	55.01	55.24
	15 cm	52.74	57.60	61.40	61.65
	Average	47.64	52.03	55.46	55.69

5.2.4 Results

From test results it is concluded that the degradation of compressive strength of concrete is about 10 to 20 percent of its original value and there is almost no difference between the post-fire and pre-fire tensile strength of reinforcement bars. As seen from the results ACI 216 gives more conservative values than the others [Table 5.8 and Table 5.9]. The Eurocode 2 and Shi et al [5] degradation models underestimated degradation of concrete compressive strength.

Table 5.8 Comparison of Post-fire Compressive Strength of Concrete

	Compressive Strength of Concrete (MPa)			
Method	Type 1A-1	Type 2A-1	Type 1B-1	Type 2B-1
Arsava Pre-Fire Test	52.7	57.6	61.4	61.6
Arsava Post-Fire Test	43.0	N.A	48.1	N.A
ACI 216 (Analytical)	38.6	42.4	44.9	45.2
Eurocode 2 (Analytical)	47.6	52.0	55.4	55.7
Shi et al (Analytical)	51.8	56.6	60.4	60.6

Table 5.9 Comparison of Tensile Strength of Reinforcement

	Tensile Strength of Steel (MPa)	
Method	Yield Strength	Ultimate Strength
Arsava Pre-Fire Test	510	613
Arsava Post-Fire Test	535	640
ACI 216 at 120th min (Analytical)	468	540
Eurocode 2 at 120th min (Analytical)	497	573
Shi et al at 120th min (Analytical)	420	485

5.3 Comparison of Structural Performances of Segments

In computation of point load capacity of segments a simple hand based computation is developed both for stressed and unstressed case.

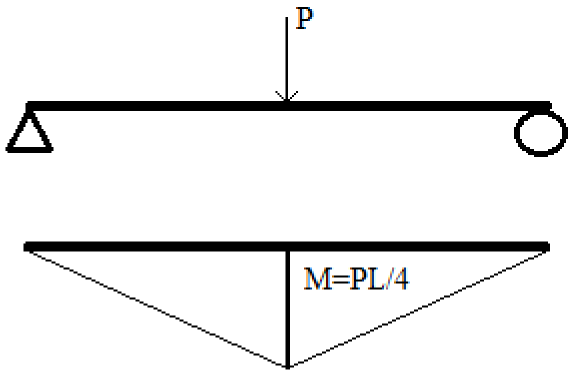

Figure 5.4 Simply Supported Beam

The load capacity can be written as:

$$P = \frac{4 \times M}{L} \qquad \text{Eqn. (5.5)}$$

Where "M" is the moment capacity of the section. For unstressed case the moment capacity can be computed using standard beam theory. The compression region is not affected from thermal loads and no degradation is accounted for compression zone.

$$M_{n,unstressed} = f_y^{PF} \times A_S \times (d - \frac{a}{2}) \qquad \text{Eqn. (5.6)}$$

$$a = \frac{A_s \times f_y}{0.85 \times f_c' \times b} \qquad \text{Eqn. (5.7)}$$

Where "f_y^{PF}" is post fire yield strength of reinforcement bar and "a" is depth of equivalent rectangular stress block.

For stressed case the moment capacity will be increased due to post-tension but also demand will be increased due to initial positive moment induced by post-tension.

$$M_{n,stressed} = M_n' - M_{Initial} \qquad \text{Eqn. (5.8)}$$

Where "M_n'" can be determined from an axial column interaction program that indicates degradation of material (FireCap). It shall be noted that the strut and tie model developed in hand analysis resulted in significant underestimation of load carrying capacity of test results.

5.3.1 FireCap Program

FireCap program is developed to evaluate load carrying capacity of reinforced concrete cross-sections based on fallowing the fire temperature-time curves. As shown in Figure 5.5 the program combines three types of strains to compute the stress at a given depth of layer. Initial fire strains due to thermal gradient are first component of primary strains that developed due to temperature profile. The layers away from hot surface will restrain the fire expansion of layers close to hot surface and forces will be equilibrated in the section. The main equation used to solve in the FireCap program is;

$$\varepsilon_{thermal\_i(t)} = \alpha_{i(t)} \times T_{i(t)} \qquad \text{Eqn. (5.9)}$$

Where "$\varepsilon_{thermal\_i(t)}$" is thermal strain in a layer, "$\alpha_{i(t)}$" is thermal coefficient of concrete at a given temperature in $1/^{o}C$ and "$T_{i(t)}$" is temperature at the layer in ^{o}C.

$$F_{thermal(t)} = \sum_{i=1}^{n} \sigma_{thermal\_i(t)} \times A_{i(t)} \qquad \text{Eqn. (5.10)}$$

Where "$F_{thermal(t)}$" is the thermal compressive force in concrete, n is total number of layers, "$\sigma_{thermal\_i(t)}$" is stress due to strain and "$A_{(t)}$" is the transformed area of the layer at a given temperature.

$$F_{equilibrate(t)} = -F_{thermal(t)} \qquad \text{Eqn. (5.11)}$$

$$M_{equilibrate(t)} = -F_{thermal(t)} \times a \qquad \text{Eqn. (5.12)}$$

Where "a" is the distance in millimeters between center of thermal compressive stresses and neutral axis of the section.

If the structure is redundant, the equilibrating forces need to be input into a representative structural analysis model to determine secondary forces. Forces can be converted not strains using standard engineer practice taking into account material degradation properties. Total strain at any layer;

$$\varepsilon_{total(t)} = \varepsilon_{thermal\_i(t)} + \varepsilon_{equilibtare\_(t)} + \varepsilon_{secondary\_i(t)} + \varepsilon_{0\_i(t)} < 0.011 \qquad \text{Eqn. (5.13)}$$

$\varepsilon_{total(t)} = 0 \rightarrow \varepsilon_{total(t)} > 0.011 \rightarrow Concrete \ldots spalled$

Where "$\varepsilon_{equilibrate\_i(t)}$" is equilibrating strain, "$\varepsilon_{secondary\_i(t)}$" is secondary strains and "$\varepsilon_{0\_i(t)}$" is strains due to creep of stress relaxation.

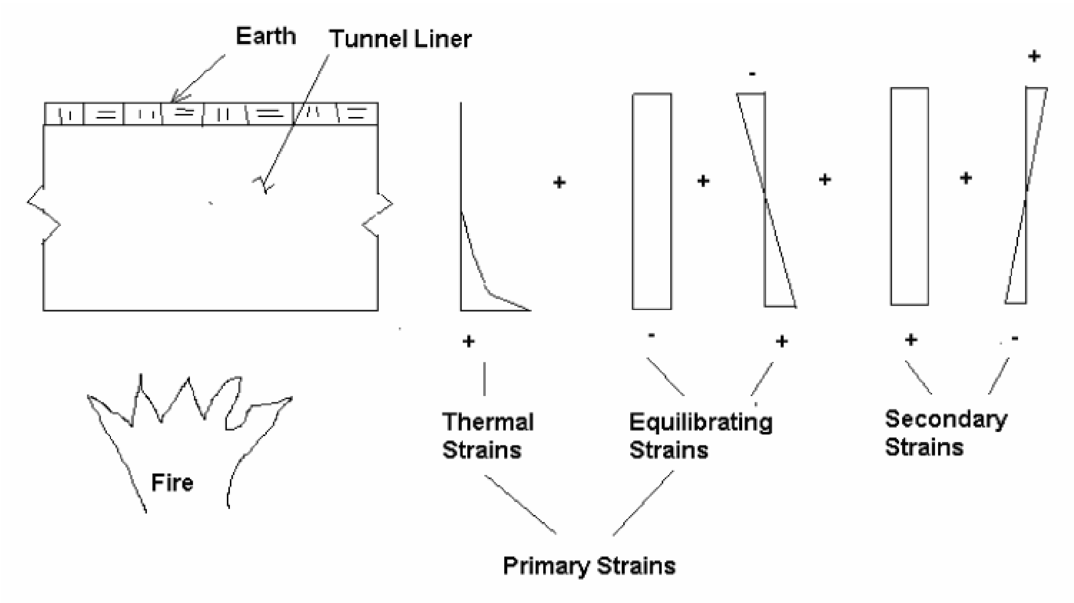

Figure 5.5 Total Strain Distribution [15]

5.3.2 Results of Calculations as Per ACI 216

ACI 216 is one of the codes which could be referenced as a guide for determining the fire endurance of concrete elements. The design approach is given in section 2.4 of this study.

The Guide contains information for determining the fire endurance of slabs and beams; also included is information on the properties of steel and concrete at high temperatures, temperature distributions within concrete members exposed to fire [2].

Consequently, the results of the capacity calculations are intended to be verified by using ACI 216 recommendations and guidelines.

Detailed calculations can be found in Appendix I.

Table 5.10 Fire Endurance and Capacity According to ACI 216

Specimen	Yield Capacity (ACI 216) (kN)	Ultimate Capacity (ACI 216) (kN)	Fire Endurance (ACI 216)
Type 1A-1	-	-	4.5 Hours
Type 1A-2	368.6	424.3	-
Type 2A-1	-	-	4.5 Hours
Type 2A-2	435.8	501.3	-
Type 1B-1	-	-	2.5 Hours
Type 1B-2	307.0	358.2	-
Type 2B-1	-	-	2.5 Hours
Type 2B-2	423.2	489.5	-

5.3.3 LARSA 4D Computer Model and Results

A manual iterative non-linear analysis has been selected to simulate the structural static loading test that can be modeled in a 2-D analysis. The components or parts of the model are shown in Figure 5.6.

Prior to selecting the manual iterative non-linear analysis, full automatic versions have been tried using LARSA, ANSYS and SOLIDWORKS. The solution convergence is not satisfactory and can not be used in predictory test results. As noticed above a simple but a labor intensive non-linear analysis is used as described below.

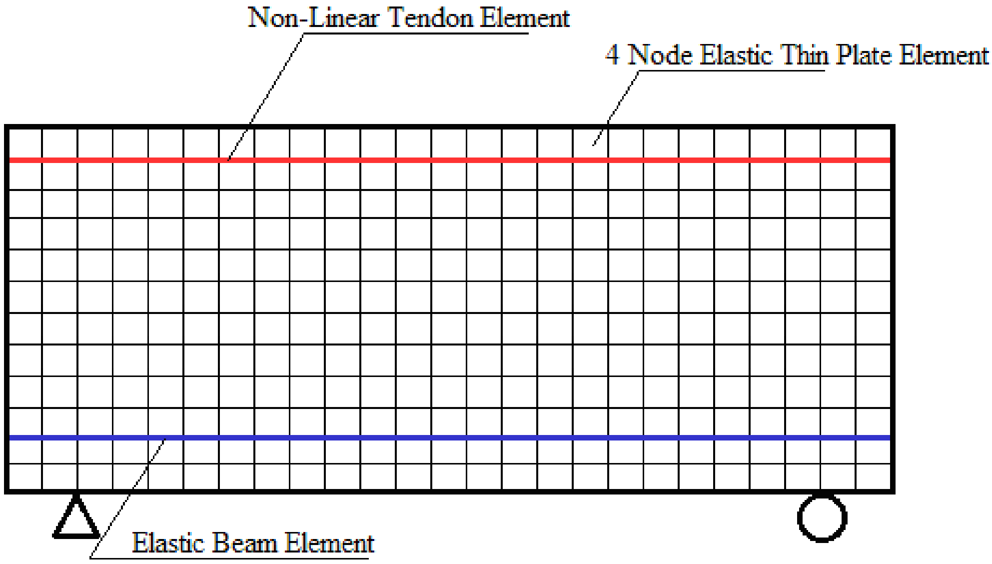

Figure 5.6 Components of the LARSA 4D Model

The point load is applied from mid region through five points located on surface of the beam. Supports are modeled similar to the conditions of test. Four node elements subjected to temperature effects of fire has been modeled with degraded properties based on the core testing. It shall be noted that core results represent the first 15 cm of concrete depth for compression strength. The model has 13 vertical layers and 40 horizontal layers and typical concrete cell has 30 mm x 30 mm dimensions. The total concrete cell elements are more then 500 elements. It is believed that this type of fine meshing is representative of the actual static loading test. The first five bottom layers have assigned degraded concrete properties. The non-linear tendon element can taken into account the change in stresses due to deformed shape during the test. The tendons are initially stressed to 0.75 f_{ps} of tendons. The analysis program can compute pre-stress loss. The steel bars are modeled with elastic beam element having the same steel area of the segment. A manual iterative procedure is used to predict the load carrying capacity at yielding of bottom steel using the following steps.

- A time stage analysis also known as construction stage analysis is used to apply the loads in time increments. At each time increment a ten kilonewton of load is applied.
- At the end of the time increment analysis, the analysis is stopped to check if any four node element simulating the concrete exceeded the pertaining tensile strength. If the tensile stress in element exceeded the limiting value, the element is deconstructed from the model prior to the next analysis step. The limiting tensile strength is taken as;

  $$f_t = 0{,}1 \times f_c^{\,f} \qquad \text{Eqn. (5.14)}$$

  Where "$f_c^{\,f}$" is the degraded concrete comparison strength. Also the rebar stresses are checked against the yielding limit of the reinforcement. If stresses reached to yielding limit, the analysis is terminated. If not, this step is repeated until the yielding limit is reached.

In the two-dimensional figure (x,y) [Figure 5.7] stresses are indicated as colors. The violet color shows the height of cracked zone. In the first picture it is at the bottom of the segment as the tensile strength of concrete is not exceeding yet and no crack have started to develop.

Following the increase of load, the segment starts to crack and the violet boundary line moves further towards the upper zone of the cross-section. This mean that the tensile strength of concrete is exceed and cracks start to occur. At every step the cracked zone of concrete (shown in yellowish color) is deconstructed and cross-section is analyzed accordingly.

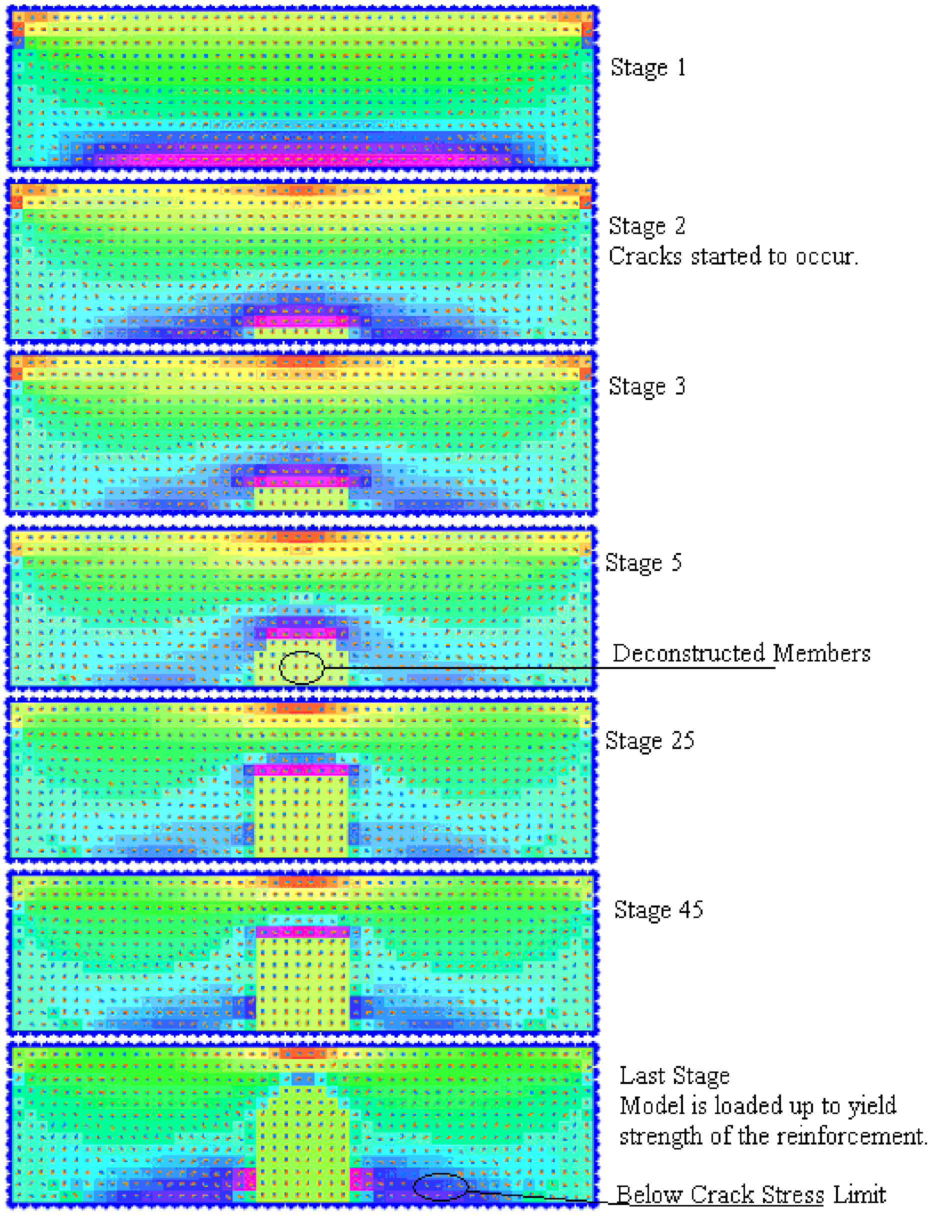

Figure 5.7 Iterative Steps in LARSA 4D

Table 5.11 Capacities According to LARSA Computer Program

Specimen	Yield Capacity (kN)	Displacement (mm)
Type 1A-1	435	0.683
Type 1A-2	447	0.680
Type 2A-1	484	0.825
Type 2A-2	517	0.714
Type 1B-1	375	0.764
Type 1B-2	438	0.655
Type 2B-1	495	0.926
Type 2B-2	517	0.825

5.3.4 Evaluation of Capacity Results

The simple beam point load is solved by practical hand computation to determine the critical moments. The cross-section analysis has been both performed by ACI 216 hand design check and FireCap program. ACI 216 methods recommends fire endurance in terms of hours for burnt segments rather then degraded capacity computation. Therefore the related cells are left blank for ACI 216. LARSA analysis can integrate system and cross-sectional analysis into one analysis. The results are listed in Table 5.12.

Table 5.12 Comparison of Capacity Results

Specimen	Yield Capacity (kN)			
	ACI 216	FireCap	LARSA	Test Results
Type 1A-1	-	317	435	450
Type 1A-2	368	384	447	460
Type 2A-1	-	427	484	495
Type 2A-2	435	456	517	490
Type 1B-1	-	333	375	353
Type 1B-2	307	369	438	467
Type 2B-1	-	441	495	490
Type 2B-2	423	467	517	520

The ACI 216 method results in 22%, the FireCap solution results in 15% and LARSA analysis results in 3% an average underestimation of test results. For design purpose the 15% to 20% is a reasonable safety factor to have in design. However for academic purposes, an advanced structural analysis such as the one described above (LARSA) could be used to simulate the test results more accurately.

5.3.5 Cut and Cover Tunnel Positive Moment Region Fire Endurance

The temperature after 2 hours of fire test is around 377 ^{o}C in 5 cm depth that is very close to mild reinforcement location. The yield strength of mild reinforcement will reduce by 10% [Figure 5.2] at that temperature. It indicates that the positive moment load carrying capacity of the section will not be significantly affected from heat during the fire.

Typically the cut and cover tunnels designed to have at least a factor of safety of 2.0 against failure under gravity loads. During extreme fires, minor repairable damage is permitted and factor of safety is desired to be above 1.0 against major damage. Therefore, 10% reduction in load carrying capacity of cut and cover tunnel subjected to 2 hours hydrocarbon fire will not result in failure of system and the minimum factor of safety will be around 1.8 to 1.9.

It has also been observed that ACI 216 temperature profile is slightly conservative as seen in Figure 5.2 and Figure 5.3 and can be used to assess the preliminary structural fire endurance positive moment region of cut and cover tunnels.

Assuming 60% of strength reduction in steel will put down the factor of safety against major damage just above 1.0; the corresponding temperature that will develop such reduction is determined to be 500 ^{o}C. [2]

The related ACI 216 tables indicate that the minimum required concrete cover is 35 mm for two hours hydrocarbon fire and is 50 mm for four hours hydrocarbon fires. Alternatively the following algorithm can be used to decide concrete cover. [Figure 5.8]

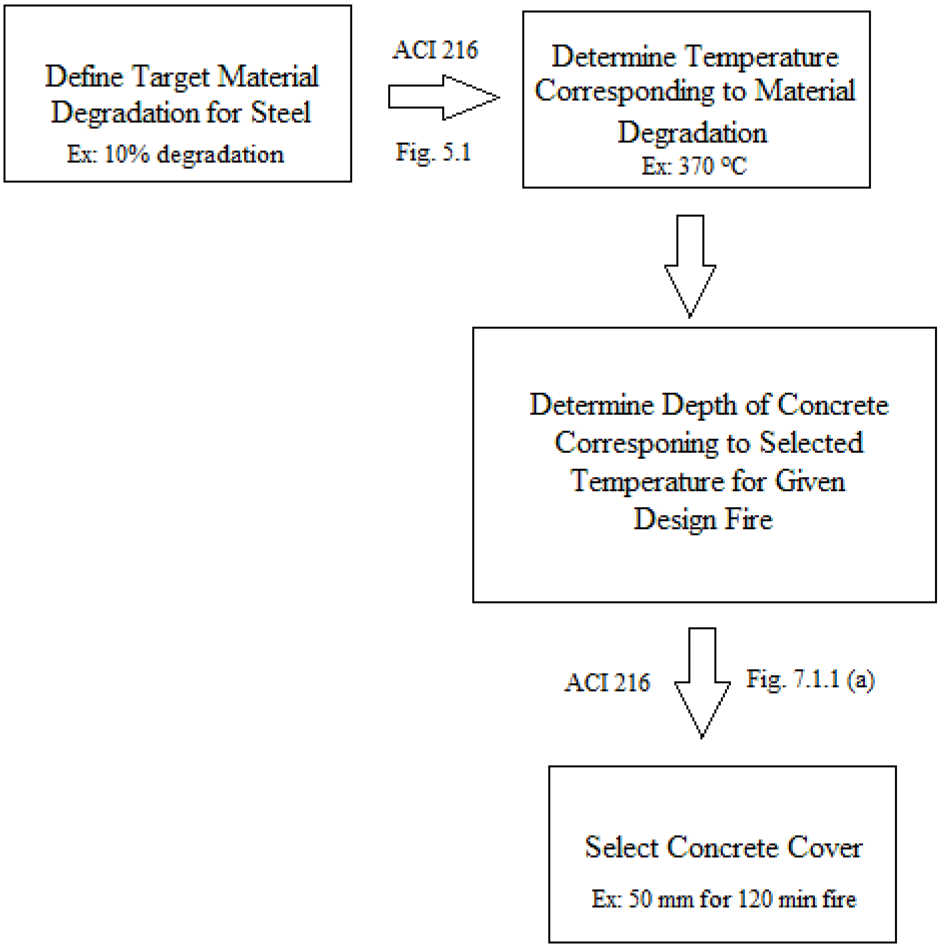

Figure 5.8 Concrete Cover Decision Algorithm

Temperature profiles in a cut and cover tunnel is expected to be lower then laboratory tests due to more cold regions surrounding the fire serving as heat sink.

CHAPTER 6

CONCLUSION

Results of the tests could be concluded as follows:

i) Two hours fire test results indicate that positive moment load carrying performance of cut and cover tunnel roof members will not be much different in the pre-fire, during fire and post-fire cases due to 60 mm concrete cover that prevents significant material degradation at steel. Due to minor spalling and rupture of concrete surfaces, repair and mitigation have to be taken into consideration. It has been estimated that 35 mm thickness of concrete over can also be used as a minimum value. For a four hour hydrocarbon fire 50 mm concrete cover is accepted as satisfactory.

ii) Temperature distribution, material degradation observed in this experimental research has similar characteristic that has been obtained into similar researches. ACI 216 temperature distribution profile developed for building type of fires is conservative compared to measured values in this tunnel fire research even if the concrete and fire is different.

iii) The difference between structural capacity of stressed, unstressed segments or segments with different mild reinforcement was not significant. In stressed segments, the moment capacity increases due to compressive axial load induced by tendons but also initial positive moment induced by tendons increase the demand that results in decrease in load carrying capacity.

iv) It is also observed that the difference of loss in load capacity between the burnt and unburnt specimens lies within 3-15 % since the reinforcement bars are placed in a safe concrete cover depth.

v) It is seen that the internal cracks develop up to 10 cm measured from surface exposed to fire as expected where the temperature effects are high during fire.

vi) It is observed that the results are compatible with the codes and standards in use for calculation and evaluation of fire on concrete structures for design purpose.

vii) For academic purposes advanced structural analysis method (LARSA 4D) suggested in this research could be used to simulate the structural fire behavior more accurately.

viii) As a preliminary design suggestion, the concrete cover for a cut and cover tunnel roof can be set to a minimum of 50 mm to serve up to critical four hours hydrocarbon fire. The four hours hydrocarbon fire is the longest tunnel design fire in terms of duration and intensity in terms of temperature-time area.

ix) The test fires are very close to two hours hydrocarbon tunnel fire in terms of area measured under temperature-time curve.

x) Minor explosive spalling observed at early minutes of fire.

REFERENCES

[1] ITA-AITES World Tunnel Congress, 7-12 May 2005, Istanbul.

[2] ACI 216 (American Concrete Institute), "Fire Endurance of Concrete Elements".

[3] Eurocode 2 "Design of concrete structures".

[4] "Structural Fire Safety of Standard Circular Railroad Tunnels Under Different Soil Conditions" A. Böncü, M.S Thesis, 2008.

[5] "Influence of Concrete Cover on Fire Resistance of Reinforced Concrete Flexural Members" Xudong Shi; Teng-Hooi Tan; Kang-Hai Tan and Zhenhai Guo, August 2004.

[6] Aestuver main brochure "Fire Safety Concepts for Underground Transport Systems", 2007.

[7] "Review of Mechanical Properties of HSC at Elevated Temperature" Long T. Phan and Nicholas J. Carino, February 1998.

[8] "Structural Fire Performance of Concrete and Shotcrete Tunnel Liners" A.Caner, S.Zlatanic, N.Munhaf, December 2005.

[9] "Use of Advanced Fire Fighting Technologies of Finely Atomized Water for Fire Protection of Metro Objects and Tunnels" A.S Chirko, A.V Karpyshev and M.D Segal, May 2005.

[10] "Cut and Cover Design and Construction In Reinforced Concrete" A.J. Powderham, 1990.

[11] "'K'(Chromel–Alumel) Type Thermocouples" , Last accessed 01.11.2010, http://www.azom.com/details.asp?ArticleID=1208#_Type_K_(Chromel

[12] "Cut and Cover Tunnels", Last accessed 01.11.2010, http://en.wikipedia.org/wiki/Tunnel

[13] "Reinforced Concrete" U. Ersoy, G. Ozcebe, T. Tankut; Department of Civil Engineering, Middle East Technical University, Ankara, Turkey, 2006.

[14] "C-S-H Gel", Last accessed 03.11.2010, http://iti.northwestern.edu/cement/monograph/Monograph5_4_2.html

[15] "Structural Fire Safety of Circular Concrete Railroad Tunnel Linings", A.Caner, A. Böncü, September 2009.

[16] "Losses in Pre-stress", Last accessed 10.11.2010, http://nptel.iitm.ac.in/courses/IIT-MADRAS/PreStressed_Concrete_Structures/pdf/2_Losses_in_Prestress/Section2.3.pdf

[17] "Spalling of Concrete Tunnel Linings In Fire"; C. Both, G.M. Wolsink, A.J. Breunese ; 2003.

[18] "Forecast of a brittle failure of concrete by fire." Zhukov, V.V, Scientific Research Institute for concrete and reinforced concrete, Moscow; 1994.

[19] Carvel R., "Fire protection in concrete tunnels", in The Handbook of Tunnel Fire Safety (Eds. Beard, A. & Carvel, R.) Thomas Telford, London, 2005.

[20] "Passive Fire Protection in Tunnels", Gabriel Alexander Khoury, Concrete for the construction industry, February 2003, Volume 7, Number 2.

[21] ASTM E 119 "Standard Test Methods for Fire Tests of Building Construction and Materials".

[22] ASTM C873 / C873M - 10 "Standard Test Method for Compressive Strength of Concrete Cylinders Cast in Place in Cylindrical Molds".

APPENDIX A

TUNNEL FIRE HISTORY

This appendix represents the major tunnel fires in order of county, year, name of the tunnel, possible causes of fire, duration and damage that fire occurred in.

Country	Year	Tunnel	Vehicle Where Fire Occurred	Most Possible Cause of Fire	Duration of Fire	Structures and Installations
Afghanistan	1982	Mazar-e-Sharif-Kabul-Salang	Soviet Military column, at least one petrol truck	Gas tanker explosion	Not available	Severe damage to structure
Australia	2007	Burnley Melbourne	Car/Truck collision	Fire due to collision	1 hour	Not available
Austria	2002	Tauern – Salzburg	Lorry	Faulty engine	Not available	Severe smoke production
Austria	2001	Gleinalm – A9 near Graz	Coach	Short circuit	> 1 hour	Severe smoke production
Austria	2001	Tauern – Salzburg	Cars	Head on collision of two cars	Not available	Not available
Austria	2000	Kitzsteinhorn – Kaprun Funicular Tunnel	Passenger train	Hydraulic oil leak onto heater	Not available	Line closed for over 1 year
Austria	2000	Tauern – Salzburg	HGV	Not available	½ hour	Not available
Austria	1999	Tauern – A10 Salzburg – Spittal	Lorry loaded with paint	Front-rear collision 4 cars and 2 lorries	15 hours	Serious damage
Austria	1995	Pfander	Lorry with trailer	Collision	1 hour	Serious damage
Austria	1989	Brenner	Dangerous goods exploded during construction	Dangerous goods	7 hours	Not available

Austria	1984	Felbertauern	Coach	Overheated brakes	> 1 hour	Damage to tunnel lining>100 m
Azerbaijan	1995	Baku	Railway/metro train	Electrical fault at rail car	Not available	Severe smoke production
Belgium	2004	Kinkempois	HGV	Not available	Not available	Closed for several days
Belgium	1987	Brussels Underground	Station fire	Not available	Not available	Dense smoke
Canada	2000	Montreal Metro	Cable fire	Cable	6 hours	Severe smoke
Canada	2000	Toronto Metro	Railway/ metro train	Not available	Not available	Line closed for 24 hours
Canada	1997	Toronto Metro	Train	Rubber matting under the track caught fire	Not available	Severe smoke
Canada	1976	Christie Street Metro Montreal	Station fire	Arson attack	Not available	Damage > $3 million
China	1998	Gueizhou-Guiyang/ Chansha	Train	Exploding gas canisters	Not available	Tunnel collapsed
Denmark	1994	Great Belt – Korsor during construction	Tunnel boring machine	Explosion at TBM	Not available	Severe damage
France	2004	Dulin – Chambery	Coach	Engine	1 hour	Not available
France	2003	Cret d’Eau	Train	Sleeper carriage	Not available	Not available
France	2003	Mornay	Train	Passenger carriage	5 hours	Not available

France	2002	A86- Versailles under construction	Cargo train	Engine Exploded	6 hours	Not available
France	2000	Toulon	Construction vehicle	Collusion of two construction vehicles	4 hours	Not available
France	1994	Castellar	HGV	Tyre caught fire	Not available	Not available
France	1986	L'Arme- Nice	Lorry with trailer	Breaking after high speed	Not available	Equipment destroyed
France	1985	Paris Metro	Station fire	Rubbish fire	Not available	Not available
France	1983	Frejus	HGV	Gearbox fire	2 hours	Severe damage
France	1979	Paris Metro	Train fire	Short circuit	Not available	Heavy smoke
France	1976	Crossing BP-A6 Paris	Lorry	High speed	4 hours	Serious damage
France	1976	Porte d'Italie B6	HGV	Engine fire	1 hour	Serious damage
France	1975	Chateau de Vincennes Metro	Train	Short circuit	Not available	Not available
France	1973	Porte d'Italie Metro	Railway Carriage	Arson attack	Not available	Not available
France	1972	Vierzy	Passenger train	Not available	Not available	Tunnel collapse
France/Italy	2004	Frejus	HGV	Breaks caught fire	2 ½ hours	Not available
France/Italy	1999	Mont Blanc	Lorry	Oil leakage	>53 hours	Serious damage

France/Italy	1990	Mont Blanc	Lorry	Motor	Not available	Equipment destroyed
France/Italy	1988	Mont Blanc	HGV	Not available	Not available	Not available
France/Italy	1981	Mont Blanc	HGV	Engine fire	Not available	Not available
France/Italy	1978	Mont Blanc	HGV	Not available	Not available	Dense smoke
France/Italy	1974	Mont Blanc	Lorry	Motor	15 minutes	Dense smoke
France/UK	1996	Channel Tunnel	HGV carrier	Polystyrene boxes	7 hours	Explosive spalling
Germany	2001	Dusseldorf U Bahn	Railway/ Metro train	Train roof caught fire	Not available	Not available
Germany	2001	Kurt Schumacher Platz station-Berlin	Train	Arc lamp	Not available	Severe smoke
Germany	2000	Berlin U Bahn	Train	Not available	Not available	Not available
Germany	1999	Leinebush-Göttingen	High speed cargo train	Train derailed	>12 hours	Not available
Germany	1984	Landungs U Bahn	Station fire	Arson attack	Not available	Severe damage $3 million
Germany	1983	Hauptbahnhof	Train	Electrical fire	Not available	Damage > $2 million
Hong Kong	2000	Cross Harbour	Car	Not available	½ hour	Not available
Italy	1997	Exilles rail -Sussa	Train transporting cars	Electrical fire	5 hours	Concrete spalling

Italy	1997	Prapontin-A32 Torino-Bardonecchia	HGV	Overheated breaks	4 hours	Explosive spalling
Japan	1980	Kajiwara	Truck	Gearbox fire	1 hour 30 min	Serious damage
Japan	1979	Shitzuoka-Nihonzaka	4 lorries, 2 cars	Front- rear collision	168 hours	Serious damage
Mexico	1985	Mexico City Underground	Metro car	Not available	Not available	Not available
Mexico	1975	Mexico City Underground	Train	Train collision	Not available	Not available
Netherlands	2001	Schiphol Airport	Not available	Electrical fire	Not available	Not available
Netherlands	1999	Amsterdam Underground	Railway/ Metro train	Train fire	Not available	Not available
New Zealand	2002	Homer-Milford	Coach	Engine fire	Not available	Not available
Norway	2000	Seljestad-E134 Drammen – Haugesund	Trailer collision	Front-rear collision	45 minutes	Serious damage
Norway	1993	Hovden-Hoyanger	Motorcycle, 2 cars	Front-rear collision	½ hour	111 m insulation material destroyed
Portugal	1976	Lisbon Underground	Train	Electrical fire	Not available	Damage over $1.8 million

Russia	1981	Okyabrskaya Underground Moscow	Station fire	Short circuit	Not available	Damage $250,000
Slovenia	2004	Trojane	Not available	Engine fire	Not available	Not available
South Africa	1994	Huguenot	Bus	Electrical fire	1 hour	Serious damage
South Korea	2003	Daegu Jungango Underground station	Train	Petrol fire	24 hours	Severe damage
Spain	2003	Guadarrama Rail	Train	Train accident	5 hours	Not available
Spain	1975	Guadarrama	Tanker	Tanker caught fire	2 hours 45 min	Severe damage
Spain	1944	Torre	Train fire	Multi train collision	>24 hours	Not available
Sweden	1960	Stockholm Underground	Train fire	Short circuit	Not available	Not available
Switzerland	2001	St. Gotthard-A2	Lorry	Collision	>48 hours	Collapse over 250 m of tunnel lining
Switzerland	1997	St. Gotthard-A2	Car transporter	Engine fire	3 hours	Slight damage
Switzerland	1994	St. Gotthard-A2	HGV	Tyre caught fire	2 hours	Severe damage
UK	1994	Kingways-Liverpool	Bus	Bus caught fire	Not available	Minor damage
UK	1984	Summit	Train with petroleum tankers	Derailment	72 hours	Severe damage
USA	2007	San Francisco McArthur bridge	Petrol tanker	Caught fire	Not available	Bridge deck collapsed

USA	2001	Howard street – Baltimore	Cargo train	Emergency brakes	12 hours	Not available
USA	1990	Los Angeles Subway	Timber supports during construction	Timber supports	Not available	45 m of tunnel collapsed
Yugoslavia	1971	Wranduk Zenica	Train fire	Engine fire	Not available	Not available

APPENDIX B

DETAILS AND RESULTS OF STRUCTURAL ANALYSIS PROGRAM

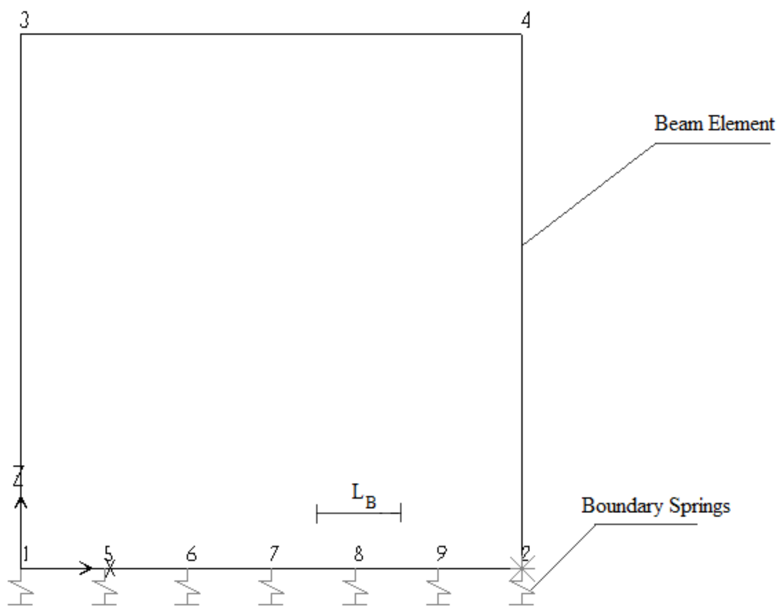

Figure B.1 Joint Labels

$$K_{soil} = K_{sg} \times A_{trib} \qquad \text{Eqn. (B.1)}$$

K_{sg}= Subgrade reaction modulus

A_{trib}= Tributary area for soil spring

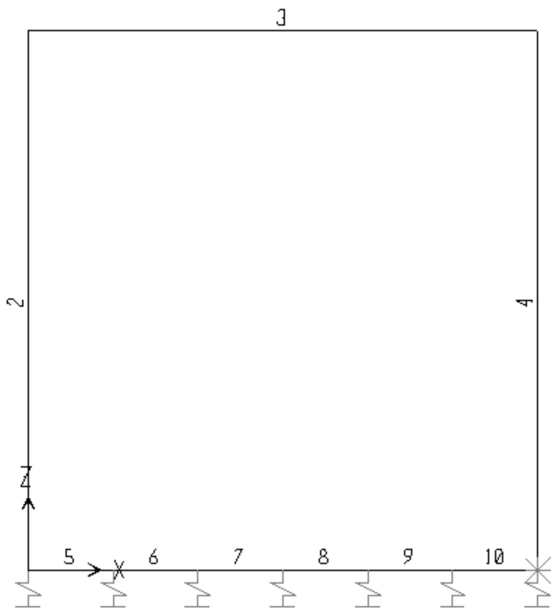

Figure B.2 Member Labels

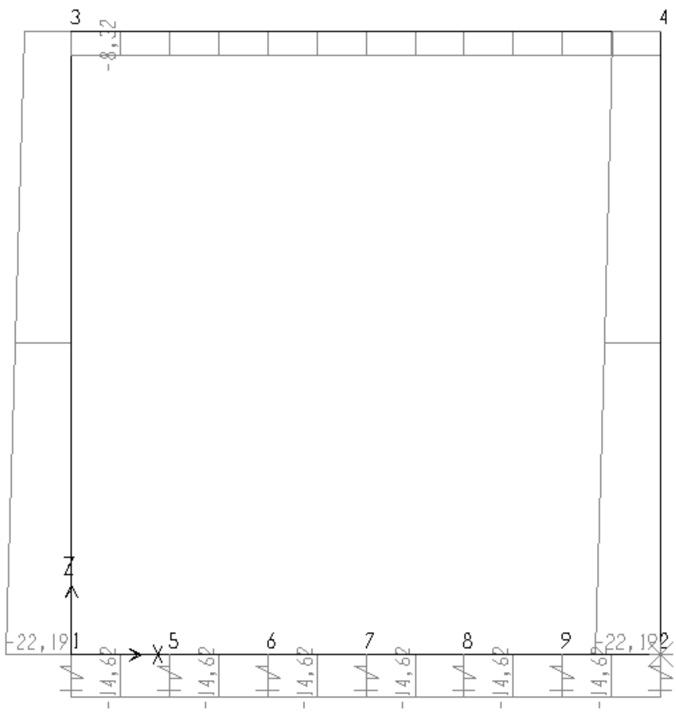

Figure B.3 Axial Load Diagram (Ton)

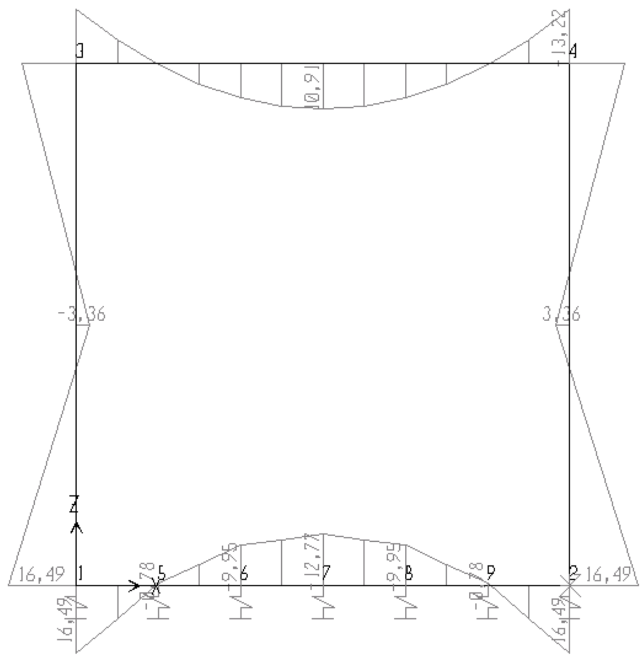

Figure B.4 Moment Diagram (M3-3) (Ton-m)

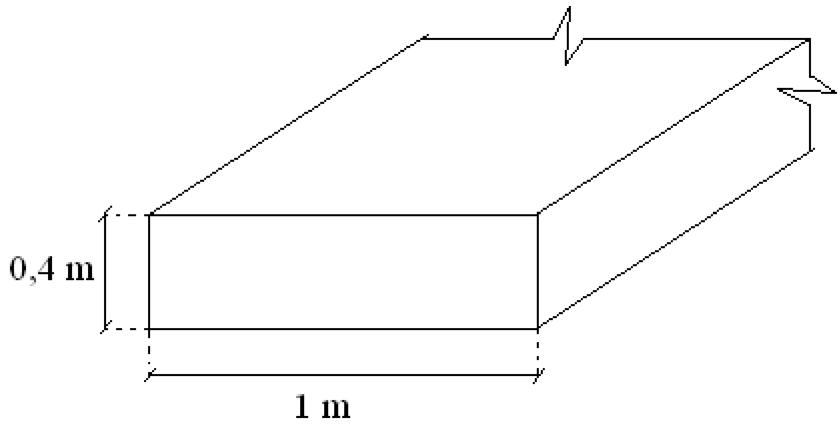

Figure B.5 Cross-Section

APPENDIX C

DESIGN OF THE SEGMENTS

Computed values for a 1 meter strip at mid-span are used for in design of test segments. The test segments are 0.6 meter wide and the analysis results have to be adjusted by 0.6 constant [Appendix B].

$M = 109.1 \times 0.6 = 68kNm$

$N = 83.2 \times 0.6 = 49.4kN$

$$K = \frac{b_w \times d^2}{M} \rightarrow K = \frac{60 \times 35^2}{68} = 108cm^2 / kN \qquad \text{Eqn. (C.1)}$$

$$A_s = \frac{M}{f_{yd} \times j \times d} \mp \frac{N}{f_{yd}} \qquad \text{Eqn. (C.2)}$$

$$A_s = \frac{68000}{0.365 \times 0.977 \times 350} - \frac{49.4}{0.365} = 405mm^2 = 4cm^2$$

Table C.1 K, J, ρ Chart for Rectangular Sections [13]

For C40 and S 420		
K (cm^2/kN)	j	ρ
13.92	0.984	0.002
9.36	0.976	0.003
7.08	0.968	0.004
5.71	0.96	0.005

As the next step it is investigated how to apply this moment to the specimen. Setting up a conventional load frame test facility in the furnace was not possible as the dimensions of the furnace were not big enough for installing such equipment. So pre-stressing seemed to be the only possibility. The method of applying pre-stressing on small specimens, finding out pre-cast factories ready to support this project, the limitations of the pre-stressing bed in this factories, transportation (although small specimens compared to actual tunnel element sizes) each had a weight of 865 kg, were restrictions and difficulties to be resolved.

After having resolved the above issues, it is decided to apply the pre-stressing with 3 strands each of 1.27 cm^2 cross-sectional area.

$$f_{pk} = 18t / cm^2 = 180kN / cm^2 \qquad \text{Eqn. (C.3)}$$

$$f_{pi} = 0.75 \times f_{pk} \qquad \text{Eqn. (C.4)}$$

$$f_{pi} = 0.75 \times 180 = 135kN / cm^2$$

Total area of the pre-stressing strands (3 x 1.27 cm^2):

$$A_{S\rho} = 2.955cm^2$$

$$P = f_{pi} \times A_{S\rho} \qquad \text{Eqn. (C.5)}$$

$$P = 135 \times 2.955 = 398.925kN$$

Losses: (Per MADRAS based AASHTO requirements)

1) Strand Relaxation Loss

If a strand is stressed and then held at constant strain, the stress decreases with time [16]. The decrease in stress is called strand relaxation loss and can be computed from the below equation. (Eqn. C.6)

$$RE = 0.08 \times f_{pi} = 0.08 * 135 = 10.80kN / cm^2 \qquad \text{Eqn. (C.6)}$$

2) Elastic Shortening Loss

When the tendons are cut and the pre-stressing force is transferred to the member, the concrete undergoes immediate shortening due to the pre-stress. The tendon also shortens by the same amount, which leads to the loss of pre-stress [16]. The equations of elastic shortening are as follows (Eqn C.7 – C.8):

$$ES = \frac{E_S}{E_c}\left(\frac{Pi}{Ac} + \frac{Pi \times e^2}{I} - \frac{Msw \times e}{I}\right) \quad \text{Eqn. (C.7)}$$

$$Ec = 1268 + 460 \times 4 = 3108 kN / cm^2$$

$$\frac{Es}{Ec} = \frac{20000}{3108} = 6.43$$

$$Pi = 0.9 \times Pj = 0.9 \times (As \times f_{pi}) = 0.9 \times (2.955 \times 135) = 359 kN \quad \text{Eqn. (C.8)}$$

$$\frac{Pi}{Ac} = \frac{359}{2400} = 0.14 kN / cm^2$$

$$\frac{Pi \times e^2}{I} = \frac{359 \times 17^2}{320000} = 0.32 kN / cm^2$$

$$\frac{Msw \times e}{I} = \frac{\frac{(0.4 \times 0.6 \times 2.5 \times 10^{-9}) \times 1.5^2}{8} \times 17}{320000} = 8.6 \times 10^{-15} kN / cm^2$$

$$ES = 6.43 \times (0.14 + 0.32 - 8.6 \times 10^{-15}) = 2.99 kN / cm^2$$

3) <u>Creep Loss</u>

Creep of concrete is defined as the increase in deformation with time under constant load. Due to the creep of concrete, the pre-stress in the tendon is reduced with time [16].

$$\varepsilon_{ce} = \frac{\sigma_{co}}{E_{c28}} \phi_{ce} \quad \text{Eqn. (C.9)}$$

σ_{co} = Stress in concrete under sustained loading

E_{c28} = Modulus of elasticity of 28 days old concrete

$Ø_{ce}$ = Creep coefficient

To find σ_{co}:

σ_p= Stress due to axial loading

$$\sigma_p = \frac{P}{A} = \frac{398.925}{2400} = 0.166 kN / cm^2 \quad \text{Eqn. (C.10)}$$

σ_{pe}= Stress due to eccentricity

$$\sigma_{pe} = \frac{P \times e \times c}{I} = \frac{398.925 \times 17 \times 20}{320000} = 0.4238 kN/cm^2 \qquad \text{Eqn. (C.11)}$$

σ_{DL}= Stress due to dead load

$$W_{DL} = 0.6t/m = 0.06kN/cm$$

$$M_{DL} = \frac{W_{DL} \times L^2}{8} = \frac{0.06 \times 150^2}{8} = 168.72 kNcm \qquad \text{Eqn. (C.12)}$$

$$\sigma_{DL} = \frac{M_{DL} \times c}{I} = \frac{168.72 \times 20}{320000} = 0.0105 kN/cm^2 \qquad \text{Eqn. (C.13)}$$

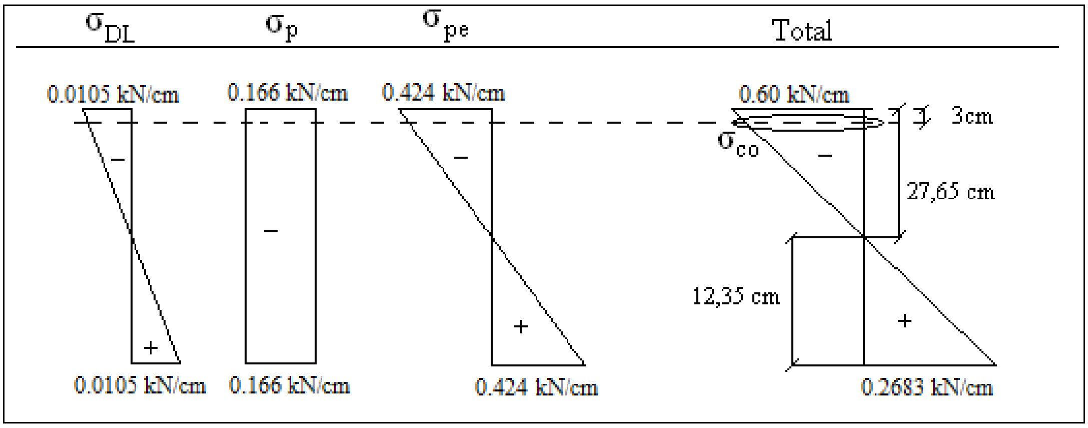

Figure C.1 Stress Distributions without Pre-stressing Losses

+ = Tension

- = Compression

$\sigma_{co} = 0.5355 kN/cm^2 \qquad E_{c28} = 3108 kN/cm^2$

<u>To find $\varnothing_{ce}$:</u>

$$\phi_{ce} = 0.4\beta_d + \phi_{f1} \times \phi_{f2} \times \beta_f \qquad \text{Eqn. (C.14)}$$

ϕ_{f1} = *Creep Coefficient*

Table C.2 Creep Coefficient ϕ_{f1} [13]

Ambient Environment	Relative Humidity	Creep Coefficient ϕ_{f1}
Water	-	0.8
Very Damp	90%	1.0
Normal	***70%***	***2.0***
Dry	40%	3.0

ϕ_{f1}=2.0

ϕ_{f2} =*Creep Coefficient*

Table C.3 Creep Coefficient ϕ_{f2} [13]

Coefficient	Fictitious Thickness l_e (mm)					
	50	100	200	400	800	≥1500
ϕ_{f2}	1.85	1.70	1.55	1.40	1.25	1.12

$$l_e = \frac{2\times A_c}{u'} = \frac{2\times(400\times600)}{2\times(400+600)} = 342.8mm \qquad \text{Eqn. (C.15)}$$

A_c = Cross-sectional Area

u' = Perimeter in contact with environment

ϕ_{f2} = 1.44

β_d and β_f Coefficient

Table C.4 Creep Coefficients β_d *and* β_f [13]

Coefficient		Period							
		5 days	10 days	30 days	2 months	***3 months***	1 years	2 years	3 years
	β_d	0.35	0.40	0.50	0.60	0.68	0.90	0.97	0.99
β_f	l_e=50mm	0.18	0.26	0.44	0.56	0.63	0.82	0.91	0.93
	100 mm	0.18	0.25	0.40	0.53	0.59	0.79	0.88	0.90
	200 mm	0.17	0.24	0.38	0.48	0.53	0.72	0.83	0.85
	400 mm	0.17	0.23	0.34	0.42	0.47	0.65	0.77	0.80
	800 mm	0.16	0.22	0.30	0.37	0.40	0.55	0.68	0.70
	≥1500mm	0.15	0.20	0.26	0.30	0.32	0.45	0.58	0.63

As the test specimens were going to be crushed after 3 months, three month values are taken into consideration in design.

β_d = 0.68

β_f = 0.48

$$\phi_{ce} = 0.4\times(0.68)+(2)\times(1.44)\times(0.48) = 1.6544$$

$$\varepsilon_{ce} = \frac{0.5355}{3108}\times1.6544 = 2.85\times10^{-4}$$

Creep Loss => $CR = \varepsilon_{ce} \times Es$ Eqn. (C.16)

$$CR = (2.85 \times 10^{-4}) \times 20000 = 5.7 kN/cm^2$$

4) Shrinkage Loss

Shrinkage of concrete is defined as the contraction due to loss of moisture. Due to the shrinkage of concrete, the pre-stress in the tendon is reduced with time [16].

$$\varepsilon_{cs} = \varepsilon_{s1} \times \varepsilon_{s2} \times \beta_s \qquad \text{Eqn. (C.17)}$$

ε_{s1}= Shrinkage Coefficient

Table C.5 Shrinkage Coefficient ε_{s1} [13]

Ambient Environment	Relative Humidity	Shrinkage Coefficient ε_{s1}	Coefficient for Thickness λ
Water	-	+0.00010	30
Very Damp	90%	-0.00013	5
Normal	***70%***	***-0.00032***	***1.5***
Dry	40%	-0.00052	1

$$l_e = \lambda \times \frac{2 \times A_c}{u'} = 1.5 \times \frac{2 \times (400 \times 600)}{2 \times (400 + 600)} = 514.3mm \qquad \text{Eqn. (C.18)}$$

ε_{s2}= *Shrinkage Coefficient*

Table C.6 Shrinkage Coefficient ε_{s2} [13]

Coefficient	Fictitious Thickness l_e (mm)					
	50	100	200	400	500	≥1500
Shrinkage, ε_{s2}	1.20	1.05	0.90	0.80	0.75	0.70

ε_{s2}= 0,75

βs= Shrinkage Coefficient

Table C.7 Shrinkage Coefficient βs [13]

l_e (mm)		Period							
		5 days	10 days	30 days	2 months	***3 months***	1 years	2 years	3 years
βs	50mm	0.30	0.36	0.55	0.68	0.75	0.90	0.94	0.97
	100 mm	0.16	0.22	0.40	0.52	0.60	0.84	0.90	0.93
	200 mm	0.07	0.10	0.21	0.32	0.40	0.65	0.80	0.87
	400 mm	0.02	0.04	0.10	0.18	0.22	0.45	0.60	0.70
	800 mm	0	0.01	0.03	0.07	0.10	0.20	0.35	0.45
	≥1500mm	0	0	0.01	0.02	0.04	0.10	0.18	0.23

$\beta s = 0.185$

$\varepsilon_{cs} = (-0.00032)\times(0.75)\times(0.185) = 4.44\times10^{-5}$

Shrinkage Loss => $SH = \varepsilon_{cs} \times Es$ Eqn. (C.19)

$SH = (4.44\times10^{-5})\times 20000 = 0.888 kN/cm^2$

<u>Total Loss</u>

$\rightarrow (135 - 10.80 - 2.995 - 5.70 - 0.888)\times 2.955 = 338.69 kN$

If the transfer length is taken as 50Ø =>$1.27\times 50 = 63.5 cm$

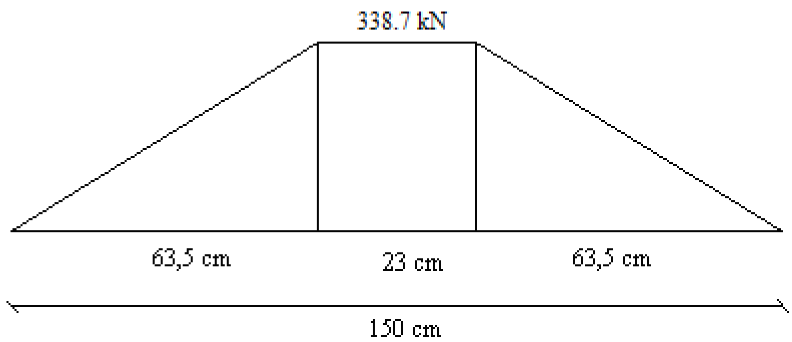

Figure C.2 Load Distributions after Pre-stressing Losses

Stress created by the pre-stressing after the losses and the amount of reinforcement required:

σ_p= Stress due to axial loading

$$\sigma_p = \frac{P}{A} = \frac{338.69}{2400} = 0.141 kN/cm^2$$

σ_p= Stress due to eccentricity

$$\sigma_{pe} = \frac{P \times e \times c}{I} = \frac{338.69 \times 17 \times 20}{320000} = 0.3598 kN/cm^2$$

σ_{DL}= Stress due to dead load

$$W_{DL} = 0.6t/m = 0.06kN/cm$$

$$M_{DL} = \frac{W_{DL} \times L^2}{8} = \frac{0.06 \times 150^2}{8} = 168.72 kNcm$$

$$\sigma_{DL} = \frac{M_{DL} \times c}{I} = \frac{168.72 \times 20}{320000} = 0.0105 kN/cm^2$$

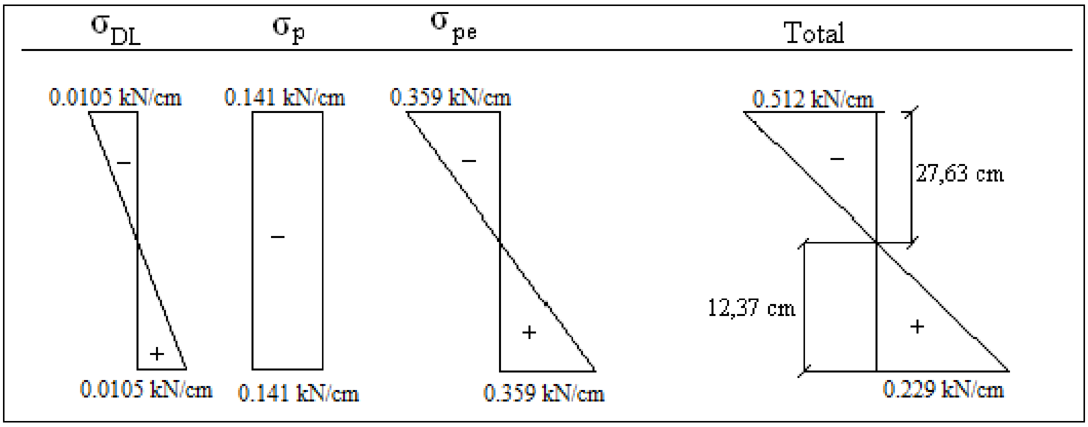

Figure C.3 Stress Distributions after Pre-stressing Losses

+ = Tension

- = Compression

$$P = \frac{0.2292 \times 12.37 \times 60}{2} = 85kN$$

$$As = \frac{8.5}{36.5} = 2.32cm^2$$

Although the results of the analysis indicate the necessity of using 4 cm^2 reinforcement, due to the restrictions of the segment sizes (only 60 cm allows for 3 strands), it was only possible to create a moment requiring reinforcement 2.32 cm^2. It was decided to use 5 cm^2 reinforcement. Stirrups are placed at even 15 cm to avoid failure under shear stresses.

APPENDIX D

SPECIMEN PROPERTIES

This appendix represents the properties of specimens in order of concrete class, additives, density of fresh concrete, density of hardened concrete, slump, temperature of fresh concrete, type of concrete, chloride content, sample dimension, cement used.

Table D.1 Specimen Properties-1

Specimen Type	**Type 1A-1**	**Type 1A-2**	**Type 2A-2**	**Type 2A-1**
Concrete Class / $f_{ck,cube}$	C40/50 /500	C40/50 /500	C40/50 /500	C40/50 /500
Additives / Properties	SIKAMENT 300 / Hyper Plasticizer	SIKAMENT 300 / Hyper Plasticizer	SIKAMENT 300 / Hyper Plasticizer	SIKAMENT 300 / Hyper Plasticizer
Density of Fresh Concrete (kg/m3) (TS EN 12350-6)	2423	2421	2425	2421
Density of Hardened Concrete (kg/m3) / Concrete Density Class (TS EN 12350-7)	2357 / Normal Weight Concrete	2357 / Normal Weight Concrete	2357 / Normal Weight Concrete	2357 Normal Weight Concrete
Slump (cm) (TS EN 12350-2)	12	14	13	13
Temp. of Fresh Concrete (^{o}C)	24	20	26	24
Ambient Temp. (^{o}C)	19	16	15	21
Dmax (mm)	22.4	22.4	22.4	22.4
Type of Concrete for Pre-cast Elements	3 No Aggregate	3 No Aggregate	3 No Aggregate	3 Aggregate
Chloride Content	Cl 0.10	Cl 0.10	Cl 0.10	Cl 0.10
Sample Type	Cube	Cube	Cube	Cube
Sample Dimension (mm) (TS EN 12390-1)	150*150*150	150*150*150	150*150*150	150*150*150
Cross-section of Sample (cm^2)	225	225	225	225
Protection of Specimen	Moisture Cure	Moisture Cure	Moisture Cure	Moisture Cure
Cement Used (TS EN 197-1)	PC-42.5	PC-42.5	PC-42.5	PC-42.5
Development of Hardening Process	Fast	Fast	Fast	Fast

Table D.2 Specimen Properties-2

Specimen Type	**Type 1B-1**	**Type 1B-2**	**Type 2B-1**	**Type 2B-2**
Concrete Class / $f_{ck,cube}$	C40/50 /500	C40/50 /500	C40/50 /500	C40/50 /500
Additives / Properties	SIKAMENT 300 / Hyper Plasticizer	SIKAMENT 300 / Hyper Plasticizer	SIKAMENT 300 / Hyper Plasticizer	SIKAMENT 300 / Hyper Plasticizer
Density of Fresh Concrete (kg/m3) (TS EN 12350-6)	2421	2419	2418	2418
Density of Hardened Concrete (kg/m3) / Concrete Density Class (TS EN 12350-7)	2357 / Normal Weight Concrete	2357 / Normal Weight Concrete	2357 / Normal Weight Concrete	2357 / Normal Weight Concrete
Slump (cm) (TS EN 12350-2)	13	13	13	12
Temp. of Fresh Concrete (^{o}C)	22	25	25	28
Ambient Temp. (^{o}C)	18	18	21	23
Dmax (mm)	22.4	22.4	22.4	22.4
Type of Concrete for Pre-cast Elements	3 No Aggregate	3 No Aggregate	3 No Aggregate	3 No Aggregate
Chloride Content	Cl 0.10	Cl 0.10	Cl 0.10	Cl 0.10
Sample Type	Cube	Cube	Cube	Cube
Sample Dimension (mm) (TS EN 12390-1)	150*150*150	150*150*150	150*150*150	150*150*150
Cross-section of Sample (cm^2)	225	225	225	225
Protection of Specimen	Moisture Cure	Moisture Cure	Moisture Cure	Moisture Cure
Cement Used (TS EN 197-1)	PC-42.5	PC-42.5	PC-42.5	PC-42.5
Development of Hardening Process	Fast	Fast	Fast	Fast

APPENDIX E

COMPARISON BETWEEN BURNT AND UNBURNT SEGMENTS

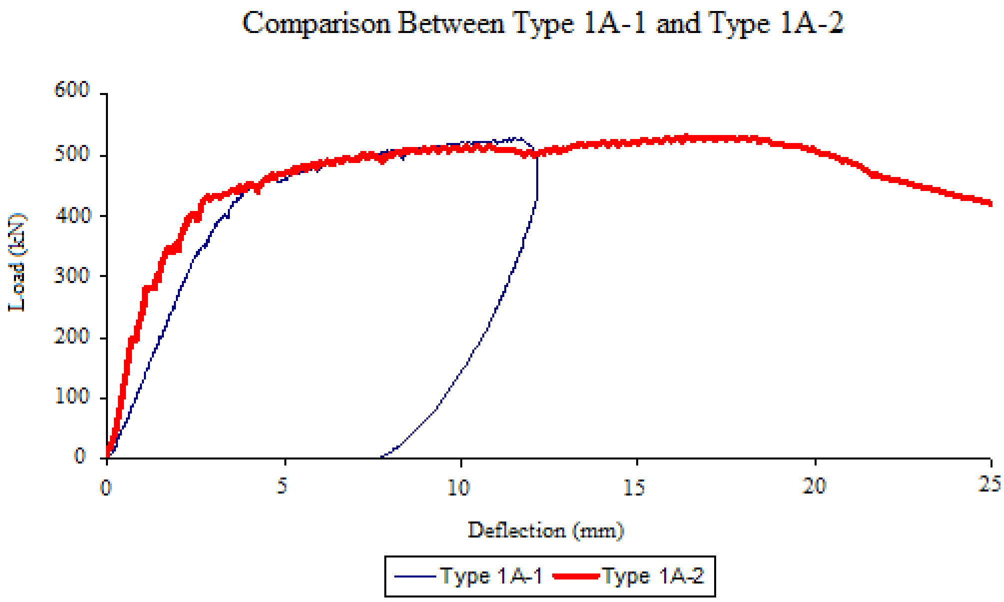

Figure E.1 Load-Deflection Diagram (Type 1A-1, Type 1A-2)
Type 1A-1: Ø12 Unstressed – Burnt
Type 1A-2: Ø12 Unstressed – Unburnt

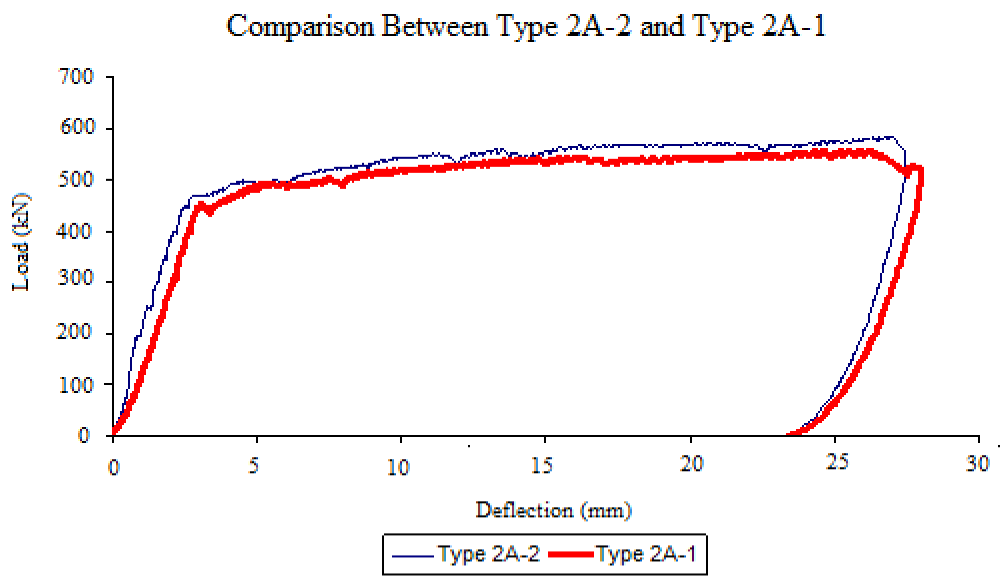

Figure E.2 Load-Deflection Diagram (Type 2A-1, Type 2A-2)
Type 2A-2: Ø14 Unstressed – Unburnt
Type 2A-1: Ø14 Unstressed – Burnt

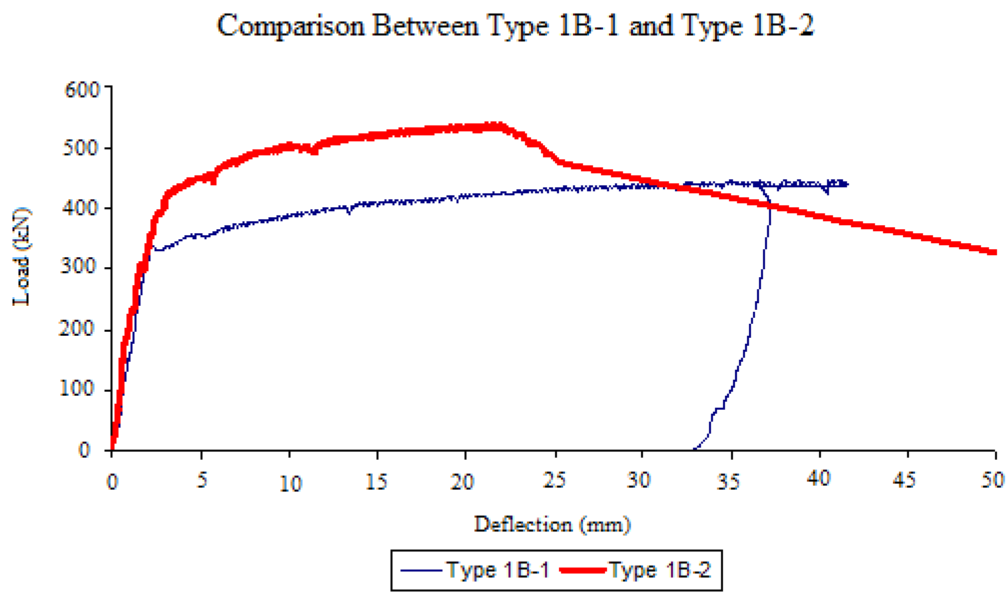

Figure E.3 Load-Deflection Diagram (Type 1B-1, Type 1B-2)
Type 1B-1: Ø12 Stressed- Burnt
Type 1B-2: Ø12 Stressed - Unburnt

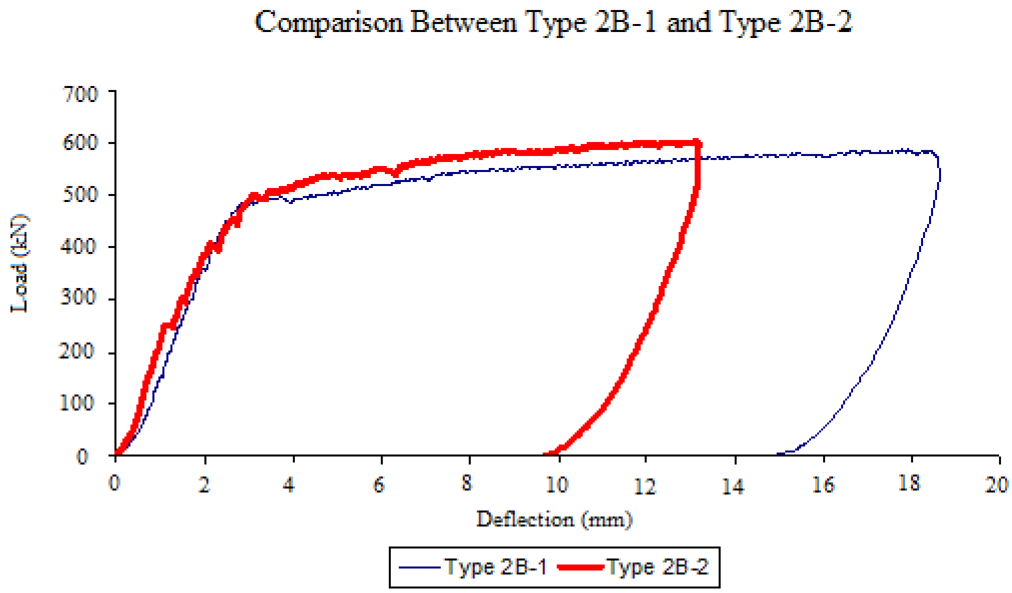

Figure E.4 Load-Deflection Diagram (Type 2B-1, Type 2B-2)
Type 2B-1: Ø14 Stressed - Burnt
Type 2B-2: Ø14 Stressed - Unburnt

APPENDIX F

COMPARISON BETWEEN STRESSED AND UNSTRESSED SEGMENTS

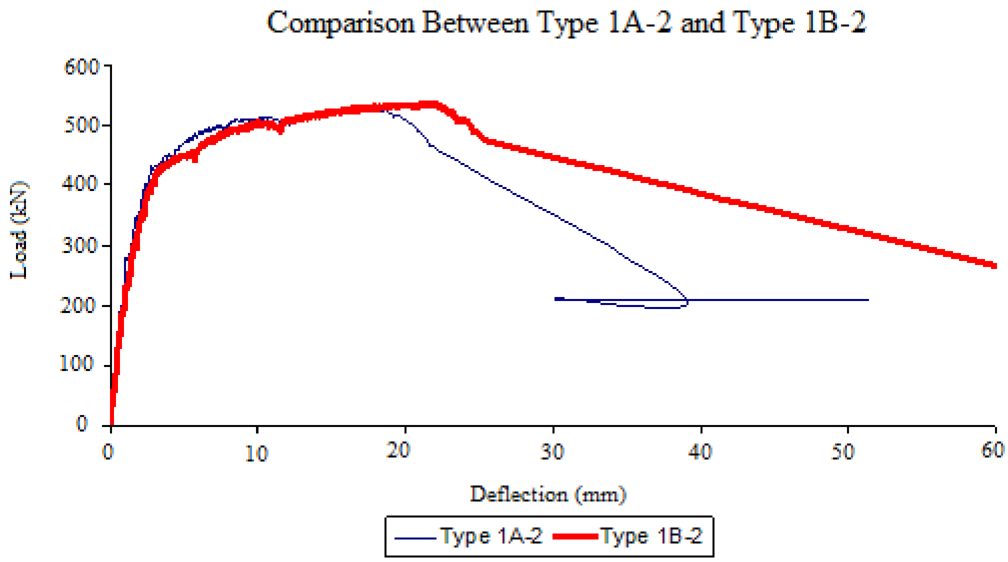

Figure F.1 Load-Deflection Diagram (Type 1A-2, Type 1B-2)
Type 1A-2: Ø12 Unstressed – Unburnt
Type 1B-2: Ø12 Stressed - Unburnt

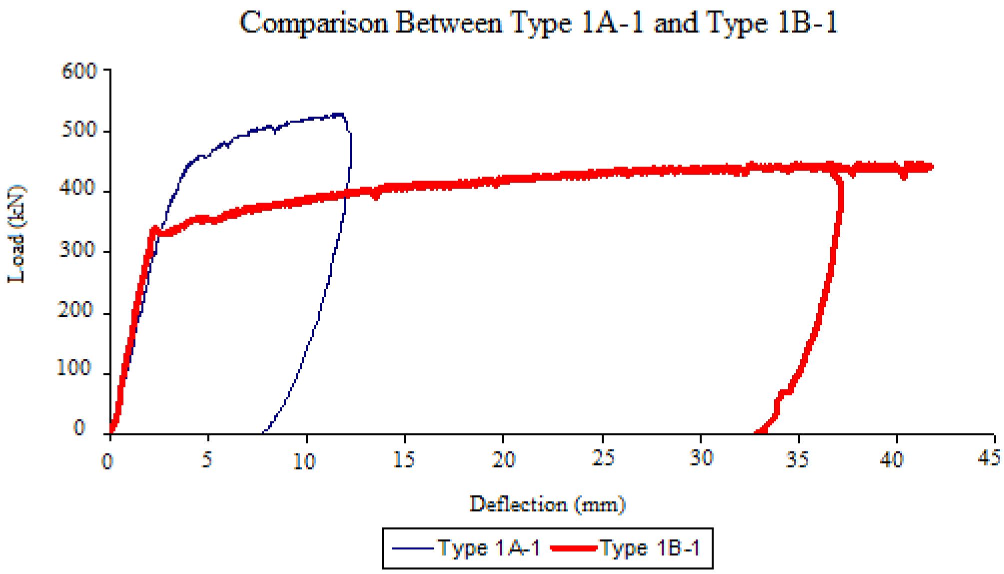

Figure F.2 Load-Deflection Diagram (Type 1A-1, Type 1B-1)
Type 1A-1: Ø12 Unstressed – Burnt
Type 1B-1: Ø12 Stressed – Burnt

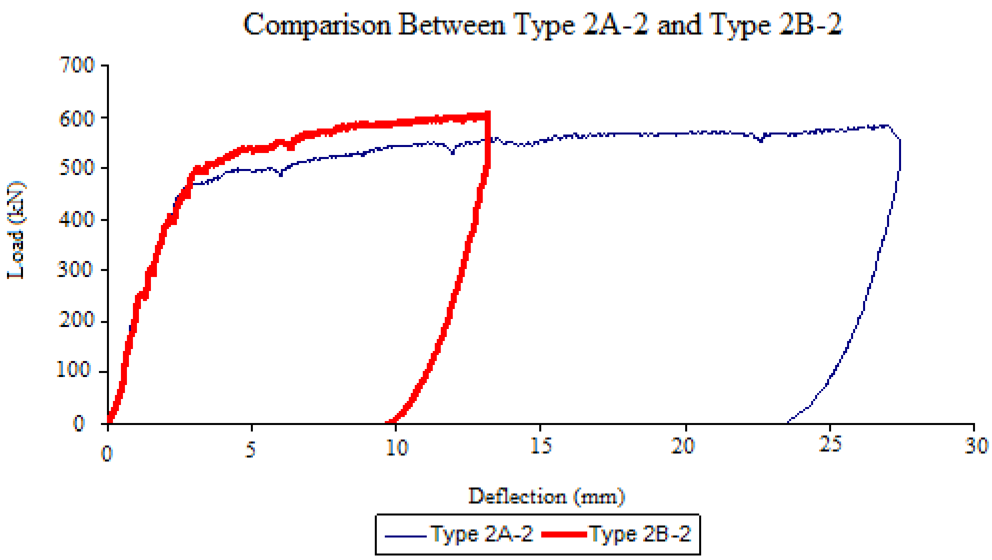

Figure F.3 Load-Deflection Diagram (Type 2A-2, Type 2B-2)
Type 2A-2: Ø14 Unstressed – Unburnt
Type 2B-2: Ø14 Stressed - Unburnt

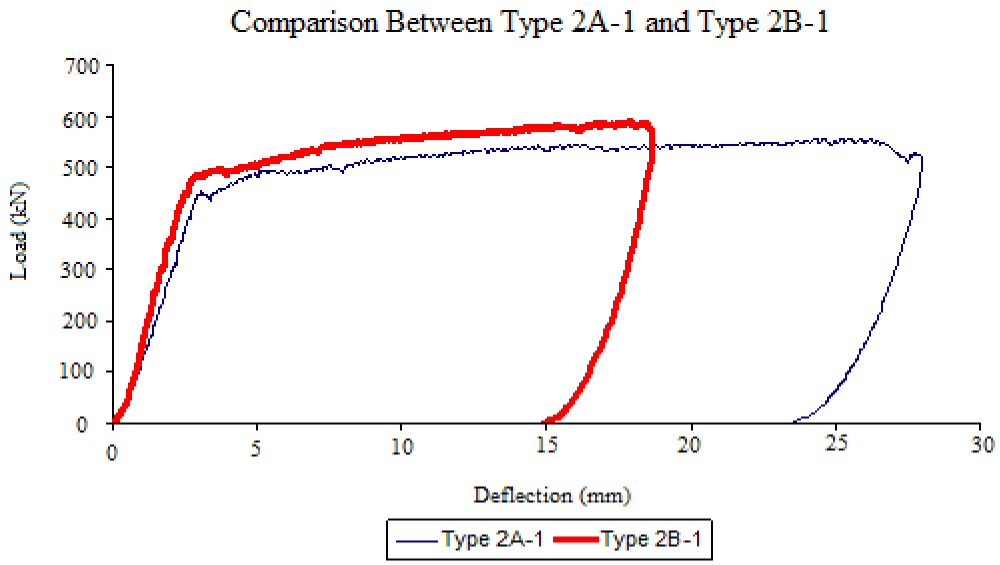

Figure F.4 Load-Deflection Diagram (Type 2A-1, Type 2B-1)
Type 2A-1: Ø14 Unstressed – Burnt
Type 2B-1: Ø14 Stressed - Burnt

APPENDIX G

GENERAL COMPARISONS OF LOAD DEFLECTION DIAGRAMS

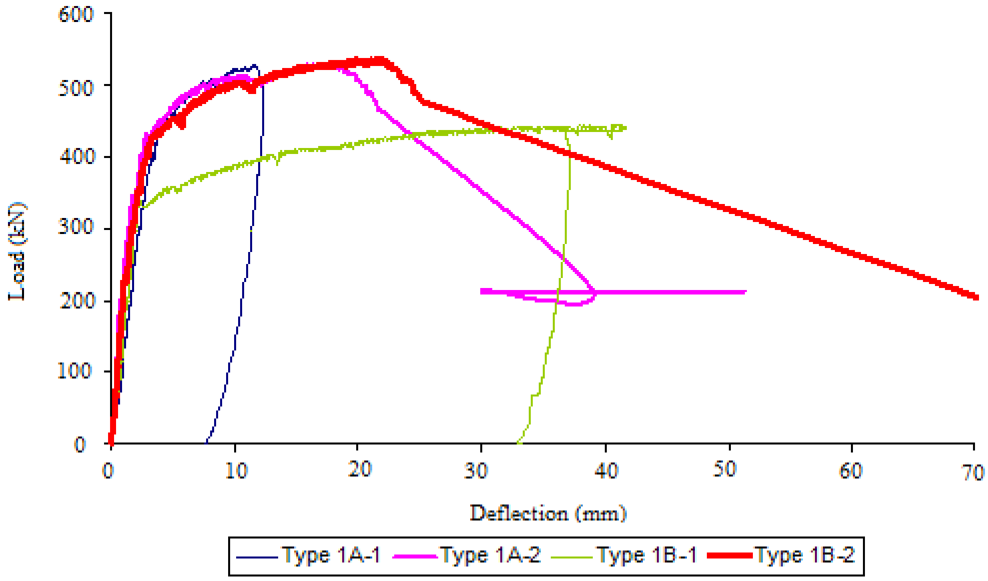

Figure G.1 Load-Deflection Diagram (Type 1A-1, 1A-2, 1B-1, 1B-2)
Type 1A-1: Ø12 Unstressed – Burnt
Type 1A-2: Ø12 Unstressed – Unburnt
Type 1B-1: Ø12 Stressed - Burnt
Type 1B-2: Ø12 Stressed - Unburnt

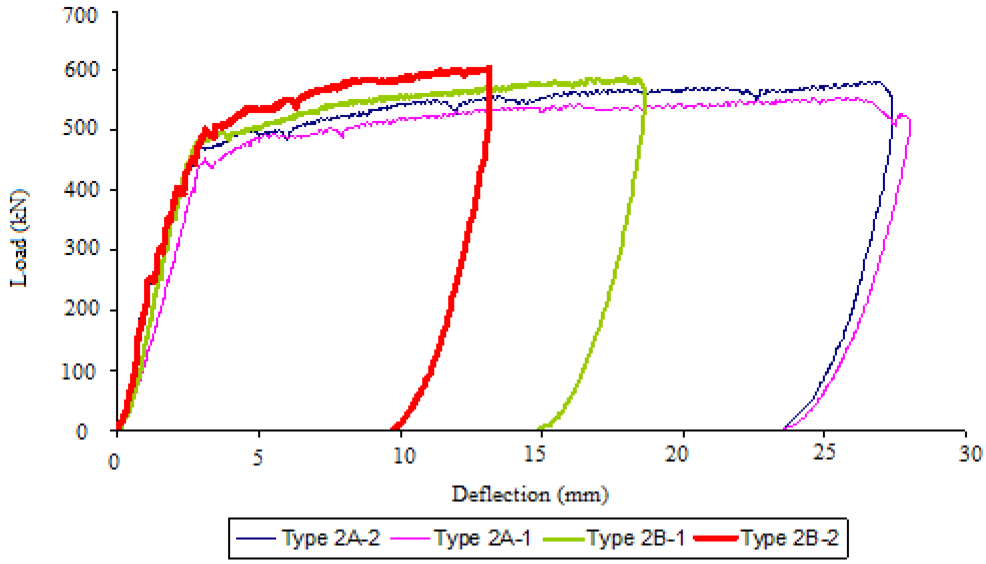

Figure G.2 Load-Deflection Diagram (Type 2A-1, 2A-2, 2B-1, 2B-2)
Type 2A-2: Ø14 Unstressed – Unburnt
Type 2A-1: Ø14 Unstressed – Burnt
Type 2B-1: Ø14 Stressed - Burnt
Type 2B-2: Ø14 Stressed - Unburnt

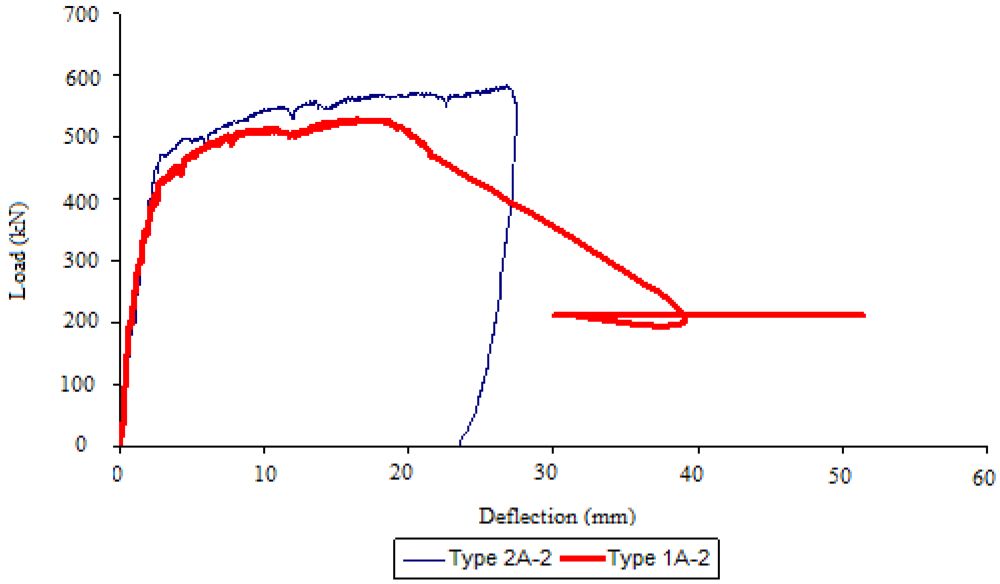

Figure G.3 Load-Deflection Diagram (Type 1A-2, Type 2A-2)
Type 1A-2: Ø12 Unstressed – Unburnt
Type 2A-2: Ø14 Unstressed – Unburnt

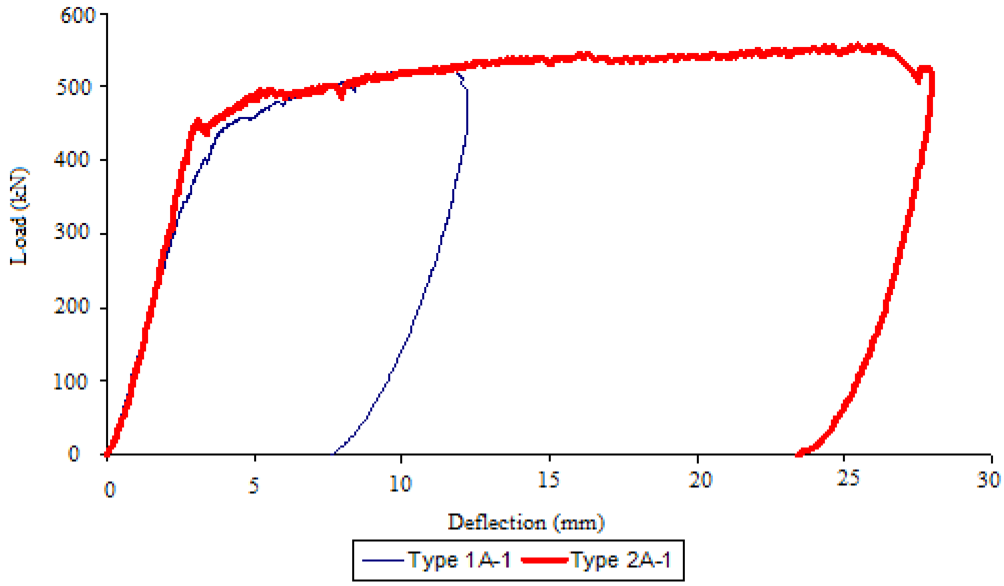

Figure G.4 Load-Deflection Diagram (Type 1A-1, Type 2A-1)
Type 1A-1: Ø12 Unstressed – Burnt
Type 2A-1: Ø14 Unstressed – Burnt

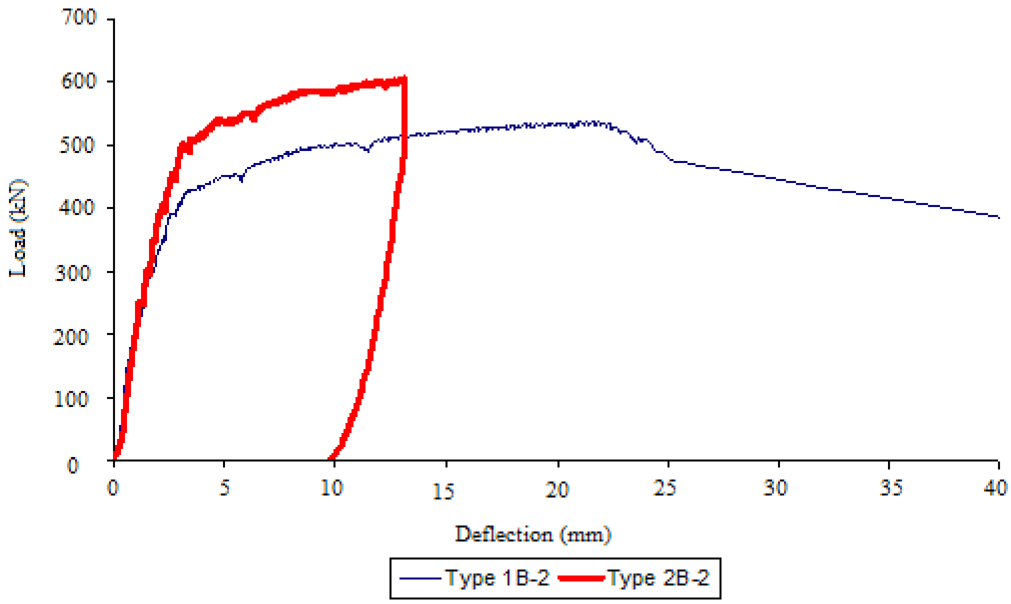

Figure G.5 Load-Deflection Diagram (Type 1B-2, Type 2B-2)
Type 1B-2: Ø12 Stressed - Unburnt
Type 2B-2: Ø14 Stressed - Unburnt

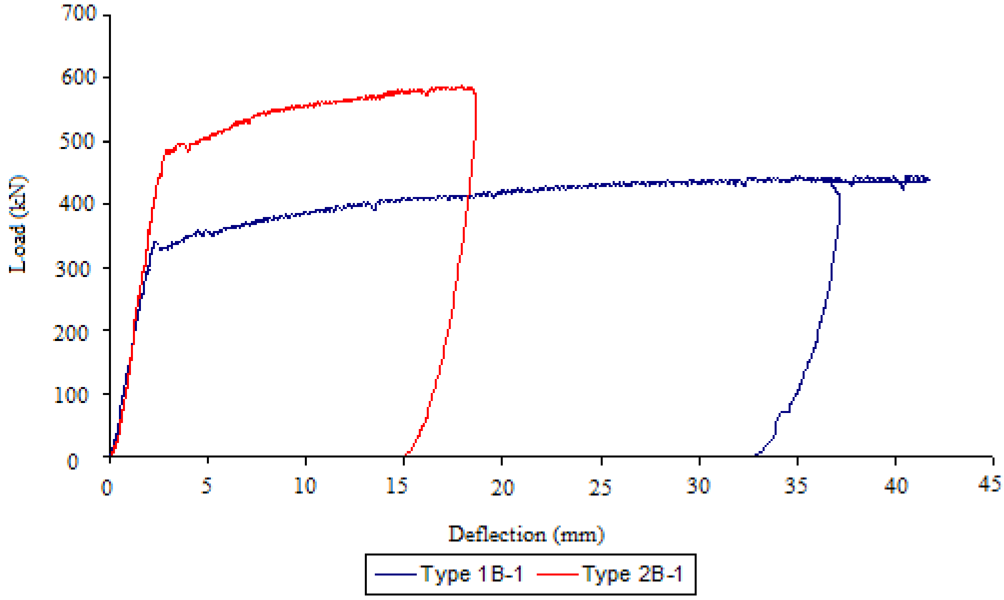

Figure G.6 Load-Deflection Diagram (Type 1B-1, Type 2B-1)
Type 1B-1: Ø12 Stressed- Burnt
Type 2B-1: Ø14 Stressed - Burnt

APPENDIX H

CALCULATION OF STEEL AND CONCRETE POST-FIRE STRENGTH ACCORDING TO [5]

a. Steel Strength

Yield Strength

$$f_y^{100^0 C} = \frac{520MPa}{1+24.4\left(\frac{377-20}{1000}\right)^{4.5}} = 420.43MPa$$

Ultimate Strength

$$f_u^{100^0 C} = \frac{600MPa}{1+24.4\left(\frac{377-20}{1000}\right)^{4.5}} = 485.12MPa$$

b. Concrete Strength

Type 1A-1

5 cm => $f_c^{373^0 C} = \frac{52.74MPa}{1+24\left(\frac{373-20}{1000}\right)^{6}} = 50.39MPa$

10 cm => $f_c^{255^0 C} = \frac{52.74MPa}{1+24\left(\frac{255-20}{1000}\right)^{6}} = 52.52MPa$ Average = 51.88 MPa

15 cm => $f_c^{100^0 C} = \frac{52.74MPa}{1+24\left(\frac{100-20}{1000}\right)^{6}} = 52.74MPa$

Type 2A-1

5 cm => $f_c^{373^0 C} = \dfrac{57.6MPa}{1+24\left(\dfrac{373-20}{1000}\right)^6} = 55.04MPa$

10 cm => $f_c^{255^0 C} = \dfrac{57.6MPa}{1+24\left(\dfrac{255-20}{1000}\right)^6} = 57.36MPa$ Average = 56.66 MPa

15 cm => $f_c^{100^0 C} = \dfrac{57.6MPa}{1+24\left(\dfrac{100-20}{1000}\right)^6} = 57.6MPa$

Type 1B-1

5 cm => $f_c^{373^0 C} = \dfrac{61.4MPa}{1+24\left(\dfrac{373-20}{1000}\right)^6} = 58.67MPa$

10 cm => $f_c^{255^0 C} = \dfrac{61.4MPa}{1+24\left(\dfrac{255-20}{1000}\right)^6} = 61.15MPa$ Average = 60.4 MPa

15 cm => $f_c^{100^0 C} = \dfrac{61.4MPa}{1+24\left(\dfrac{100-20}{1000}\right)^6} = 61.4MPa$

Type 2B-1

5 cm => $f_c^{373^0 C} = \dfrac{61.65MPa}{1+24\left(\dfrac{373-20}{1000}\right)^6} = 58.91MPa$

10 cm => $f_c^{255^0 C} = \dfrac{61.65MPa}{1+24\left(\dfrac{255-20}{1000}\right)^6} = 61.4MPa$ Average = 60.65 MPa

15 cm => $f_c^{100^0 C} = \dfrac{61.65MPa}{1+24\left(\dfrac{100-20}{1000}\right)^6} = 61.65MPa$

APPENDIX I

CALCULATION OF STEEL AND CONCRETE POST-FIRE STRENGTH ACCORDING TO ACI 216

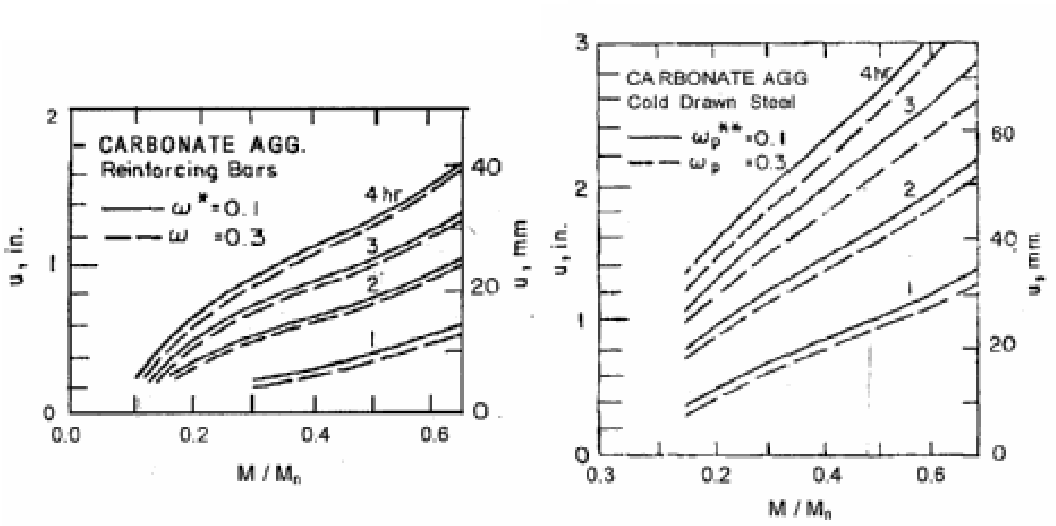

Figure I.1 Fire Endurance of Concrete Slabs as Influenced by Aggregate Type, Reinforcing steel Type, Moment Intensity and u [2]

<u>Type 1A-1</u> (Ø12, Unstressed, Burnt)

<u>General Properties</u>:

$d_b = 12mm$ $f_y = 530MPa$ $f_u = 600MPa$ $f_c' = 52.74MPa$

$A_s = 565.48mm^2$ $Cover = 60mm$ $L = 1200mm$ $u = 15mm$

$h = 400mm$

<u>Fire Endurance Calculations</u>:

Dead Load=> $2.5t/m^3 \times 0.4 \times 0.6 \times 1.5 = 0.9Ton = 9kN$

$$M = \frac{W \times l^2}{8} = \frac{9 \times 1.2^2}{8} = 1.62kNm \qquad \text{Eqn. (I.1)}$$

$$d = h - \text{cov}er - \frac{d_b}{2} = 400 - 60 - \frac{12}{2} = 334mm \qquad \text{Eqn. (I.2)}$$

$$a = \frac{A_s \times f_y}{0.85 \times f_c' \times b} = \frac{565.48 \times 530}{0.85 \times 52.74 \times 600} = 11.14mm \qquad \text{Eqn. (I.3)}$$

$$M_n = A_s \times f_y \times (d - \frac{a}{2}) = \frac{565.48 \times 530 \times (334 - \frac{11.14}{2})}{1000 \times 1000} = 98.43kNm \qquad \text{Eqn. (I.4)}$$

$$\frac{M}{M_n} = \frac{1.62}{98.43} = 0.0164$$

$$w = \frac{A_s \times f_y}{b \times d \times f_c'} = \frac{565.48 \times 530}{600 \times 334 \times 52.74} = 0{,}028 \qquad \text{Eqn. (I.5)}$$

If I assume M/M_n=0.1 and w=0.1; fire endurance is about 4.5 hours [Figure I.1].

<u>Type 1A-2</u> (Ø12, Unstressed, Unburnt)

<u>General Properties</u>:

$d_b = (2 \times \phi 14) + (3 \times \phi 12)$ $\quad f_y = 520MPa$ $\quad f_u = 600MPa$ $\quad f_c' = 61.83MPa$

$A_s = (153.9 \times 2) + (113.1 \times 3) = 647.1mm^2$ $\quad Cover = 60mm$ $\quad L = 1200mm$

$h = 400mm$

<u>Yield Capacity</u>

$$d = h - \text{cov}er - \frac{d_b}{2} = 400 - 60 - \frac{12}{2} = 334mm$$

$$a = \frac{A_s \times f_y}{0.85 \times f_c' \times b} = \frac{647.1 \times 520}{0.85 \times 61.83 \times 600} = 10.67mm$$

$$M_n = A_s \times f_y \times (d - \frac{a}{2}) = \frac{647.1 \times 520 \times (334 - \frac{10.67}{2})}{1000 \times 1000} = 110.59kNm$$

$$M_n = \frac{P \times L}{4} \Rightarrow P = \frac{4 \times 110.59}{1.2} = 36.86Ton$$

Ultimate Capacity

$$a=\frac{A_s\times f_y}{0.85\times f_c'\times b}=\frac{647.1\times 600}{0.85\times 61.83\times 600}=12.31mm$$

$$M_n=A_s\times f_y\times(d-\frac{a}{2})=\frac{647.1\times 600\times(334-\frac{12.31}{2})}{1000\times 1000}=127.29kNm$$

$$M_n=\frac{P\times L}{4}\Rightarrow P=\frac{4\times 127.29}{1.2}=424.3kN$$

Type 2A-1 (Ø14, Unstressed, Burnt)

General Properties:

$d_b=14mm$ $f_y=530MPa$ $f_u=600MPa$ $f_c'=57.6MPa$

$A_s=769.7mm^2$ $Cover=60mm$ $L=1200mm$ $u=15mm$

$h=400mm$

Fire Endurance Calculations:

Dead Load=> $2.5t/m^3\times 0.4\times 0.6\times 1.5=0.9Ton=9kN$

$$M=\frac{W\times l^2}{8}=\frac{9\times 1.2^2}{8}=1.62kNm$$

$$d=h-\text{cover}-\frac{d_b}{2}=400-60-\frac{14}{2}=333mm$$

$$a=\frac{A_s\times f_y}{0.85\times f_c'\times b}=\frac{769.7\times 530}{0.85\times 57.6\times 600}=13.88mm$$

$$M_n=A_s\times f_y\times(d-\frac{a}{2})=\frac{769.7\times 530\times(333-\frac{13.88}{2})}{1000\times 1000}=133.kNm$$

$$\frac{M}{M_n}=\frac{1.62}{133}=0.012$$

$$w=\frac{A_s\times f_y}{b\times d\times f_c'}=\frac{769.7\times 530}{600\times 333\times 57.6}=0.035$$

If I assume M/M_n=0.1 and w=0.1; fire endurance is about 4.5 hours [Figure I.1].

Type 2A-2 (Ø14, Unstressed, Unburnt)

General Properties:

$d_b = 14mm$ $f_y = 520MPa$ $f_u = 600MPa$ $f_c' = 61.8MPa$

$A_s = 769.7mm^2$ $Cover = 60mm$ $L = 1200mm$ $h = 400mm$

Yield Capacity

$$d = h - \text{cov}er - \frac{d_b}{2} = 400 - 60 - \frac{14}{2} = 333mm$$

$$a = \frac{A_s \times f_y}{0.85 \times f_c' \times b} = \frac{769.7 \times 520}{0.85 \times 61.8 \times 600} = 12.7mm$$

$$M_n = A_s \times f_y \times (d - \frac{a}{2}) = \frac{769.7 \times 520 \times (333 - \frac{12.7}{2})}{1000 \times 1000} = 130.74kNm$$

$$M_n = \frac{P \times L}{4} \Rightarrow P = \frac{4 \times 130.74}{1.2} = 435.8kN$$

Ultimate Capacity

$$a = \frac{A_s \times f_y}{0.85 \times f_c' \times b} = \frac{769.7 \times 600}{0.85 \times 61.8 \times 600} = 14.65mm$$

$$M_n = A_s \times f_y \times (d - \frac{a}{2}) = \frac{769.7 \times 600 \times (333 - \frac{14.65}{2})}{1000 \times 1000} = 150.4kNm$$

$$M_n = \frac{P \times L}{4} \Rightarrow P = \frac{4 \times 150.4}{1.2} = 501.3kN$$

Type 1B-1 (Ø12, Stressed, Burnt)

General Properties:

$d_b = 12mm$ $f_y = 530MPa$ $f_u = 600MPa$ $f_c' = 61.47MPa$

$A_s = 565.48mm^2$ $Cover = 60mm$ $L = 1200mm$ $h = 400mm$

Fire Endurance Calculations:

Dead Load=> $2.5t/m^3 \times 0.4 \times 0.6 \times 1.5 = 0.9Ton = 9kN$

$$M = \frac{W \times l^2}{8} = \frac{9 \times 1.2^2}{8} = 1.62kNm$$

Pre-stressing Moment=> $e \times P = 0.17 \times 34.6 = 5.882tonm = 58.82kNm$

$$d = h - \text{cover} - \frac{d_b}{2} = 400 - 60 - \frac{12}{2} = 334mm$$

$$a = \frac{A_s \times f_y}{0.85 \times f_c' \times b} = \frac{565.48 \times 530}{0.85 \times 61.47 \times 600} = 9.56mm$$

$$M_n = A_s \times f_y \times (d - \frac{a}{2}) = \frac{565.48 \times 530 \times (334 - \frac{9.56}{2})}{1000 \times 1000} = 98.66kNm$$

$$\frac{M}{M_n} = \frac{1.62 + 58.82}{98.66} = 0.61$$

Interior Bars=> $u = \text{cover} + \frac{d_b}{2} = 60 + 6 = 66mm$ Eqn. (I.6)

Corner Bars=> $u = \frac{u}{2} = 33mm$ Eqn. (I.7)

Effective u=> $u = \frac{(3 \times 66) + (2 \times 33)}{5} = 52.8mm$

$$w_p = \frac{A_{ps} \times f_{pu}}{b \times d \times f_c'} = \frac{295.5 \times 13500}{600 \times 334 \times 61.47} = 0.32$$

According to diagram in ACI 216, fire endurance is about 2.5-3 hours [Figure I.1].

Type 1B-2 (Ø12, Stressed, Unburnt)

General Properties:

$d_b = 12mm$	$f_y = 520MPa$	$f_u = 600MPa$	$f_c' = 60.57MPa$
$A_s = 565.48mm^2$	$Cover = 60mm$	$L = 1200mm$	$h = 400mm$

Yield Capacity

$$d = h - \text{cover} - \frac{d_b}{2} = 400 - 60 - \frac{12}{2} = 334mm$$

$$a = \frac{A_s \times f_y}{0.85 \times f_c' \times b} = \frac{565.48 \times 520}{0.85 \times 60.57 \times 600} = 9.52mm$$

$$M=\frac{(565.48\times520)\times(334-\frac{9.52}{2})}{1000\times1000}-\frac{346\times(17-\frac{9.52}{2})}{1000}=96.81-4.26=92.55kNm$$

$$M=\frac{P\times L}{4}\Rightarrow P=\frac{4\times92.55}{1.2}=307kN$$

Ultimate Capacity

$$a=\frac{A_s\times f_y}{0.85\times f_c'\times b}=\frac{565.48\times600}{0.85\times60.57\times600}=10.98mm$$

$$M=\frac{565.48\times600\times(334-\frac{10.98}{2})}{1000\times1000}-\frac{346\times(17-\frac{10.98}{2})}{1000}=111.46-3.99=107.47kNm$$

$$M=\frac{P\times L}{4}\Rightarrow P=\frac{4\times107.47}{1.2}=358.2kN$$

Type 2B-1 (Ø14, Stressed, Burnt)

General Properties:

$d_b=14mm$	$f_y=530MPa$	$f_u=600MPa$	$f_c'=61.65MPa$
$A_s=769.7mm^2$	$Cover=60mm$	$L=1200mm$	$h=400mm$

Fire Endurance Calculations:

Dead Load=> $2.5t/m^3\times0.4\times0.6\times1.5=0.9Ton=9kN$

$$M=\frac{W\times l^2}{8}=\frac{9\times1.2^2}{8}=1.62kNm$$

Pre-stressing Moment=> $e\times P=0.17\times34.6=5.882tonm=58.82kNm$

$$d=h-cover-\frac{d_b}{2}=400-60-\frac{14}{2}=333mm$$

$$a=\frac{A_s\times f_y}{0.85\times f_c'\times b}=\frac{769.7\times530}{0.85\times61.65\times600}=12.97mm$$

$$M_n=A_s\times f_y\times(d-\frac{a}{2})=\frac{769.7\times530\times(333-\frac{12.97}{2})}{1000\times1000}=133.2kNm$$

$$\frac{M}{M_n}=\frac{1.62+58.82}{133.2}=0.45$$

Interior Bars=> $u = \text{cover} + \frac{d_b}{2} = 60 + 7 = 67mm$

Corner Bars=> $u = \frac{u}{2} = 33.5mm$

Effective u=> $u = \frac{(3\times 67)+(2\times 33.5)}{5} = 53.6mm$

$$w_p = \frac{A_{ps}\times f_{pu}}{b\times d\times f_c'} = \frac{295.5\times 13500}{600\times 334\times 61.65} = 0.32$$

According to diagram in ACI 216, fire endurance is about 2.5-3 hours [Figure I.1].

<u>Type 2B-2</u> (Ø14, Stressed, Unburnt)

<u>General Properties</u>:

$d_b = 14mm$ $f_y = 520MPa$ $f_u = 600MPa$ $f_c' = 50.58MPa$

$A_s = 769.7mm^2$ $Cover = 60mm$ $L = 1200mm$ $h = 400mm$

<u>Yield Capacity</u>

$$d = h - \text{cover} - \frac{d_b}{2} = 400 - 60 - \frac{14}{2} = 333mm$$

$$a = \frac{A_s\times f_y}{0.85\times f_c'\times b} = \frac{769.7\times 520}{0.85\times 50.58\times 600} = 15.51mm$$

$$M = \frac{(769.7\times 520)\times(333-\frac{15.51}{2})}{1000\times 1000} - \frac{346\times(17-\frac{15.51}{2})}{1000} = 130.17 - 3.19 = 126.98kNm$$

$$M = \frac{P\times L}{4} \Rightarrow P = \frac{4\times 126.98}{1.2} = 423.2kN$$

<u>Ultimate Capacity</u>

$$a = \frac{A_s\times f_y}{0.85\times f_c'\times b} = \frac{769.7\times 600}{0.85\times 50.58\times 600} = 17.9mm$$

$$M = \frac{(769.7\times 600)\times(333-\frac{17.9}{2})}{1000\times 1000} - \frac{346\times(17-\frac{17.9}{2})}{1000} = 149.65 - 2.78 = 146.87kNm$$

$$M_n = \frac{P\times L}{4} \Rightarrow P = \frac{4\times 146.87}{1.2} = 489.5kN$$